Continuum Sensitivity Method for Nonlinear Dynamic Aeroelasticity

Shaobin Liu

Dissertation submitted to the Faculty of the
Virginia Polytechnic Institute and State University
in partial fulfillment of the requirements for the degree of

Doctor of Philosophy
in
Aerospace Engineering

Robert A. Canfield, Chair
Rakesh K. Kapania
Mayuresh J. Patil
Christopher J. Roy
Muhammad R. Hajj

June 13, 2013
Blacksburg, Virginia

Keywords: Continuum Sensitivity, Shape Sensitivity, Aeroelasticity, Optimization,
Fluid-structure interaction

Continuum Sensitivity Method for Nonlinear Dynamic Aeroelasticity

Shaobin Liu

(ABSTRACT)

In this dissertation, a continuum sensitivity method is developed for efficient and accurate computation of design derivatives for nonlinear aeroelastic structures subject to transient aerodynamic loads. The continuum sensitivity equations (CSE) are a set of linear partial differential equations (PDEs) obtained by differentiating the original governing equations of the physical system. The linear CSEs may be solved by using the same numerical method used for the original analysis problem. The material (total) derivative, the local (partial) derivative, and their relationship is introduced for shape sensitivity analysis. The CSEs are often posed in terms of local derivatives (local form) for fluid applications and in terms of total derivatives (total form) for structural applications. The local form CSE avoids computing mesh sensitivity throughout the domain, as required by discrete analytic sensitivity methods. The application of local form CSEs to built-up structures is investigated. The difficulty of implementing local form CSEs for built-up structures due to the discontinuity of local sensitivity variables is pointed out and a special treatment is introduced. The application of the local form and the total form CSE methods to aeroelastic problems are compared. Their advantages and disadvantages are discussed, based on their derivations, efficiency, and accuracy. Under certain conditions, the total form continuum method is shown to be equivalent to the analytic discrete method, after discretization, for systems governed by a general second-order PDE. The advantage of the continuum sensitivity method is that less information of the source code of the analysis solver is required. Verification examples are solved for shape sensitivity of elastic, fluid and aeroelastic problems.

This work has been supported by Dr. Fariba Fahroo under the Air Force Office of Scientific Research Grant FA9550-09-1-0354.

Attribution

Robert A. Canfield is co-author for the manuscripts of Chapters 2, 3, and 4. His contributions include strategic advice and review of the articles for technical accuracy, completeness, and grammatical correctness.

Dedication

This dissertation is dedicated to my beloved family

for their endless love, support and encouragement.

Acknowledgments

First and foremost, I would like to express my deepest gratitude to my advisor, Dr. Robert Canfield, for his support, patient guidance and encouragement during my PhD study. His wide horizons and insightful thoughts have greatly helped to advance this research work. He is more than an excellent advisor, but a mentor and role model who always gives me positive energy. I believe that the experience working with him would have lifelong benefits for me.

I would like to thank my dissertation committee members, Dr. Rakesh K. Kapania, Dr. Mayuresh Patil, Dr. Christopher Roy and Dr. Muhammad R. Hajj, for their precious time, inspiring comments and valuable feedback for my research. Their courses I took laid the useful knowledge foundations for this research and for my future career development. Talking with them always enlightens me with critical thinking and professionalism.

My special thanks goes to my friends and officemates: Anthony P. Ricciardi who patiently answer almost any questions I have about language, culture, Latex and others. It's really fun and helpful to work with him; David P. Cross with whom I discussed intensively about the design sensitivity methods.

I am very grateful to all my friends met in Blacksburg, especially Yu Lei, Qing Yang, Zhiye Zhang, Yumeng Li, Zhibing Xu, Song Xue, Shengzhi Shao and Haiyang Fu, for their friendship and support. My life at Virginia Tech would not be colorful and meaningful without them.

I devote my deepest gratitude to my parents, my sisters and brother-in-laws for all their unlimited love and endless encouragement. Without their support and patience, I can not complete my study in United States.

Contents

List of Figures

Chapter 1

Introduction

1.1 Motivation

More than ever, in these days of frugal budgets, cost is an important constraint for acquisition of commercial and military vehicles. Designing air vehicle systems with "cost as an independent variable" is driven by fiscal constraints that demand the best performance for the budget available, not the best performance at any cost. Because cost and performance are affected most by decisions made early in the design process, accurate and efficient modeling are paramount to the designer. The development of numerical modeling methods for predicting and optimizing the performance, stability, and safety of coupled aero-structural systems will improve the performance and minimize the cost for any air vehicle that responds flexibly to aerodynamic loads. NASA's experience with the highly flexible Helios (Fig. 1.1), a High Altitude, Long Endurance (HALE) aircraft, strongly indicates the need for better numerical methods for predicting gust response in the transient nonlinear regime. After investigating its crash, "the board determined that the mishap resulted from the inability to predict, using available analysis methods, the aircraft's increased sensitivity to atmospheric

disturbances such as turbulence, following vehicle configuration changes required for the long-duration flight demonstration." (NASA, 2004). Gust loads due to atmospheric turbulence is one of the most critical load cases for aircraft across a broad spectrum of vehicle sizes. HALE aircraft with lightweight requirements and large aspect ratios are very sensitive to gust loads. This is true for applications such as the next-generation Sensorcraft (Fig. 1.2) for which the Air Force is planning as a Global Hawk replacement (Johnson, 2001) and DARPAs Vulture program (Trimble, 2009). Exploratory design studies by the Air Force Research Laboratory (AFRL) (Lucia, 2005) and Boeing (Omar, 2003) confirm that gusts are critical loads for the Sensorcraft mission. At the other end of the spectrum, wind gusts are one of the most critical challenges for designing a micro air vehicle (MAV) that can be as small as 15 centimeters. Clearly a better understanding of how changes to an aircraft configuration can improve response to turbulent gusts is imperative for meeting aggressive performance requirements of the next generation of air vehicles.

Computational aeroelasticity is a challenging area that deals with the interaction of the two fields. Although modeling the structural and fluid fields is becoming mature and efficient, the accurate calculation of the coupling of these two fields with high fidelity models for nonlinear dynamic problems is still problematic due to the computational expense involved. The multidisciplinary design and shape optimization of structures and aerodynamics is extremely challenging (Sobieszczanski-Sobiesk and Haftka, 1997). With respect to aeroelastic design, Livne (1994) comments that "much less is known in the area of aeroservoelastic approximations when shape design variables are added to the sizing type design variables." Since the optimization typically requires the calculation of the change of a performance measure or an objective function to variations of the design parameters in each iteration, the sensitivity analysis becomes one of the most time consuming steps of optimization of aeroelastic problems. A contribution in developing computationally efficient sensitivity analysis methods for

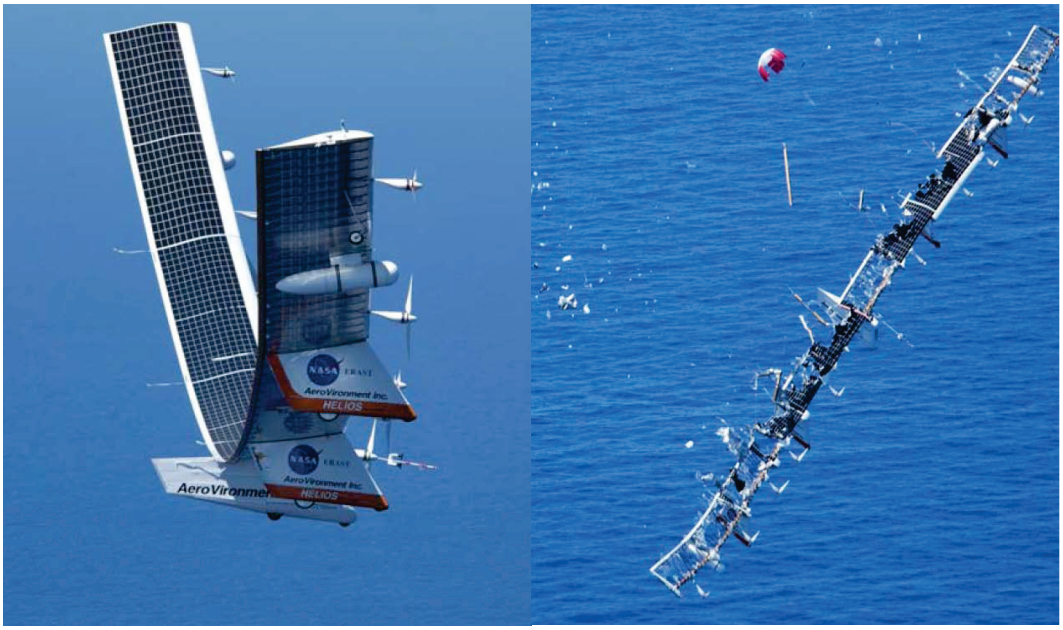

Figure 1.1: Helios prototype at high wing dihedral prior to structural failure and in-flight breakup (NASA, 2004).

fluid-structure interaction problems will have significant benefits for aeroelastic design.

The objectives of this research are to implement, demonstrate, and apply a newly derived computational method for obtaining the sensitivity of dynamic aeroelastic systems with respect to their shape or configuration changes. The ultimate goal is to reduce the design cycle time for evaluating new design models of high performance aircraft. Although modern computer aided design and analysis tools expedite the design process in the early, conceptual design stage, the design methods are still predominantly based on empirical or low fidelity models due to the computational expenses. In this research, the goal is to develop aeroelastic sensitivity analysis tools to enable computationally efficient methods for design optimization of the high fidelity, physics-based models of future flexible aerospace vehicles early in the design process, when the most critical design decisions are being made.

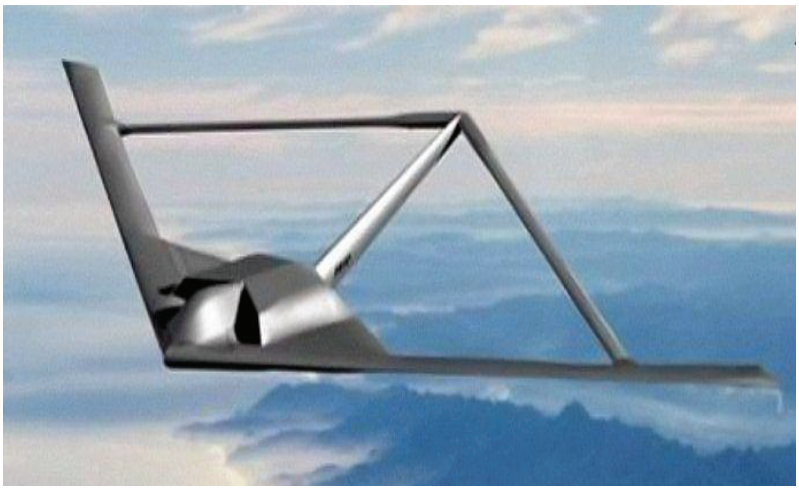

Figure 1.2: Boeing sensorcraft configuration (Johnson, 2001) used under fair use, 2013

1.2 Design sensitivity methods

One of the most widely used classes of optimization algorithms are gradient-based algorithms, in which the gradients of the performance measures (objective or constraint functions) with respect to the design parameter are required. The gradients of performance measures are often referred to as design sensitivities. There are several ways of calculating the sensitivity. As can be seen from the taxonomy in Fig. 1.3, the design sensitivity analysis (DSA) methods may be classified as numeric, analytic, or automatic differentiation.

The finite difference (FD) method is one of the most commonly used numerical methods due to its simplicity of implementation. However, the FD method suffers from inefficiency and the need to find an appropriate step size that balances truncation and roundoff errors. More recently the complex step method has seen increased use due to its greater accuracy for machine precision step sizes (Squire and Trapp, 1998; Martins, 2003); however, its implementation is limited to analytic functions that can operate on complex arguments. Automatic

differentiation similarly provides high accuracy, but does require access to all the source code. The automatic differentiation method has been widely used for sensitivity analysis of general purpose computational fluid dynamics packages (Carle et al., 1998; Bischof et al., 2007). The application of automatic differentiation for flutter instability problems have been investigated (Kapania and Issac, 1994; Issac et al., 1995; Issac and Kapania, 1997).

The taxonomy of analytic methods may be further refined as discrete and continuum (or continuous) approaches. In the discrete approach, the governing equations are first discretized and then used to carry out the DSA, while in the continuum method, the continuum equations are first differentiated, then discretized. Heretofore, the discrete analytic methods generally have been the method of choice to most efficiently achieve high accuracy, when the details of the analysis procedure are available (Braibant and Fleury, 1984; Braibant, 1986; Pandey and Bakshi, 1999). A general way of implementing the discrete analytic method is to approximate the derivatives of the stiffness matrix by finite differences. This is known as the semi-analytic method. Hence it has advantages and disadvantages similar to the FD method. The discrete analytic and semi-analytic methods have been applied to calculate the shape sensitivity of wing flutter and aeroelastic response with respect to changes in shape parameters (Kapania et al., 1991, 1993).

The continuum sensitivity method, also known as variational shape design (Haug et al., 1986), the variational sensitivity method (Haftka and Gurdal, 1986), and the continuous sensitivity equation method (Borggaard and Burns, 1997) can be derived by differentiating the continuous governing equations. The resulting linearized system of equations, called continuum sensitivity equations (CSEs), are solved for the gradients of dependent variables with respect to the design variables. For shape design problems, the CSEs can be posed in terms of material derivatives (total form) or local derivatives (local form). For value design problems, in which the domain shape does not change with the design parameters, total

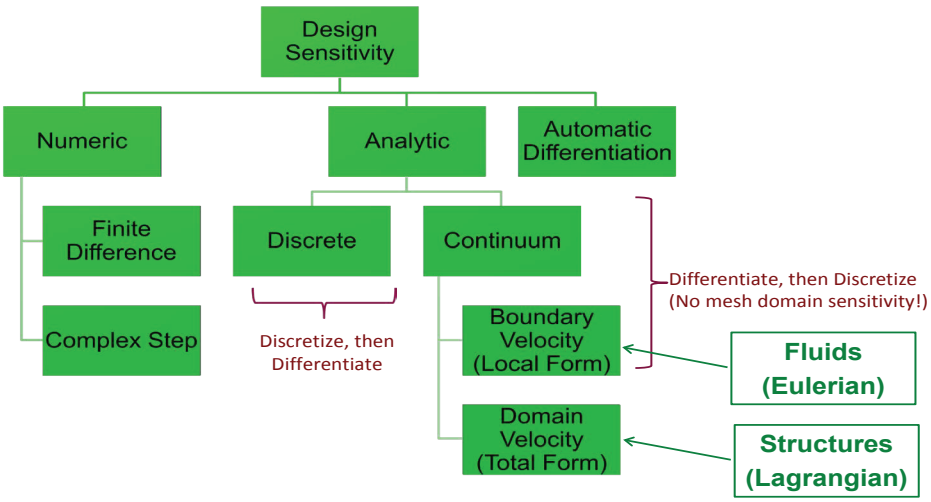

Figure 1.3: Taxonomy of design sensitivity methods.

form and local form CSE are identical. Continuum shape sensitivity systems are often posed in terms of local derivatives (an Eulerian reference frame) for fluids (Borggaard and Burns, 1997; Etienne and Pelletier, 2005) and total derivatives (Lagrangian reference frame) for solids (Haug et al., 1986; Choi and Kim, 2005). For shape optimization of fluid applications, an Eulerian description of the flow sensitivity is often adequate. Thus, much of the fluid mechanics literature does not emphasize the distinction between the local and total derivatives, except Charlot et al. (2012) introduced the continuous lagrangian sensitivity equation method (total form) for fluid applications. For structural optimization problems, however, the design sensitivity at a material point is usually required, which necessitates a means to calculate total sensitivities at a given material point.

The local form CSE is usually derived by taking partial derivatives of the governing equations and posing the resulting PDEs in terms of local sensitivity variables. Only boundary design velocities that define the rate of change of the spatial coordinates with respect to the design are required for solving the local sensitivities. If the total sensitivities are of

interest, the local derivative can be converted to total derivative (Wickert et al., 2012). Liu and Canfield (2011) point out that the dependent variables of the CSE, namely the local sensitivity variables, are not continuous at the interfaces of a built-up structure because they are locations where strain is discontinuous, Hence, the implementation of local form CSE is more complicated for indeterminate structures. The total derivative form is more generally applicable for built-up structures with strain discontinuities. An article on the detailed derivation and application of local form CSE has been published online (http://dx.doi.org/10.1016/j.jfluidstructs.2013.05.003) in *Journal of Fluids and Structures* (Chapter 2).

Liu and Canfield (2012b) made a comparison between local and total form CSE, which showed that the total form CSE for shape sensitivity may be more accurate than the local form when the displacement finite element method (FEM) was used for the analysis problem. The local form requires design velocity only at the boundaries of the domain, while the total form requires the design velocity in the whole domain. An additional linear system may have to be solved for the design velocity field for use of the total form. The local form CSE requires higher order derivatives of the analysis solution than the total form, which affects the accuracy of sensitivity results. The accuracy of local form CSE method may be improved by using higher order finite elements for the analysis problem. Cross and Canfield (2012a) proposed a spatial gradient reconstruction method for obtaining accurate gradients of the analysis solution for the local form CSE boundary conditions. An article that presents a comparison between local form and total form CSE will be submitted to *AIAA Journal* (Chapter 3).

The total form CSE method, once discretized, was proven to be equivalent to the discrete analytic method for nonlinear second-order field problems under certain conditions. The conditions are that the two methods use the same: (1) numerical approximation of the field

variables and sensitivity variables, (2) integration of the finite element matrices, (3) design velocity fields that are linear with respect to the design variable, and (4) shape functions for domain transformation and for design velocity field calculation. Although, under these conditions, the discrete analytic method is identical to the total form CSE method, the total form CSE can be implemented without satisfying all these conditions. For instance, different shape functions or meshes can be used for solving the CSE system (Burns et al., 1997). The advantage of the CSE method is that the discrete analytic method requires the knowledge of the implementation details of the original analysis codes, which may be inaccessible or very complex, while the continuum method requires minimum information of the source codes. The continuum method only requires knowledge of the governing equations, the numerical solutions and the spatial gradients of the solutions for the governing equations. Thus, the CSE method can be implemented by treating the existing analysis solver as a "black box" as described in Cross and Canfield (2012b). The proof of equivalence between discrete analytic and total form CSE method is presented in an article that has been accepted for publication in *Journal of Structural and Multidisciplinary Optimization* (Chapter 4).

1.3 Literature review of continuum sensitivity methods

The purpose of this section is to outline the prior research of continuum design sensitivity analysis methods. For an extensive list of references for design sensitivity analysis methods in general see Olhoff and Taylor (1983), Haug et al. (1986), Haftka and Grandhi (1986), Haftka and Adelman (1989), Tortorelli and Michaleris (1994), and Keulen et al. (2005). This review mainly focuses on the literature concerning continuum sensitivity methods and its applications to fluids and structures. The literature review in this chapter is grouped into

three subsections according to the areas of application of the continuum sensitivity method: Structures (1.3.1), Fluids (1.3.2), Fluid-Structure Interaction (1.3.3).

1.3.1 Structures

The theory of the continuum sensitivity method was first developed for structural elasticity in a series of works (Choi and Haug, 1983; Dems and Mroz, 1983, 1984, 1985). They called it the variational approach for sensitivity. A textbook published by Haug et al. (1986) was one of the first textbooks to introduce the material derivative for shape sensitivity analysis. A more recent textbook by Choi and Kim (2005) gives many examples for using material derivatives for structural shape sensitivity analysis and extends this method for nonlinear structural problems. Choi and Kim (2005) are the first authors to name this method the continuum sensitivity method. Arora (1993) explains the material derivative approach for structural shape sensitivity analysis and derives both the direct and the adjoint sensitivity formulas. Arora et al. (1992) investigated the relationship between material derivative and control volume approaches. They showed that the final design sensitivity expression for one approach can be obtained from the other. Thus, the two approaches are theoretically equivalent. Several authors have proposed formulations using the adjoint method with boundary integrals (Choi and Haug, 1983; Chun and Haug, 1983; Choi, 1985; Haug et al., 1986). Unfortunately, there are considerable numerical difficulties associated with the evaluation of boundary integrals (Yang and Choi, 1985, 1986; Yang and Botkin, 1986), especially for low-order elements which do not accurately approximate a curved boundary.

The domain integral approach in a direct formulation was introduced by Braibant and Fleury (1984, 1985) to avoid these numerical difficulties. The domain integral method can also be used with the adjoint formulation (Choi and Seong, 1986). The domain integral method

avoids the numerical difficulties associated with the boundary integral approach, but it is more expensive, since an initial strain field and design velocity field are required, which requires additional computational resources. The domain integral method, referred to as the "domain shape design sensitivity method " in Haug et al. (1986), was also named total form CSE method in Liu and Canfield (2012b, 2013b). Akbari et al. (2010) proved that the domain integral approach (or total form CSE) is equivalent to the discrete analytic method for linear elasticity problems when they use the same numerical approximation, numerical integration, and design velocity fields that are linear with respect to the design variable. Liu and Canfield (2013a) extended this proof to general nonlinear field problems, such as geometrically nonlinear structures and potential flow problems. In addition to the conditions given in Akbari et al. (2010), the shape functions used for domain transformation also should be the same as those for design velocity calculation.

Dems and Haftka (1988) introduced the concept that continuum equations can also be posed in terms of local derivatives of the dependent variable with respect to shape parameters. After that, for more than two decades, no other literature revised the local derivative form of continuum sensitivity method for structures. More recently, Wickert et al. (2009) applied the local derivative form continuum sensitivity method to a 1D Euler Bernoulli beam using the least-squares finite element method. Following that, Liu and Canfield (2011) pointed out that the implementation of the local form CSE to built-up structures is more difficult due to the discontinuity of local sensitivity values at the interfaces where strains are discontinuous. The advantages and disadvantages of both local and total form CSE methods are discussed in Liu and Canfield (2012a,b, 2013b).

1.3.2 Fluids

In fluid mechanics, the continuum sensitivity method was first developed for aerodynamic shape sensitivity using the adjoint formulation (Jameson, 1988). Borggaard and Burns (1994) introduced a direct formulation for shape optimization of fluid flow and named it the PDE or continuous sensitivity equation method. Since then, the application of the CSE method for fluid applications has been well documented (Borggaard and Burns, 1997; Borggaard and Verma, 2000; Stanley and Stewart, 2002). Based on their research, the CSE method was implemented in a commercial software, SENSE, by AeroSoft Inc. (Burns and Cliff, 1998). In the same period, Pelletier and his students began examining fluid sensitivity using continuous sensitivity methods (Turgeon et al., 1999, 2005; Pelletier, 2003; Hristova et al., 2004; Colin et al., 2005; Duvigneau and Pelletier, 2006). Continuum sensitivity systems are most often posed in terms of the local derivative (an Eulerian reference frame) for fluids. A well-known advantage of local derivative form CSE is that mesh sensitivity is avoided. It requires only the geometric sensitivity at the boundaries in order to specify the boundary conditions for the sensitivity equations. However, extra effort is required for obtaining accurate derivatives of the analysis solutions at boundaries. Recently, Charlot et al. (2008) began investigating the application for fluid problems of the so-called continuous Lagrangian sensitivity equation method (CLSEM), which is the CSE posed in terms of total derivatives (Charlot et al., 2009, 2012). They conclude that the CLSEM delivers more accurate shape sensitivities at a lower cost than the Eulerian technique (local form CSE). However, Liu and Canfield (2013a) proved that the total form CSE method is equivalent to the discrete analytical method under certain conditions.

1.3.3 Fluid-structure interaction

The coupled, or multidisciplinary, problem of optimizing shape for desired structural and aerodynamic response is an extremely challenging problem. Barthelemy and Bergen (1989) derived the analytic shape sensitivity equations for aeroelasticity. Previous work by Ghattas and Li (1998), Lund et al. (2001, 2003) and Fernandez and Moubachir (2001) investigated the design sensitivity of fluid-structure interaction problems, but they mainly focused on the application of the discrete analytic method. Bhaskaran and Berkooz (1997) present the earliest continuum sensitivity application for fluid-structure interaction, albeit for one-way structure to fluid coupling. Etienne and Pelletier (2005) first applied the CSE method to both fluid and structural domains in a fully coupled fashion. Pelletier et al. have employed continuum sensitivity methods for a range of fluid-structure interaction problems (Etienne and Pelletier, 2005; Etienne et al., 2006, 2007) with prominent success; however, much of their work focuses on flow variable sensitivities. Subsequently, Wickert et al. (2008) derived CSE for FSI for the first time using a least-squares finite element method for both fluids and structures. They were also the first to use local form CSE for gust sensitivity (Wickert et al., 2009). Whereas Etienne, Pelletier and co-workers focused on flow sensitivity in the FSI problem, (Liu et al., 2010) were most interested in structural sensitivity in the FSI problem. Liu and Canfield (2011) first applied the local form CSE method for shape sensitivity of a built-up structure under gust loads. Liu and Canfield (2012a) solved the FSI shape sensitivity of an aeroelastic problem for the first time using total form CSE method.

1.4 Research contributions

The work completed here has new and unique aspects relevant to the multidisciplinary design optimization research community. Design sensitivity analysis is one of the most important

steps for design optimization of multidisciplinary problems, such as aeroelastic systems. Relatively little research has been conducted for the CSE of fluid-structure interaction applications. The research on continuum sensitivity methods has been somewhat isolated between the structures and fluids communities. They both adopted the concept of "differentiate then discretize," but used different forms of the continuum sensitivity method. In fact, no one has previously investigated the application of those different forms of the continuum sensitivity method for both fluid and structure problems. This dissertation makes several significant contributions to the state of the knowledge for the application of the continuum sensitivity methods to not only fluid-structure interaction problems, but also for more fundamental problems, such as structural and aerodynamic shape design problems. The following contributions are explained in more detail in the rest of the dissertation.

- The total form continuum sensitivity method was applied for the first time to nonlinear transient gust response. For nonlinear problems, it is shown in this dissertation that, when the Newton-Raphson method is used, the tangent stiffness matrix yields the desired sensitivity coefficient matrix for solving the linear sensitivity equations in the Galerkin finite element formulation.

- The local form CSE using the boundary velocity method was applied for the first time to built-up indeterminate structures. It has been recognized that the local sensitivity variables in the local form CSE are discontinuous at the interfaces of the built-up structure where the strains are discontinuous. The difficulty in implementation of the assembly the sensitivity coefficient matrix has been resolved. Otherwise, the total form CSE is more generally applicable and easier to implement for built-up structures or other structures with strain discontinuities.

- First comparison of the local form and the total form CSE method for static and

transient aeroelastic problems has been made. The total form CSE exhibited higher accuracy than local form, when the same numerical method was used for solving fluid and structures benchmark problems. The local form requires design velocity only at the boundaries, and the continuity requirements for the design velocity is lower than the total form CSE method. On the other hand, local form requires higher order spatial derivatives to specify its sensitivity boundary conditions than does total form CSE.

- First proof of the equivalence of the discrete analytic method and the total form CSE method is given for general nonlinear transient second-order partial differential equations that govern many field problems. The equivalence of these two methods is demonstrated for general transient geometric nonlinear elasticity and potential flow, as specific examples.

1.5 Outline of dissertation

In this dissertation, Chapters 2 and 4 contain journal articles that have been accepted in archival journals for publication. Chapter 2 presents the application of boundary velocity (local form CSE) method for continuum shape sensitivity of nonlinear fluid-structure interaction problems, including built-up structures with discontinuous local derivatives. In this chapter, we detail the application of local form CSE for built-up structures under aerodynamic loads. Chapter 3 which is in preparation for submission as a journal article, compares the local form and the total form continuum sensitivity methods. The advantages and disadvantages of the two methods are discussed based on their accuracy, efficiency and their implementations. Chapter 4 presents a proof of the equivalence between the discrete analytic method and the total form CSE method. In the proof, a general way of deriving sensitivity equations is given for a general transient nonlinear second-order partial differential equation.

Chapter 5 provides conclusions drawn from this work and suggests the future work to be done in the design sensitivity analysis for aeroelasticity.

Bibliography

Akbari, J., Kim, N., Ahmadi, M., 2010. Shape sensitivity analysis with design-dependent loadings–equivalence between continuum and discrete derivatives. Structural and Multidisciplinary Optimization 40 (1-6), 353–364.

Arora, J. S., 1993. An exposition of the material derivatives approach for structural shape sensitivity analysis. Computer Methods in Applied Mechanics and Engineering 105, 41–62.

Arora, J. S., Lee, T. H., Cardoso, J. B., 1992. Structural shape sensitivity analysis: Relationship between material derivative and control volume approaches. AIAA Journal 30 (6), 1638–1648.

Barthelemy, J.-F., Bergen, F. D., 1989. Shape sensitivity analysis of wing static aeroelastic characteristics. Journal of Aircraft. 26 (8), 712–717.

Bhaskaran, R., Berkooz, G., 1997. Optimization of fluid-structure interaction using the sensitivity equation approach. Fluid-Structure Interaction, Aeroelasticity, Flow-Induced Vibrations and Noise. 1 (53-1), 49–56.

Bischof, C. H., Bucker, H. M., Rasch, A., Slusanschi, E., Lang, B., 2007. Automatic differentiation of the general-purpose computational fluid dynamics package FLUENT. Journal of Fluids Engineering 129 (5), 652–658.

Borggaard, J., Burns, J., 1994. A sensitivity equation approach to shape optimization in fluid flows. Tech. rep., Langley Research Center.

Borggaard, J., Burns, J., 1997. A pde sensitivity equation method for optimal aerodynamic design. Journal of Computational Physics. 136, 366–384.

Borggaard, J., Verma, A., 2000. On efficient solutions to the continuous sensitivity equation using automatic differentiation. SIAM J. SCI. COMPUT. 22 (1), 39–62.

Braibant, V., 1986. Shape sensitivity by finite elements. Journal of structural mechanics 14 (2), 209–228.

Braibant, V., Fleury, C., 1984. Shape optimal design using B-splines. Computer Methods in Applied Mechanics and Engineering. 44 (3), 247–267.

Braibant, V., Fleury, C., 1985. An approximation concepts approach to shape optimal design. Computer Methods in Applied Mechanics and Engineering. 53 (3), 119–148.

Burns, J. A., Cliff, E. M., 1998. Pre and post processing for large scale computations in optimal design and control. Tech. rep., Virginia Polytechnic Inst and State Univ Blacksburg Interdisciplinary Center of Applied Mathmatics., Blacksburg, VA.

Burns, J. A., Stanley, L. G., Stewart, D. L., 1997. A projection method for accurate computation of design sensitivities. Optimal Control: Theory, Algorithms and Applications, 40–66.

Carle, A., Fagan, M., Green, L. L., 1998. Preliminary results from the application of automated code generation to cfl3d. In: Proceedings, 12th AIAA/USAF/NASA/ISSMO Symposium on Multidisciplinary Analysis and. pp. 98–4807.

Charlot, L., Etienne, S., Pelletier, D., 2008. Lagrangian sensitivity equation method for shape parameters. In: 16th Annual Conference of the Computational Fluid Dynamics Society of Canada.

Charlot, L., Etienne, S., Pelletier, D., 2009. A continuous lagrangian sensitivity equation method for shape parameters. In: 46th AIAA ASM.

Charlot, L., Etienne, S., Pelletier, D., 2012. A continuous lagrangian sensitivity equation method for incompressible flow. Journal of Computational Physics 231, 5989–6011.

Choi, K. K., 1985. Shape design sensitivity analysis of displacement and stress constraints,. Journal of Structural Mechanics. 13, 27–41.

Choi, K. K., Haug, E. J., 1983. Shape design sensitivity analysis of elastic structures. Journal of Structural Mechanics. 11 (2), 231–269.

Choi, K. K., Kim, N.-H., 2005. Structural sensitivity analysis and optimization. Springer Science+Business media, New York.

Choi, K. K., Seong, H. W., 1986. A domain method for shape design of built-up structures. Computer Methods in Applied Mechanics and Engineering. 57, 1–15.

Chun, Y. W., Haug, E. J., 1983. Shape optimization of a solid of revolution. Journal of Engineeringl Mechanics. 109 (1), 30–46.

Colin, E., Pelletier, D., Borggaard, J., 2005. Application of a sensitivity equation method to turbulent flows with heat transfer. International Journal of Thermal Sciences 44 (1), 1024–1038.

Cross, D. M., Canfield, R. A., September, 17-19 2012a. Continuum shape sensitivity with spatial gradient reconstruction of nonlinear aeroelastic gust response. In: 14th AIAA/ISSMO Multidisciplinary Analysis and Optimization Conference. No. AIAA 2012-55597. Indianapolis, Indiana.

Cross, D. M., Canfield, R. A., April, 23-26 2012b. Solving continuum shape sensitivity with existing tools for nonlinear aeroelastic gust analysis. In: 53rd

AIAA/ASME/ASCE/AHS/ASC Structures, Structural Dynamics, and Materials Conference. No. AIAA 2012-1923. Honolulu, Hawaii.

Dems, K., Haftka, R. T., 1988. Two approaches to sensitivity analysis for shape variation of structures. Mech. Struct.& Mach. 16 (4), 501.

Dems, K., Mroz, Z., 1983. Variational approach by means of adjoint systems to structural optimization and sensitivity analysis. part I - variation of material parameters within fixed domain. International Journal of Solids and Structures. 19 (8), 677–692.

Dems, K., Mroz, Z., 1984. Variational approach by means of adjoint systems to structural optimization and sensitivity analysis. part II - structure shape variation. International Journal of Solids and Structures 20, 527–552.

Dems, K., Mroz, Z., 1985. Variational approach to first- and second-order sensitivity analysis of elastic structures. International Journal for Numerical Methods in Engineering 21, 637–661.

Duvigneau, R., Pelletier, D., 2006. On accurate boundary conditions for a shape sensitivity equation method. International Journal for Numerical Methods in Fluids. 50 (2), 147–164.

Etienne, S., Hay, A., Garon, A., 2006. Shape sensitivity analysis of fluid-structure interaction problems. In: 36th AIAA Fluid Dynamics Conference and Exhibit. No. AIAA 2006-3217. San Francisco, California.

Etienne, S., Hay, A., Garon, A., 2007. Sensitivity analysis of unsteady fluid-structure interaction problems. In: 45th AIAA Aerospace Sciences Meeting and Exhibit. No. AIAA-2007-332. Reno, Nevada.

Etienne, S., Pelletier, D., 2005. A general approach to sensitivity analysis of fluid-structure interactions. Numerical Heat Transfer Part B-Fundamentals 42 (6), 485–498.

Fernandez, M., Moubachir, M., 2001. Investigation of sensitivity analysis of fluidstructure interaction systems. the First M.I.T. Conference on Computational Fluid and Solid Mechanics. 11.

Ghattas, O., Li, X., 1998. Domain decomposition methods for sensitivity analysis of a nonlinear aeroelasticity problem. International Journal of Computational Fluid Dynamics. 11, 113–130.

Haftka, R. T., Adelman, H. M., 1989. Recent developments in structural sensitivity analysis. Structural Optimization 1, 137–151.

Haftka, R. T., Grandhi, R. V., 1986. Structural shape optimization–a survey. Computer Methods in Applied Mechanics and Engineering. 57, 91–106.

Haftka, R. T., Gurdal, Z., 1986. Design sensitivity analysis of structural systems, Mathematics in science and engineering. Vol. 177. Academic Press, Orlando.

Haug, E. J., Choi, K. K., Komkov, V., 1986. Design sensitivity analysis of structural systems, Mathematics in science and engineering. Vol. 177. Academic Press, Orlando.

Hristova, H., Etienne, S., Pelletier, D., Borggaard, J., 2004. A general sensitivity equation formulation for unsteady laminar flows. In: 34th AIAA Fluid Dynamics Conference and Exhibit.

Issac, J. C., Kapania, R. K., 1997. Aeroelastic sensitivity analysis of wings using automatic differentiation. AIAA Journal 35 (3), 519–525.

Issac, J. C., Kapania, R. K., Barthelemy, J. M., 1995. Sensitivity analysis of flutter responses of a wing to shape and modal parameters. AIAA Journal 33 (10), 1983–1986.

Jameson, A., 1988. Aerodynamic design via control theory. Journal of Scientific Computing 3, 233–260, 10.1007/BF01061285.
URL http://dx.doi.org/10.1007/BF01061285

Johnson, F. P., August, 6-9 2001. Sensorcraft–tomorrow's eyes and ears of the warfighter. In: AIAA Modeling and Simulation Technologies Conference and Exhibit. No. AIAA 2001-4370. Montreal, Canada.

Kapania, R. K., Bergen, F. D., Barthelemy, J. M., 1991. Shape sensitivity analysis of flutter response of a laminated wing. AIAA Journal 29 (2), 611–612.

Kapania, R. K., Bergen, F. D., Barthelemy, J. M., 1993. Sensitivity analysis of a wing aeroelastic response. Journal of Aircraft 30 (4), 496–504.

Kapania, R. K., Issac, J. C., 1994. Sensitivity analysis of flutter response of a wing in transonic flow. AIAA Journal 32 (4), 350–356.

Keulen, F. v., Haftka, R. T., Kim, N. H., 2005. Review of options for structural design sensitivity analysis. part 1: Linear systems. Computer Methods in Applied Mechanics and Engineering. 194, 3213–3243.

Liu, S., Canfield, R. A., April, 4-7 2011. Continuum shape sensitivity for nonlinear transient aeroelastic gust response. In: 52nd AIAA/ASME/ASCE/AHS/ASC Structures, Structural Dynamics, and Materials Conference. No. AIAA 2011-1971. Denver, Colorado.

Liu, S., Canfield, R. A., September, 17-19 2012a. Continuum sensitivity method for aeroelastic shape design problems. In: 14th AIAA/ISSMO Multidisciplinary Analysis and Optimization Conference. No. AIAA 2012-5480. Indianapolis, Indiana.

Liu, S., Canfield, R. A., April, 23-26 2012b. Continuum shape sensitivity method for fluid

flow around an airfoil. In: 53st AIAA/ASME/ASCE/AHS/ASC Structures, Structural Dynamics, and Materials Conference. No. AIAA 2012-1426. Honolulu, Hawaii.

Liu, S., Canfield, R. A., 2013a. Equivalence of discrete analytic and continuum sensitivity methods for nonlinear differential equations. Accepted for publication in Structural and Multidisciplinary Optimization.

Liu, S., Canfield, R. A., 2013b. Two forms of continuum shape sensitivity method for fluid-structure interaction problems. Submitted to AIAA Journal.

Liu, S., Wickert, D. P., Canfield, R. A., April,12-15 2010. Fluid-structure transient gust response sensitivity for a nonlinear joined wing model. In: 51st AIAA/ASME/ASCE/AHS/ASC Structures, Structural Dynamics, and Materials Conference. No. AIAA 2010-3118. Orlando,Florda.

Livne, E., 1994. Equivalent plate structural modeling for wing shape optimization including transverse shear. AIAA Journal 32 (6), 1278–1288.

Lucia, D. J., April, 18-21 2005. The sensorcraft configurations: A non-linear aeroservoelastic challenge for aviation. In: 46th AIAA/ASME/ASCE/AHS/ASC Structures, Structural Dynamics and Materials Conference. No. AIAA 2005-1943. Austin, Texas.

Lund, E., Moller, H., Jakobsen, L., 2001. Shape design optimization of steady fluid-structure interaction problems with large displacements. In: 42nd AIAA/ASME/ASCE/AHS/ASC Structures, Structural Dynamics and Materials Conference and Exhibit. No. AIAA 2001-1624. Seattle, Washington.

Lund, E., Moller, H., Jakobsen, L., 2003. Shape design optimization of stationary fluid-structure interaction problems with large displacements and turbulence. Structural and Multidisciplinary Optimization. 25, 383–392.

Martins, J. R. R. A., 2003. The complex-step derivative approximation. ACM Transactions on Mathematical Software. 29 (3), 245–262.

NASA, 2004. Helios prototype. NASA Dryden Flight Research Center. URL `http://www.nasa.gov/centers/dryden/news/ResearchUpdate/Helios/index.html`

Olhoff, N., Taylor, J. E., 1983. On structural optimization. Journal of Applied Mechanics 50 (4), 1139–1151.

Omar, E., 2003. Sensor integration study for sensorcraft UAV mid-term review. The Boeing Company, Seattle, Washington.

Pandey, P., Bakshi, P., 1999. Analytical response sensitivity computation using hybrid finite elements. Computers & structures 71 (5), 525–534.

Pelletier, D., 2003. Second order sensitivity equation method for laminar flows. In: AIAA Aerospace Sciences Meeting.

Sobieszczanski-Sobiesk, J., Haftka, R. T., 1997. Multidisciplinary aerospace design optimization: survey of recent developments. Structural and Multidisciplinary Optimization 14 (1), 1–23.

Squire, W., Trapp, G., 1998. Using complex variables to estimate derivatives of real functions. SIAM Review 40 (1), 110–112.

Stanley, L. G. D., Stewart, D., 2002. Design sensitivity analysis : computational issues of sensitivity equation methods. Academic Press, Philadelphia.

Tortorelli, D., Michaleris, P., 1994. Design sensitivity analysis: Overview and review. Inverse Problems in Engineering 1 (1), 71–105.

Trimble, S., 2009. DARPA re-thinks aircraft acquisition and operations with Vulture . URL http://www.flightglobal.com/articles/2009/11/30/335535/darpa-re-thinks-aircraft-acquisitionand-operations-with-vulture.html

Turgeon, E., Pelletier, D., Borggaard, J., 1999. A continuous sensitivity equation approach to optimal design in mixed convection. No. AIAA 99-3625.

Turgeon, E., Pelletier, D., Borggaard, J., 2005. A general continuous sensitivity equation formulation for complex flows. Numerical Heat Transfer Part B-Fundamentals 42 (6), 485–498.

Wickert, D. P., Canfield, R. A., Reddy, J. N., May 4-7 2009. Fluid-structure transient gust sensitivity using least-squares continuous sensitivity analysis. In: 50th AIAA/ASME/ASCE/AHS/ASC Structures, Structural Dynamics, and Materials Conference. No. AIAA-2008-1821. Palm Springs, California.

Wickert, D. P., Canfield, R. A., Reddy, J. N., 2012. Least-squares continuous sensitivity shape optimization for structural elasticity applications. AIAA Journal 48 (12), 2752–2762.

Wickert, D. P., Roberts, R. W., Canfield, R. A., April 7-10 2008. Least-squares continuous sensitivity equations for an infinite plate with a hole. In: 49th AIAA/ASME/ASCE/AHS/ASC Structures, Structural Dynamics, and Materials Conference. No. AIAA-2008-1797. Schaumburg,IL.

Yang, R. J., Botkin, M. E., 1986. The relationship between the variational approach and the implicit differentiation approach to shape design sensitivities. Bennett JA, Botkin ME (eds) The optimum shape: automated structural design. Plenum, New York, 61–77.

Yang, R. J., Choi, K. K., 1985. Accuracy of finite element based shape design sensity analysis. Journal of Structural Mechanics. 13 (2), 223–239.

Yang, R. J., Choi, K. K., 1986. Numerical considerations in structural component shape optimization. Journal of Mechanisms, Transmissions, and Automation in Design 107 (3), 334–339.

Chapter 2

Boundary Velocity Method for Continuum Shape Sensitivity of Nonlinear Fluid-Structure Interaction Problems[1]

Abstract

A Continuum Sensitivity Equation (CSE) method was developed in local derivative form for fluid-structure shape design problems. The boundary velocity method was used to derive the continuum sensitivity equations and sensitivity boundary conditions in local derivative form for a built-up joined beam structure under transient aerodynamic loads. For nonlinear problems, when the Newton-Raphson method is used, the tangent stiffness matrix yields the desired sensitivity coefficient matrix for solving the linear sensitivity equations in the Galerkin finite element formulation. For built-up structures with strain discontinuity, the local sensitivity variables are not continuous at the joints, requiring special treatment to assemble the elemental local sensitivities and the generalized force vector. The coupled fluid-structure physics and continuum sensitivity equations for gust response of a nonlinear joined beam with an airfoil model were posed and solved. The results were compared to the results obtained by finite difference (FD) method.

[1]Published online (http://dx.doi.org/10.1016/j.jfluidstructs.2013.05.003) in *Journal of Fluids and Structures* co-authored with Robert A. Canfield

Keywords: Shape Sensitivity Analysis, Continuum Sensitivity Method, Fluid-Structure Interaction, Boundary Velocity Method

---

2.1 Introduction

In the continuum sensitivity equation (CSE) method, also known as variational shape design (Haug et al., 1986), the variational sensitivity method (Haftka and Gurdal, 1992), and the continuous sensitivity equation method (Borggaard and Burns, 1997), the design parameter gradients are calculated by solving the continuum sensitivity equations. Since the CSE system in local derivative form is posed as a continuous system, it can efficiently produce shape parameter gradients without calculating the mesh sensitivity inside the discrete domain. Further, the sensitivity system is always a linear system of equations, even when the analysis problem is nonlinear. If Newton-Raphson iteration is used for nonlinear problems, the tangent stiffness matrix gives the sensitivity coefficient matrix for the CSE linear system as previous researchers, Borggaard and Burns (1994), and Wickert (2009), have noted.

CSE methods were first introduced for structural problems (Dems and Mroz, 1985; Haftka and Gurdal, 1992). Jameson (1988) first introduced the continuum sensitivity concept in adjoint equation form for aerodynamic design problems. Borggaard and Burns (1994) introduced the CSE nomenclature in a fluid setting and several fluid flow optimization applications followed (Borggaard and Burns, 1997; Bhaskaran and Berkooz, 1997; Stanley and Stewart, 2002; Turgeon et al., 1999). Choi and Kim (2005) cite the lion's share of structural elasticity applications that employ continuum sensitivity methods. Bhaskaran and Berkooz (1997) present one of the earliest uses of CSE for a fluid-structure interaction problem, although it involved CSE only for the fluid with respect to structural mode shapes for the purpose of creating an aerodynamic influence coefficient matrix for flutter calculation. Pelletier et al.

have employed CSE methods for a range of fluid-structure interaction (FSI) problems with prominent success (Etienne and Pelletier, 2005; Etienne et al., 2006, 2007); however, much of their work focuses on flow sensitivities. Wickert and Canfield recently applied the CSE method to the gust sensitivity for an airfoil mounted to an Euler Bernoulli beam (Wickert et al., 2009). They used least-squares finite elements and solved the nonlinear system with successive substitution for which the nonlinear coefficient matrix is different than the sensitivity matrix. Recent work has applied the CSE method to built-up structures, such as joined beam structures, with only static results (Liu et al., 2010). The current effort extends this method to a transient nonlinear joined beam with an airfoil, using the Galerkin finite element method. The Newton-Raphson method is used for the nonlinear problem and for obtaining the sensitivity coefficient matrix for the linear CSE system. Boundary conditions are also derived for CSE of built-up structure sensitivity problems.

CSE systems are often posed in terms of local derivatives (an Eulerian reference frame) for fluid flow, although it is possible to derive the fluid CSE system in total derivative form (Lagrangian reference frame) (Charlot et al., 2009, 2012). For shape optimization of fluid applications, an Eulerian description of the flow sensitivity is often adequate, once accuracy of the spatial derivatives of the solution on the boundary are addressed, since often only local sensitivities for flow are of interest. Thus, much of the fluid mechanics literature does not emphasize the distinction between the local and total derivative. For structural optimization problems, however, the design sensitivity at a material point is usually required, which necessitates a means to calculate total sensitivities at a given material point. In this work, local derivative form CSE system is solved and then the local derivatives are transformed to the total derivative when needed. The difficulty of implementing the local derivative form for structures with stress discontinuity, such as built-up structures, is pointed out and a remedy is suggested.

Section 2.2 begins with a derivation of the CSE system and its associated boundary conditions. In the next section, CSE boundary conditions at the joint of a built-up structure are discussed. Section 2.4 gives the finite element model and the local form CSE for both structure and fluid domains of the nonlinear joined beam and airfoil model. The model is fairly simple, yet complex enough to capture all the salient aspects of the CSE method for a coupled domain, nonlinear, transient system. This is followed by a brief description of the computational results for a simplified nonlinear beam with potential flow about an airfoil model and a joined beam structure under static and transient aerodynamic load.

2.2 Continuum sensitivity equations

Consider the following general, nonlinear boundary value system defined in a domain Ω with a boundary Γ for which we seek a solution $u(x,t;b)$ of the equations

$$\mathcal{A}\left(u, L(u)\right) = f\left(x,t;b\right) \quad \text{on } \Omega, \tag{2.1}$$

with geometric and natural boundary conditions

$$\mathcal{B}\left(u, L(u)\right) = g\left(x,t;b\right) \quad \text{on } \Gamma, \tag{2.2}$$

where $u = u(x,t;b)$ is dependent on design variable b implicitly, L is a linear differential operator, such as $\left\{\frac{\partial}{\partial t}, \frac{\partial}{\partial x}, \frac{\partial}{\partial y}, \frac{\partial^2}{\partial x^2}, \frac{\partial^2}{\partial y^2} \ldots\right\}$, that appears in the governing differential equations or boundary conditions, $\mathcal{A}$ and $\mathcal{B}$ are vectors of algebraic functions of u and $L(u)$, and $\mathcal{B}\left(u, L(u)\right)$ can be a simple function of u, such as a prescribed boundary condition $u = \bar{u}$ for Dirichlet boundary conditions, or involve a differential operator for von Neumann boundary conditions.

Discrete sensitivity analysis methods discretize the original governing equations (2.1) and obtain a system of discrete equations first. For example, in the static case

$$\mathbf{K}\mathbf{u} = \mathbf{f}. \tag{2.3}$$

Then, the sensitivity with respect to the design parameters, $\frac{D\mathbf{u}}{Db}$, can be calculated by using the finite difference method or discrete analytical methods.

The total derivative of solution vector $\mathbf{u}$ with respect to design parameter b is $\frac{D\mathbf{u}}{Db}$. The finite difference method can be used for approximating $\frac{D\mathbf{u}}{Db}$. For example, the forward difference approximation is

$$\frac{D\mathbf{u}}{Db} \simeq \frac{\mathbf{u}(b + \Delta b) - \mathbf{u}(b)}{\Delta b}. \tag{2.4}$$

A drawback of the finite difference method is the challenge of determining the optimum step size. Large step sizes are dominated by truncation error and small step sizes are dominated by numerical round-off error. Furthermore, it involves solving the original analysis problem $n+1$ times for n design variables, which makes finite difference method inefficient, especially for nonlinear problems.

Discrete analytical methods require the derivatives of the stiffness matrix and load vectors with respect to the design variables. The direct method differentiates Eq. (2.3) and solves for

$$\frac{D\mathbf{u}}{Db} = \mathbf{K}^{-1}\left(\frac{D\mathbf{f}}{Db} - \frac{D\mathbf{K}}{Db}\mathbf{u}\right), \tag{2.5}$$

where $\mathbf{K}$ is the stiffness matrix of the discretized equation of Eq. (2.1). If the design parameter is a shape parameter, the mesh sensitivity in the whole domain should be calculated for $\frac{D\mathbf{K}}{Db}$, which is computationally inefficient.

The CSE method avoids these shortcomings by directly differentiating the governing equa-

tion. Taking the partial derivative of the governing equations (2.1), the CSEs can be obtained in terms of local sensitivity variable $u' = \frac{\partial u}{\partial b}$ as

$$\frac{\partial \mathcal{A}}{\partial u} u' + \frac{\partial \mathcal{A}}{\partial L} L(u') = \frac{\partial f(x,t;b)}{\partial b}. \tag{2.6}$$

Henceforth, the prime notation will be used to indicate a local sensitivity variable as unknown to be solved for. The dot notation is reserved for a total sensitivity variable, such as $\dot{u} = \frac{Du}{Db}$. Spatial and temporal derivatives will be abbreviated in sections applying CSE method to particular examples using indices with a comma, such as $\frac{\partial(\cdot)}{\partial x} = (\cdot)_{,x}$. The boundary conditions for (2.6) may be derived by taking material derivative of the boundary condition (2.2) and writing the material derivatives in terms of local derivatives and convective terms as

$$\frac{Du}{Db} = \frac{\partial u}{\partial b} + V(x) \cdot \nabla u, \tag{2.7}$$

or $\dot{u} = u' + V(x) \cdot \nabla u$, where ∇u is the gradient of u with respect to the spatial coordinates, $V(x) = \frac{\partial x_b}{\partial b}$ is the geometric sensitivity or design velocity, which is dependent on the parameterization of the computational domain. Equation (2.7) requires that the domain changes linearly with respect to the design parameter b as described by the following domain mapping

$$x_b(x,b) = x + bV(x), \tag{2.8}$$

where x_b is the perturbed coordinates. After taking material derivatives of (2.2) and moving the convective terms to the right hand side, the CSE boundary conditions are given as

$$\frac{\partial \mathcal{B}}{\partial u} u' + \frac{\partial \mathcal{B}}{\partial L} L(u') = \dot{g}\left(x,t;b\right) - V(x) \cdot \left(\frac{\partial \mathcal{B}}{\partial u} \nabla u + \frac{\partial \mathcal{B}}{\partial L} L\left(\nabla u\right) \right), \tag{2.9}$$

where $\dot{g}\left(x,t;b\right)$ is the material derivative of the boundary condition. The commutation of

derivatives on the left side of Eq. (2.9) is possible when the derivatives are local. The CSE (2.6) with the boundary conditions in Eq. (2.9) is a well posed linear system of equations in terms of sensitivity variable u', which can be solved by the same numerical method used for solving the analysis problem. The solution u can be obtained from the analysis solution of Eq. (2.1) for use in Eq. (2.6) and Eq. (2.9). The CSE in local form only requires the design velocity, $V(x)$, at the boundaries. The boundary velocity method is more efficient when only sensitivities at boundaries are of interest, since it avoids calculating design velocity inside the whole domain. As seen from the last term of (2.9), the derivative of the analysis solution required by the CSE boundary condition is one order higher than the derivatives in the original boundary condition for analysis. The gradient of solution is evaluated by postprocessing the finite element solution on the boundary. It is well known that results of finite element analysis on the boundary may not be satisfactory (Babuska and Aziz, 1972). For accurate sensitivity boundary conditions, additional effort may be required for calculating derivatives of the analysis solution on the design dependent boundary, such as by increasing the order of elements, or by adapting the mesh to obtain finer mesh at boundaries, or using spatial gradient reconstruction (Cross and Canfield, 2012a,b).

For shape sensitivity, the solution of CSE equations, $\frac{\partial u}{\partial b}$, is local sensitivity. The total derivative of u with respect to design parameter b at a material point consists of the local derivative and the convective term. The latter accounts for how u changes as the material point moves in response to design variable changes. The accuracy of Eulerian sensitivities depends on how accurately the derivatives of solution in the sensitivity boundary conditions are evaluated. If the sensitivity boundary conditions are accurate enough to obtain the local (Eulerian) sensitivity and to compute the convective sensitivity term, then the local sensitivities can be transformed to the total derivatives by adding the convective terms as in equation (2.7).

The CSE method is especially efficient for nonlinear problems, since the CSE is always linear. If Newton-Raphson's method is used for solving the nonlinear analysis problem associated with a Galerkin finite element method, the tangent stiffness matrix gives the required matrix to solve the linear CSE system. Although Wickert (2009) states that it is not generally true for other weighted-residual forms such as Least Squares finite element methods, it is true for Galerkin finite element method. The weighted residual form of the analysis equation is denoted as

$$\iint v\mathcal{A}\left(u, L(u)\right) u\Omega = \iint v f d\Omega, \tag{2.10}$$

where v is the test function. The weighted residual form of the CSE system is

$$\iint v\left[\frac{\partial \mathcal{A}}{\partial u}u' + \frac{\partial \mathcal{A}}{\partial L}L(u')\right] d\Omega = \iint v\frac{\partial f}{\partial b}d\Omega. \tag{2.11}$$

The weighted residual form of the analysis problem and CSE system may be discretized using the same shape functions,

$$u \approxeq \sum_j u_j\phi_j, \tag{2.12}$$

and

$$u' \approxeq \sum_j u'_j\phi_j. \tag{2.13}$$

Substituting Eq. (2.12) into Eq. (2.10) and taking shape function ϕ_i as the test function v, the discrete equations for analysis problem is obtained as

$$\iint \phi_i\mathcal{A}\left(\sum_j u_j\phi_j, L\left(\sum_j u_j\phi_j\right)\right) d\Omega = \iint \phi_i f d\Omega. \tag{2.14}$$

The tangent stiffness matrix for Newton-Raphson's method is obtained by taking partial

derivatives of Eq. (2.14) with respect to u_j as (Reddy, 2006)

$$T_{ij} = \iint \left[\frac{\partial \mathcal{A}}{\partial u} \phi_i \phi_j + \frac{\partial \mathcal{A}}{\partial L} \phi_i L(\phi_j) \right] d\Omega. \tag{2.15}$$

The discrete CSE is derived by substituting Eq. (2.13) into Eq. (2.11),

$$\sum_{j=1}^{n} \iint \left[\frac{\partial \mathcal{A}}{\partial u} \phi_i \phi_j + \frac{\partial \mathcal{A}}{\partial L} \phi_i L(\phi_j) \right] d\Omega \; u'_j = \iint \phi_i \frac{\partial f}{\partial b} d\Omega; i = 1, 2, \ldots, n. \tag{2.16}$$

Each term in the first integral in Eq. (2.16) is an element of the coefficient matrix for the CSE system, which corresponds exactly to an element of the tangent stiffness matrix in Eq. (2.15).

To summarize, the CSE system is derived by taking the derivatives of the original field equations (2.1) and boundary conditions (2.2). It is a linear boundary value problem even for nonlinear problems. If Newton-Raphson's method is used for solving the nonlinear analysis problem associated with a Galerkin finite element method, the tangent stiffness matrix can be used as the required coefficient matrix for solving the discretized linear CSE system. The boundary velocity method only needs design velocity on the boundary. It poses the CSE in local derivative form and parameterizes the boundary, which avoids the complexity and numerical expense of calculating the mesh Jacobian inside the whole domain. The local derivative formulation of CSE method is generally applicable and efficient for flow problems, provided that spatial derivatives of the solution are recovered accurately, but care must be taken in its implementation for structures with strain discontinuity, such as built-up structures discussed in the following section.

2.3 CSE boundary conditions for built-up structures

For built-up structures, the solution of the FSI problem lies in the space of C^0 continuous functions. At the joints, displacement of the structure is continuous, but the first derivative of the displacements may not be continuous. For local shape sensitivities, solution of the CSE lies in the space of piecewise C^0 continuous functions, although the material derivatives are C^0 continuous in the whole domain. A remedy is to divide the domain into subdomains over which the solution is C^o continuous. For built-up structures like the joined beam structure in Figure 2.1 used in subsequent examples in Section 2.4, the domain is divided into subdomains, which are connected together at the joint.

The design velocity $V(x)$ in (2.8) that defines the rate of the domain change with respect to design parameter can be parameterized linearly or nonlinearly with respect to the spatial coordinates. The design velocity fields used for the results in this paper are parameterized linearly as

$$V(x) = \frac{x}{L}\delta L, \tag{2.17}$$

where δL is the tip perturbation of the beam and x is the axial coordinates of the beam. The design velocity is required only on the boundaries of the domain, Eq. (2.45).

Figure 2.2 shows the three interconnected subdomains at the joint of joined beam structure. The displacements at the joint are assumed to be continuous. The continuous boundary condition at the joint is

$$u_I(x_j) = u_{II}(x_j) \quad \text{and} \quad u_I(x_j) = T^T \bar{u}_{III}(\bar{x}_j), \tag{2.18}$$

where $u(x)$ is the vector of displacements expressed in global coordinates, the subscript represents the subdomain index and T is the rotation matrix that transforms the displacements

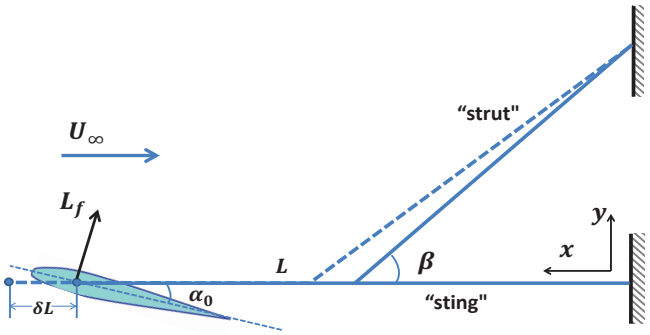

Figure 2.1: Joined beam with an airfoil model and the structural perturbation.

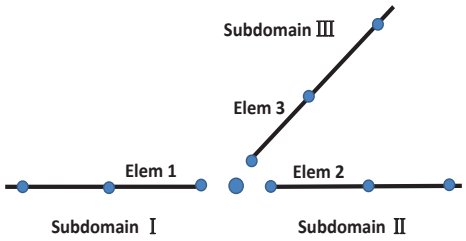

Figure 2.2: Subdomains and elements at joint for joined beam structure.

in local coordinates to global coordinates. T is a function of the angle between sting and strut, β. And x_j is the spatial coordinates at the joint. Taking the material derivative of the first equation of (2.18) with respect to the design variable b and writing the material derivatives in terms of local derivatives and convective terms using Eq. (2.7), the CSE boundary condition at the domain interface is obtained as

$$u'_I(x_j) = u'_{II}(x_j) + f_{12}, \tag{2.19}$$

and

$$u'_I(x_j) = T^T \bar{u}'_{III}(x_j) + f_{13}, \tag{2.20}$$

where

$$f_{12} = \left(\frac{\partial u_{II}(x_j)}{\partial x} - \frac{\partial u_I(x_j)}{\partial x} \right) V_j, \tag{2.21}$$

and

$$f_{13} = \left(T^T \frac{\partial \bar{u}_{III}(\bar{x}_j)}{\partial \bar{x}} \bar{V}_j - \frac{\partial u_I(x_j)}{\partial x} V_j \right) + \dot{T}^T \bar{u}_{III}(\bar{x}_j), \tag{2.22}$$

and V_j is the design velocity at the joint node, the variables with a bar indicate that they are in local axial coordinates of the strut, T is the rotation matrix for transforming the displacements and forces in local coordinates to the global. From Eq. (2.19) and Eq. (2.21), if $\frac{\partial u_{II}(x_j)}{\partial x} \neq \frac{\partial u_I(x_j)}{\partial x}$, the local sensitivity variables are not continuous. As a result, when a displacement-based finite element method is used for solving the CSE system, the associated element stiffness matrix at the joint cannot be assembled directly without special treatment.

Similarly, if no external forces are applied on the joint node, the summation of internal force at the joint node should be zero, which is

$$F_I(x_j) + F_{II}(x_j) + T^T \bar{F}_{III}(\bar{x}_j) = 0, \tag{2.23}$$

where $F_i(x_j)$ is the internal force vector expressed in global coordinates for the i^{th} subdomain at $x = x_j$, $\bar{F}_{III}(\bar{x}_j)$ is the internal force vector of strut in local coordinates at the joint. For local sensitivity variables, if the spatial derivatives of the internal forces do not cancel, the summation of the force sensitivity components are not equal to zero. Rather, by taking the

material derivative of Eq. (2.23) and rearranging terms

$$\begin{aligned}\frac{\partial F_I(x_j)}{\partial b}+\frac{\partial F_{II}(x_j)}{\partial b}+T^T\frac{\partial \bar{F}_{III}(\bar{x}_j)}{\partial b} &= -T^T\frac{\partial \bar{F}_{III}(\bar{x}_j)}{\partial \bar{x}}\bar{V}_j-\dot{T}^T\bar{F}_{III}(\bar{x}_j)\\ &- \left(\frac{\partial F_I(x_j)}{\partial x}+\frac{\partial F_{II}(x_j)}{\partial x}\right)V_j. \qquad (2.24)\end{aligned}$$

For every joint node, spatial derivatives of internal force would have to be obtained from the analysis solution in conjunction with the design velocity at the joint. A fictitious force boundary condition, Eq. (2.24), should be applied to the CSE system at the subdomain interface.

Local sensitivities are not continuous at the locations where the strains are discontinuous. The finite element stiffness matrix for solving local CSE equations cannot be assembled directly based on the continuity of the dependent variables. The sum of derivatives of the internal forces does not vanish at the joint even for the case without external forces. The implementation differs from the FEM for analysis, since at any strain discontinuity special treatment is needed, which makes the implementation more involved.

In this paper, a special treatment to deal with the CSE boundary conditions at the joint, Eqs. (2.19),(2.20) and (2.24), was implemented. Assume nodal degree of freedom for the FEM discretization at the joint

$$u_{1j} = u_I(x_j), \qquad (2.25)$$

$$u_{2j} = u_{II}(x_j), \qquad (2.26)$$

$$u_{3j} = u_{III}(x_j), \qquad (2.27)$$

where u_{ij} denotes the nodal displacements at i^{th} element at joint node j. The local sensitivities of one of the elements at the joint node can be chosen as the global unknown

sensitivity variables to be determined at the joint node. The local sensitivities in the other elements can be written in terms of the global sensitivities. For instance, if local sensitivities of the first element u'_{1j} were used as the global sensitivities, then from Eq. (2.19), elemental displacements of the second element at the joint can be written as

$$u'_{2j} = u'_{1j} - f_{12}. \tag{2.28}$$

Accordingly, the discrete equation for the second element can be written as

$$[K_j \;\; K_o] \begin{pmatrix} u'_{2j} \\ u'_o \end{pmatrix} = [K_j \;\; K_o] \begin{pmatrix} u'_{1j} - f_{12} \\ u'_o \end{pmatrix} = \frac{\partial F_2(x_j)}{\partial b}. \tag{2.29}$$

where $[K_j \;\; K_o]$ is the partitioned CSE elemental coefficient matrix with K_j associated with the nodal degree of freedoms, u'_{2j}, and u'_o is the elemental displacement sensitivity values at other degree of freedoms of element 2. The discrete equation (2.29) for element 2 in terms of global degree freedom u'_{12} for the left nodal values can be written as

$$[K_j \;\; K_o] \begin{pmatrix} u'_{1j} \\ u'_o \end{pmatrix} = K_j f_{12} + \frac{\partial F_2(x_j)}{\partial b}. \tag{2.30}$$

The elemental coefficient matrix does not change, but a pseudo force term $K_j f_{12}$ should be added accordingly to the right hand side of the elemental force vector. Likewise, the equilibrium equation for the third element may be partitioned so that the chosen global sensitivity variables may be assembled into the sensitivity coefficient matrix. Hence, the assembled tangent stiffness matrix can still be used as the assembled coefficient matrix of CSE. The right hand side terms in Eq. (2.24) should also be applied as external force term at joint node to account for the force discontinuity.

2.4 Applications

2.4.1 Nonlinear Timoshenko beam with an airfoil

In this subsection, the nonlinear Timoshenko beam with an airfoil model, which is the joined beam shown in Fig. 2.1 without the strut, was investigated. This is a determinate structure without strain discontinuity in the structural domain. The sting is modeled as nonlinear Timoshenko beams capable of large deflections as described in subsection 2.4.1. At a positive angle of attack, the airfoil generates lift, deflecting the beam in the fluid, resulting in an increased angle of attack. Equilibrium deflection of the sting occurs when the force and moments generated by the lifting airfoil balance the internal sting force and moments resisting the bending. The airfoil is assumed to be rigid without considering the aeroelastic effects due to the flexibility of the airfoil (Berci et al., 2013). For shape sensitivity analysis, the sting length L is taken as a shape design parameter.

Finite element model for structure domain

Nonlinear Timoshenko beam theory accounts for moderately large rotations and nonlinear strains (Reddy, 2006). The displacement field can be given as

$$u_1 = u_x(x) - y\psi; \quad u_2 = u_y(x); \quad u_3 = 0,$$

where ψ is the rotation of the cross section. Using the nonlinear strain-displacement relations

$$\epsilon_{ij} = \frac{1}{2}(u_{i,j} + u_{j,i}) + \frac{1}{2}(u_{m,i}u_{m,j}),$$

and retaining only the square of rotation of a transverse normal line in the beam as the only nonlinear strain term, we obtain

$$\epsilon_{xx} = \left[\frac{\partial u_x}{\partial x} + \frac{1}{2}\left(\frac{\partial u_y}{\partial x}\right)^2\right] - y\frac{\partial \psi}{\partial x}; \quad \gamma_{xy} = \frac{\partial u_y}{\partial x} - \psi,$$

where u_y is the vertical deflection, u_x is the axial displacement, ψ is the cross section rotation angle. By using extended Hamilton's principle and assuming linear elastic material behavior, the governing equations for the nonlinear Timoshenko beam with the rotational inertia can be derived, which gives a specific example of (2.1). The left hand side of (2.1) is given as

$$\mathcal{A}\left(u, L(u)\right) = \begin{pmatrix} \rho A u_{x,tt} - \left[EA(u_{x,x} + \frac{1}{2}u_{y,x}^2)\right]_{,x} \\ \rho A u_{y,tt} - \left[EAu_{y,x}(u_{x,x} + \frac{1}{2}u_{y,x}^2)\right]_{,x} - \left[kGA(u_{y,x} - \psi)\right]_{,x} \\ \rho I \psi_{,tt} - \left(EI\psi_{,x}\right)_{,x} - kGA(u_{y,x} - \psi) \end{pmatrix}, \tag{2.31}$$

and the right hand force vector is given as

$$f\left(x, t; b\right) = \begin{pmatrix} f_1(x, t; b) \\ f_2(x, t; b) \\ 0 \end{pmatrix}, \tag{2.32}$$

where $f_1(x, t; b)$ is the axially distributed load and $f_2(x, t; b)$ is the laterally distributed load. EA, EI and kGA are the flexural rigidity of membrane, bending and shear, respectively. ρ, I and A are the material density, the moment of inertia, and the cross-sectional area, respectively. The list of dependent variables u here includes u_x, u_y and ψ. The linear derivatives of the dependent variables $L(u)$ includes $u_{x,tt}, u_{y,tt}, \psi_{,tt}, u_{x,xx}, u_{y,x}, u_{y,xx}, \psi_{,x}$ and $\psi_{,xx}$. Multiplying each row of the governing equations (2.1) by a test function, the weighted

residual form of each row can be obtained as

$$\int_{x_a}^{x_b} v_i \mathcal{A}_i dx = \int_{x_a}^{x_b} v_i f_i \; dx; \quad i = 1, 2, 3. \tag{2.33}$$

Integrating (2.33) by parts, and substituting equations (2.31) and (2.32) for this example, the weak form of the nonlinear Timoshenko beam model is obtained as

$$\int_{x_a}^{x_b} \rho A u_{x,tt} v_1 dx + \int_{x_a}^{x_b} EA(u_{x,x} + \frac{1}{2}u_{y,x}^2) v_{1,x} dx = \int_{x_a}^{x_b} v_1 f_1 dx + N_{xx} v_1|_{x_a}^{x_b}, \tag{2.34}$$

$$\int_{x_a}^{x_b} \rho A u_{y,tt} v_2 dx + \int_{x_a}^{x_b} EA u_{y,x}(u_{x,x} + \frac{1}{2}u_{y,x}^2) v_{2,x} dx + \int_{x_a}^{x_b} kGA(u_{y,x} - \psi) v_{2,x} dx$$
$$= \int_{x_a}^{x_b} v_2 f_2 dx + V_f v_2|_{x_a}^{x_b}, \tag{2.35}$$

$$\int_{x_a}^{x_b} \rho I \psi_{,tt} v_3 dx + \int_{x_a}^{x_b} EI \psi_{,x} v_{3,x} dx - \int_{x_a}^{x_b} kGA(u_{y,x} - \psi) v_3 dx = M_{xx} v_3|_{x_a}^{x_b}, \tag{2.36}$$

where v_1, v_2 and v_3 are test functions. A set of natural boundary conditions of (2.2) is given as

$$\begin{pmatrix} EA(u_{x,x} + \frac{1}{2}u_{y,x}^2) \\ EI\psi_{,x} \\ EAu_{y,x}(u_{x,x} + \frac{1}{2}u_{y,x}^2) + kGA(u_{y,x} - \psi) \end{pmatrix} = \begin{pmatrix} N_{xx} \\ M_{xx} \\ V_f \end{pmatrix}, \tag{2.37}$$

where N_{xx} is the axial force, M_{xx} is the moment, V_f is the vertical force. Equation (2.37) is a specific example of the general boundary condition (2.2). $\mathcal{B}(u, L(u))$ here is the left side of (2.37) and $g(x, t; b)$ is the right side of (2.37).

CSE for structure domain

The CSE in local derivative form can be derived by taking partial derivative of the governing equations with respect to the design variable b directly as in (2.6). The CSE is a specific

example of (2.6) with

$$\frac{\partial \mathcal{A}}{\partial u} = \begin{pmatrix} 0 & 0 & 0 \\ 0 & 0 & 0 \\ 0 & 0 & kGA \end{pmatrix}, \tag{2.38}$$

and

$$\frac{\partial \mathcal{A}}{\partial L} = \begin{pmatrix} \rho A & 0 & 0 & 0 & -EAu_{y,xx} & 0 & -EA & -EAu_{y,x} & 0 \\ \rho A & 0 & 0 & -EAu_{y,xx} & \mathcal{A}^l_{25} & kGA & -EAu_{y,x} & \mathcal{A}^l_{28} & 0 \\ \rho I & 0 & 0 & 0 & -kGA & 0 & 0 & 0 & -EI \end{pmatrix}, \tag{2.39}$$

where

$$\mathcal{A}^l_{25} = -EA(u_{x,xx} + 3u_{y,x}u_{y,xx}), \tag{2.40}$$

and

$$\mathcal{A}^l_{28} = -EA(u_{,x} + \frac{3}{2}u^2_{y,x}) - kGA. \tag{2.41}$$

The sensitivity variable vector $u' = [u'_x, u'_y, \psi']^T$ and the linear derivatives of the sensitivity variables in (2.6) is given as

$$L(u') = [u'_{x,tt}, u'_{y,tt}, \psi'_{,tt}, u'_{x,x}, u'_{y,x}, \psi'_{,x}, u'_{x,xx}, u'_{y,xx}, \psi'_{,xx}]^T. \tag{2.42}$$

The partial derivatives of the force terms in the right hand side of (2.6) is

$$\frac{\partial f(x,t;b)}{\partial b} = \begin{pmatrix} f_{1,b} \\ f_{2,b} \\ 0 \end{pmatrix} = \begin{pmatrix} 0 \\ 0 \\ 0 \end{pmatrix}. \tag{2.43}$$

The sensitivity boundary conditions at the root for the cantilevered beam case in Fig. 2.1 are found by differentiating the homogeneous boundary condition for the analysis problem.

$$\begin{pmatrix} u'_x \\ u'_y \\ \psi' \end{pmatrix} = \mathbf{0}. \tag{2.44}$$

The sensitivity boundary conditions at the tip of the beam are found by taking the material derivative of (2.37) and solving for the local derivatives

$$\begin{pmatrix} N'_{xx} \\ M'_{xx} \\ V'_f \end{pmatrix} = \begin{pmatrix} \dot{N}_{xx} \\ \dot{M}_{xx} \\ \dot{V}_f \end{pmatrix} - \begin{pmatrix} EA\left[u_{x,xx} + u_{y,x}u_{y,xx}\right]V(x)|_{x=L} \\ EI\psi_{,xx}V(x)|_{x=L} \\ \left[N_{xx,x}u_{y,x} + N_{xx}u_{y,xx} - Q_{x,x}\right]V(x)|_{x=L} \end{pmatrix}, \tag{2.45}$$

where in Eq. (2.45)

$$N_{xx,x} = EA\left[u_{x,xx} + u_{y,x}u_{y,xx}\right], \tag{2.46}$$

$$Q_{x,x} = -kGA(u_{y,xx} - \psi_{,x}), \tag{2.47}$$

and the material derivatives of the external forces are given by equations (2.63)-(2.65) in Section 2.4.1. Then a set of new equations of (2.6) formed by terms in Eqs. (2.38)-(2.43), with boundary conditions (2.44) and (2.45), in terms of the local sensitivity variables can be solved for the local sensitivities. If needed, total sensitivities can be obtained by the conversion, Eq. (2.7), given in Section 2.2.

Finite element model for fluid domain

For verifying the method and codes in two dimensions, we consider linear potential flow around an airfoil, which is sufficient for demonstrating the application of the CSE method to two dimensional flow problems. The finite element model and CSE method are developed for inviscid, incompressible flow around an airfoil. In an irrotational flow, the governing equation for the stream function Ψ is

$$\nabla^2 \Psi = 0. \tag{2.48}$$

The x and y-component velocity, v_x and v_y, can be found from the streamfunction, Ψ, in two dimensional flows,

$$v_x = \frac{\partial \Psi}{\partial y}, \qquad v_y = -\frac{\partial \Psi}{\partial x}. \tag{2.49}$$

The essential boundary condition on the far field boundaries of the domain is given as

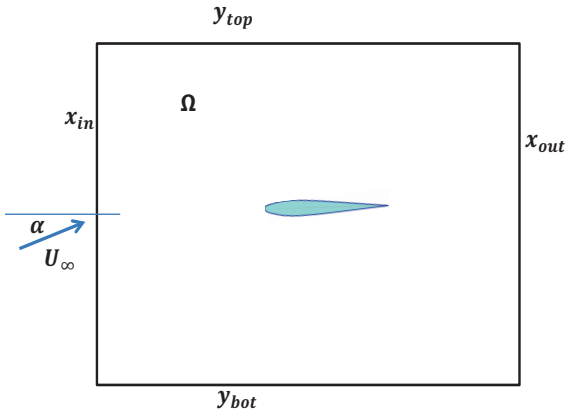

Figure 2.3: Potential flow around an airfoil model.

$$\Psi = U_\infty y \cos(\alpha) - U_\infty x \sin(\alpha). \tag{2.50}$$

The boundary condition on the airfoil is the no-penetration condition. If the airfoil boundary is a streamline, then the velocity is always tangential to the airfoil. Thus, the no-penetration condition becomes an essential boundary condition on the airfoil,

$$\Psi|_{\Gamma_a} = \Psi_a, \tag{2.51}$$

where Ψ_a is a constant along the airfoil, but it is not known prior to the simulation. For implementation of the essential boundary condition on the airfoil, Eq. (2.51), the nodal values of the streamfunction on the airfoil are all given by the single unknown Ψ_a. The Kutta condition was used as a constraint. It requires the flow to leave the trailing edge smoothly. To enforce this condition, we require that flow at the trailing edge be aligned along the bisector of the trailing edge. The geometry of the trailing edge is shown in Fig. 2.4. For the flow to be aligned to n_{te}, the velocity normal to the bisector n_{te} should be zero. Thus, at the trailing edge, the Kutta condition becomes

$$\nabla\Psi \cdot \vec{n}_{te} = 0. \tag{2.52}$$

The finite element method is used for solving the analysis problem. The weak form of Eq. (2.48) is

$$\iint_\Omega \nabla v \cdot \nabla\Psi dA = \oint_\Gamma v q_n ds, \tag{2.53}$$

where v is the test function, Ω is the fluid domain, Γ is the boundary of the domain and $q_n = \frac{\partial\Psi}{\partial x}n_x + \frac{\partial\Psi}{\partial y}n_y$ is the flux through the boundaries. Within the finite element discretization, the Kutta condition is implemented in a weighted residual form known as the collocation method, specifically,

$$\iint_\Omega v_{te} \nabla\Psi \cdot \vec{n}_{te} dA = 0, \tag{2.54}$$

where v_{te} is the shape function evaluated at the trailing edge node.

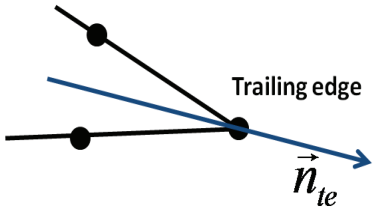

Figure 2.4: Trailing edge geometry.

CSE for fluid domain

The CSE method was used for evaluating the steady pressure coefficient sensitivity to the inflow angle of attack. We keep the mesh fixed and change the inflow angle to obtain different angles of attack determined by tip rotation of the sting and the initial angle, $\alpha = \alpha_0 + \psi_{\text{tip}}$. The angle of attack α is a value parameter, since a change in α does not change the shape of airfoil. In other words, the design velocity is zero. Hence, from equation (2.7), taking the material derivative of the boundary conditions reduces to simply taking the local derivative. Taking partial derivatives of the governing equation (2.48), the boundary conditions (2.50)-(2.51), and the Kutta condition (2.52), we have the CSE for fluid in terms of local sensitivity variable Ψ',

$$\nabla^2 \Psi' = 0, \tag{2.55}$$

and the CSE boundary condition from Kutta condition,

$$\nabla \Psi' \cdot \vec{n}_{te} = 0. \tag{2.56}$$

The other boundary conditions for the CSE system are

$$\Psi'|_{\Gamma_a} = \Psi'_a \qquad \text{on airfoil,}$$

and

$$\Psi' = -U_\infty y \sin\alpha - U_\infty x \cos\alpha \quad \text{on the far field boundaries.}$$

Comparing with the analysis equations, the CSE has the same form. The CSE can be solved by using the same solver as for the original analysis problem, except for the change of boundary conditions. The velocity sensitivity can be evaluated by differentiating Eq. (2.49) with respect to the coordinates and commuting the order of differentiation.

$$v'_x = \frac{\partial \Psi'}{\partial y}, \qquad v'_y = -\frac{\partial \Psi'}{\partial x}.$$

The pressure coefficient in an inviscid, incompressible flow can be found using Bernoulli's equation,

$$C_p = \frac{p - p_\infty}{\frac{1}{2}\rho_a U_\infty^2} = 1 - \left(\frac{\bar{v}}{U_\infty}\right)^2 \tag{2.57}$$

where $\bar{v} = \sqrt{v_x^2 + v_y^2}$ is the local flow speed. The partial derivative of C_p with respect the design variable α can be obtained

$$\frac{\partial C_p}{\partial \alpha} = -\frac{2(v_x v'_x + v_y v'_y)}{U_\infty^2}, \tag{2.58}$$

The lift force sensitivity with respect to the angle of attack is given as

$$\frac{\partial L_f}{\partial \alpha} = \oint_{\Gamma_a} \frac{1}{2}\rho_a c U_\infty^2 \frac{\partial C_p}{\partial \alpha}\, ds. \tag{2.59}$$

Fluid structure interaction boundary conditions

In the joined beam with an airfoil model, the airfoil is mounted on the tip of the sting at the aerodynamic center. The aerodynamic force, L_f, serves as a follower force on the tip of the sting. The axial force N_{xx}, the moment M_{xx} and the shear force V_f at the beam tip are given as

$$N_{xx} = -L_f \sin(\alpha_0 + \psi_{\text{tip}}), \tag{2.60}$$

$$M_{xx} = 0, \tag{2.61}$$

$$V_f = L_f \cos(\alpha_0 + \psi_{\text{tip}}), \tag{2.62}$$

where α_0 is the initial angle of attack, ψ_{tip} is the rotation angle of the beam tip. As seen in Eq. (2.45), the CSE boundary condition requires the total derivative of the external forces. If the external forces are constants or independent of the design variables, then the total derivatives are zero. If the external forces depend on the design parameters implicitly, then the natural sensitivity boundary conditions should be given in terms of the local sensitivity variables. Hence, the total derivatives of axial force $\dot{N}_{xx}$, and the shear force $\dot{V}_f$ in Eq. (2.45) required by the CSE boundary conditions can be obtained using the chain rule as

$$\dot{N}_{xx} = A_1 \psi'_{\text{tip}} + B_1 w'_{,t} + C_1, \tag{2.63}$$

$$\dot{M}_{xx} = 0, \tag{2.64}$$

$$\dot{V}_f = A_2 \psi'_{\text{tip}} + B_2 w'_{,t} + C_2, \tag{2.65}$$

where

$$A_1 = \left(-\frac{\partial L_f}{\partial \alpha}\sin(\alpha_0+\psi_{\text{tip}}) - L_f\cos(\alpha_0+\psi_{\text{tip}})\right), \tag{2.66}$$

$$A_2 = \left(\frac{\partial L_f}{\partial \alpha}\cos(\alpha_0+\psi_{\text{tip}}) - L_f\sin(\alpha_0+\psi_{\text{tip}})\right), \tag{2.67}$$

$$B_1 = \frac{\partial L_f}{\partial \alpha}\frac{\sin(\theta_{\text{tip}})}{U_\infty}, \tag{2.68}$$

$$B_2 = \frac{\partial L_f}{\partial \alpha}\frac{\cos(\theta_{\text{tip}})}{U_\infty}, \tag{2.69}$$

$$C_1 = \left(-\frac{\partial L_f}{\partial \alpha}\sin(\theta_{\text{tip}})\left(\psi_{\text{tip},x}+\frac{w_{,xt}}{U_\infty}\right) - L_f\cos(\theta_{\text{tip}})\psi_{\text{tip},x}\right)V(x), \tag{2.70}$$

$$C_2 = \left(\frac{\partial L_f}{\partial \alpha}\cos(\theta_{\text{tip}})\left(\psi_{\text{tip},x}-\frac{w_{,xt}}{U_\infty}\right) - L_f\sin(\theta_{\text{tip}})\psi_{\text{tip},x}\right)V(x). \tag{2.71}$$

For steady-state fluid structure interaction, the aerodynamic force can be obtained by solving the steady state potential flow equations given in Section 2.4.1, and the lift force sensitivity with respect to the angle of attack, $\frac{\partial L_f}{\partial \alpha}$, can be calculated by using Eq. (2.59). The sensitivity boundary conditions for the steady state case can be obtained by leaving out all the time dependent terms in Eqs. (2.63)-(2.71).

Numerical results for nonlinear Timoshenko beam with an airfoil

The sensitivities of the static fluid-structure response with respect to the beam length L were calculated by using local derivative form CSE. The design velocity was parameterized linearly using Eq. (2.17) with $\delta L = 1$. The static case of the dynamic equations for structure domain in Section 2.4.1 were used. The fluid force was obtained by solving the linear potential flow around the airfoil as described in Section 2.4.1 and resulting aerodynamic force exerted on the tip of the beam. The static structural problem was implemented by using p-version Galerkin finite element method (Szabo and Babuska, 1991). As seen for the CSE boundary

conditions Eq. (2.45), second derivatives of displacement are required. The derivatives of the analysis solution were obtained by differentiating the shape functions. For accurate results using limited number of elements, at least $p = 3$ is required. Twenty elements with order $p = 3$ were used here. Since the actual order of the solution for this Timoshenko beam with tip load problem is dominated by cubic and lower order terms, further increase of the order of elements for the structure does not significantly increase the accuracy of the sensitivity boundary conditions. The numerical results were obtained for a sting with length $L = 6\ m$, membrane rigidity $EA = 1e8\ N$, shear rigidity $kGA = 1e7\ N$, bending rigidity $EI = 3e6\ N \cdot m^2$, rotary inertia $\rho I = 50\ kg \cdot m$ and mass per unit length $\rho A = 600\ kg/m$.

The finite element solver was implemented for potential flow around an airfoil with inflow velocity $U_\infty = 70\ m/s$ and air density $\rho_a = 1.2kg/m^3$. The chord length of the airfoil is $3\ m$ with a 3 degree initial angle of attack, α_0. The finite element model for the fluid and the CSE for the fluid were discussed in Section 2.4.1 and Section 2.4.1, respectively. Linear triangular elements were used. The number of elements used was 1324 and the number of nodes associated was 726. The finite element mesh is fixed. For different angle of attack cases, the angle between the airfoil cord and the inflow velocity changes, rather than changing the mesh. The numerical results for the fluid analysis are shown in Figure 2.5, which are non-dimensionalized by the inflow velocity U_∞. The angle of attack α is 10 deg. The velocity in x direction in subfigure (a) increases on the upper airfoil surface and decreases on the lower airfoil surface. The velocity in y direction increases rapidly at the upper leading edge. Hence, the pressure coefficient has positive values at the upper leading edge and has negative values at the lower leading edge. As seen in subfigure (d), the pressure coefficient around the airfoil closely matches a vortex panel code solution (Marchman, 1999). As the angle of attack increases, the velocities at the upper airfoil surface increase and the velocities at the lower airfoil surface decrease. Hence, the velocity sensitivities shown in Fig. 2.6 are positive on the

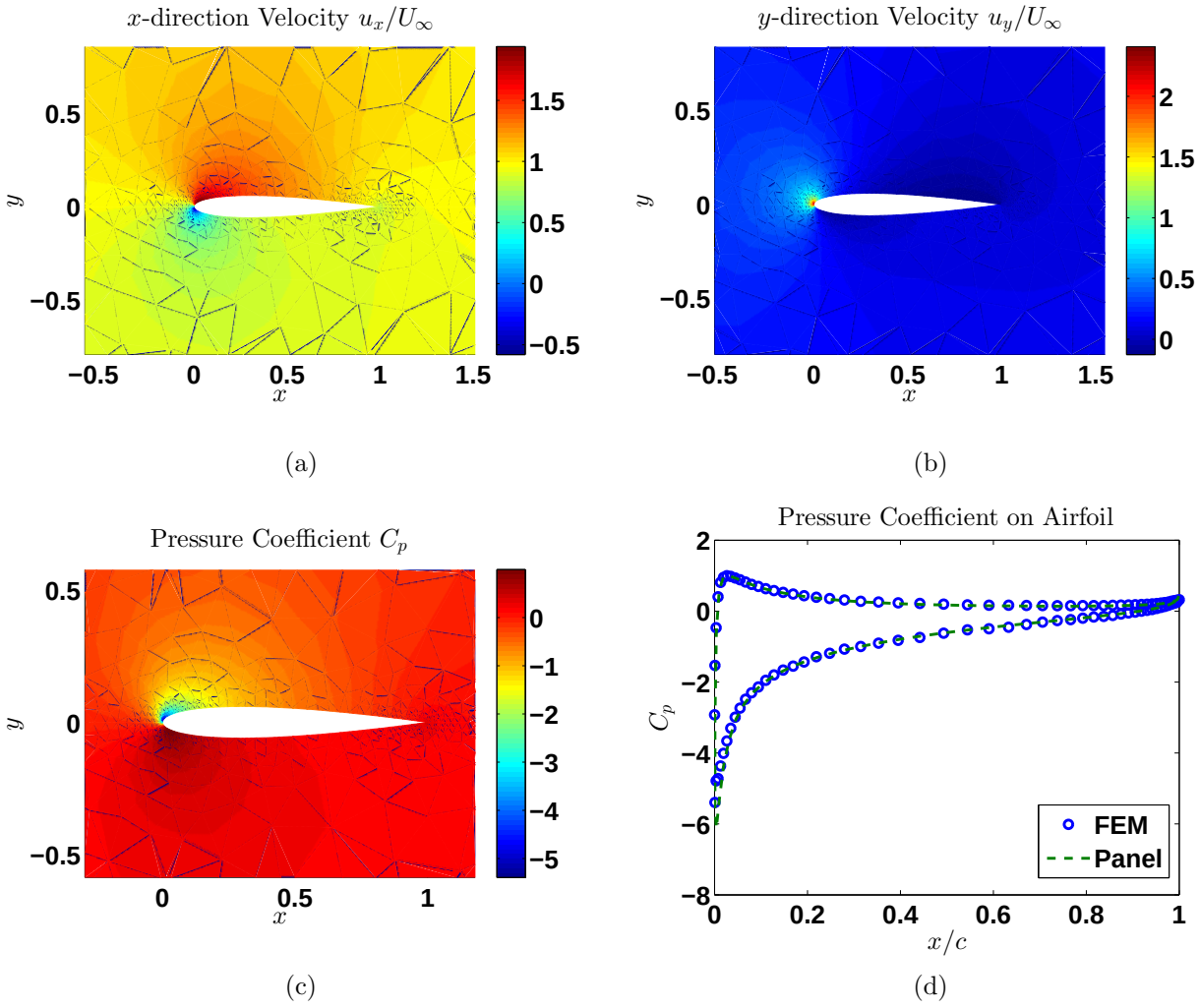

Figure 2.5: Finite element solutions for NACA 0012 airfoil at $\alpha = 10$ deg

upper surface and negative on the lower surface, while the pressure coefficient sensitivity is negative on the upper surface and positive on the lower surface. As seen from subfigure (d), the pressure coefficient sensitivity on the airfoil surface closely matches the finite difference solution. The lift force sensitivity to angle of attack can be obtained by integrating the pressure coefficient sensitivity around the airfoil surface as indicated in Section 2.4.1.

For fluid-structure interaction problems, the material derivative of the forces term in Eq. (2.45) is the fluid lift force sensitivity, which depends on the deformation sensitivity of the struc-

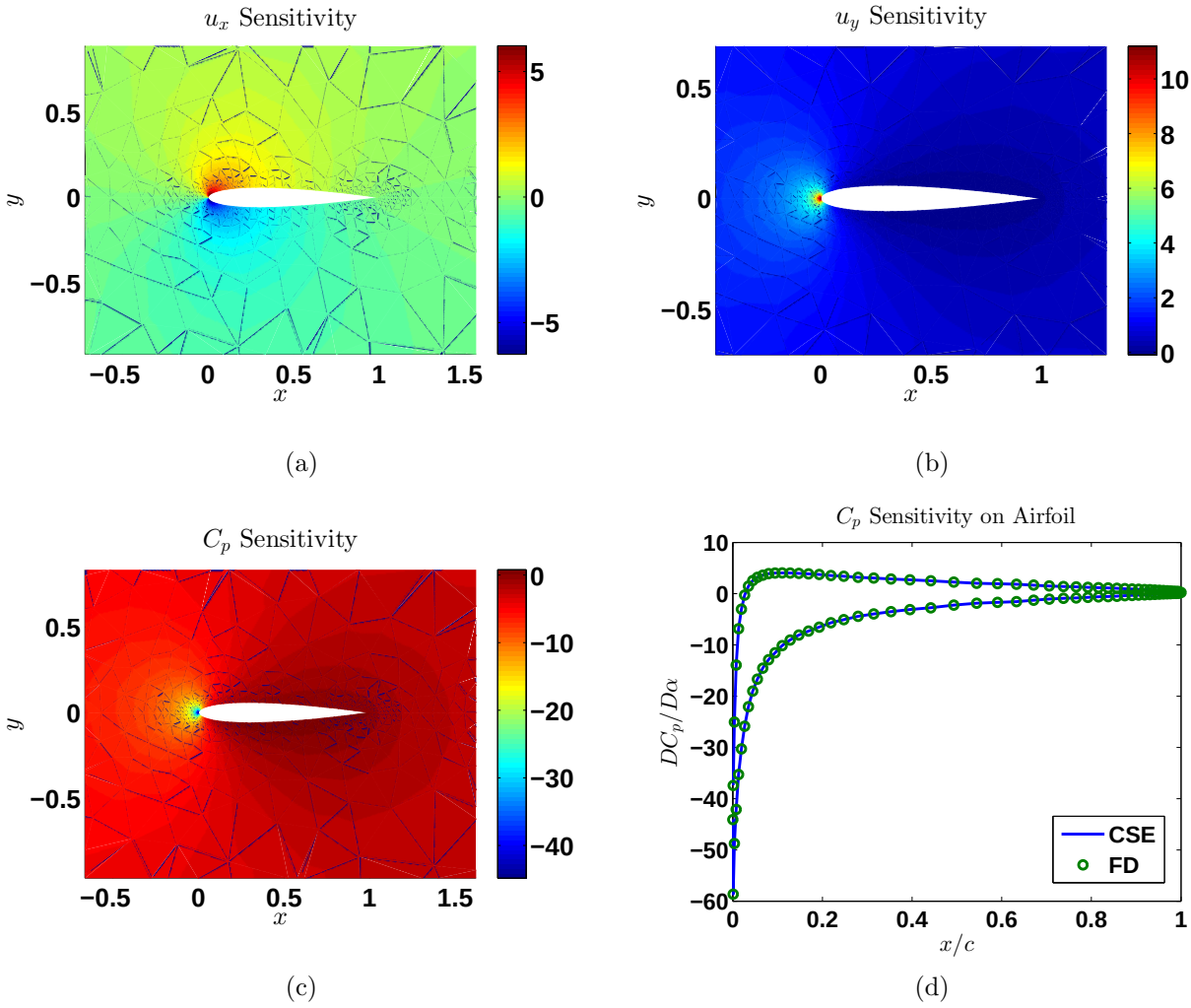

Figure 2.6: Sensitivity of flow velocity and pressure with respect to angle of attack.

ture. Hence, the CSE system can be solved by forming a fully coupled system of equations in a similar way as solving the original fluid-structure problem. However, the CSE system is linear even though the beam is nonlinear. The tangent stiffness matrix for solving the analysis problem was used as the CSE coefficient matrix. The results are shown in Fig. 2.7. As seen from the plots, the CSE total sensitivities closely match with the finite difference solution. The local sensitivity was first calculated by solving the CSE system in local derivative form. The total sensitivity was then obtained by adding the convective term as given in

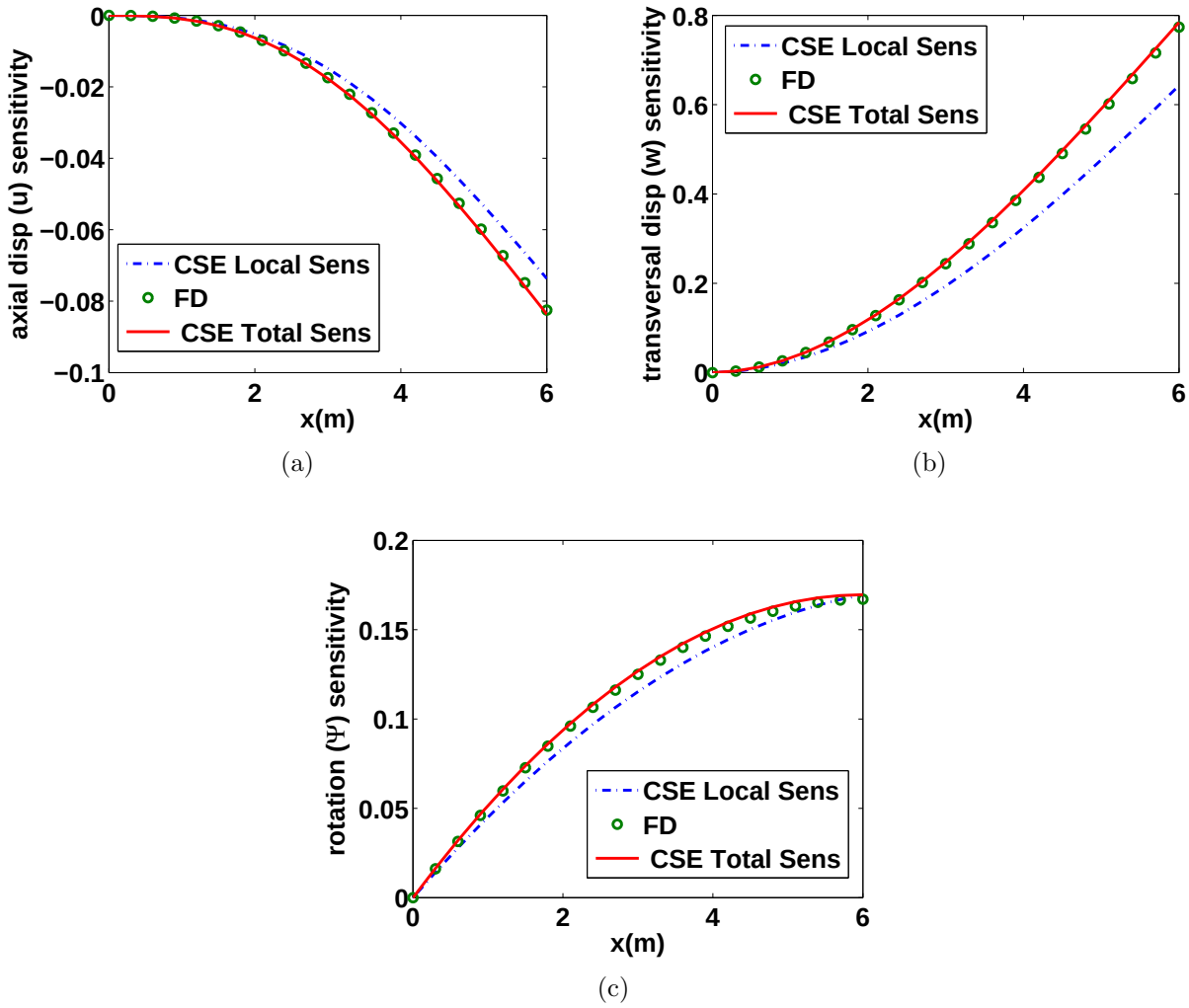

Figure 2.7: Static FSI response sensitivity with respect to beam length.

Eq. (2.7). Note that the local sensitivities are continuous throughout the domain, since the first derivatives of the beam displacements are continuous. The elemental matrix for this CSE system can be assembled based on the continuity of the sensitivity variables without difficulty for this simple determinate structure with continuous strain.

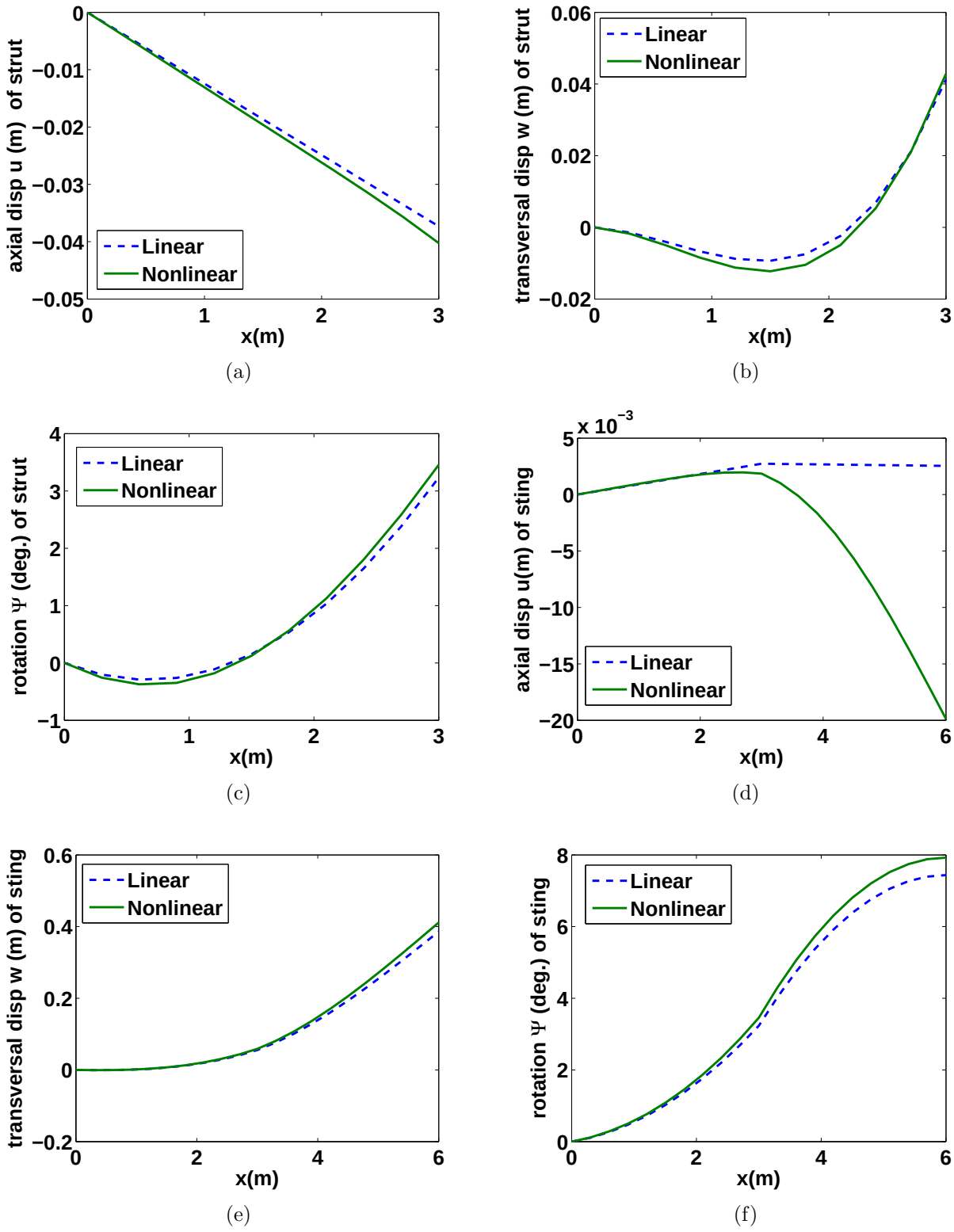

Figure 2.8: Static FSI response of the joined beam strut (a-c) and sting (d-f).

2.4.2 Joined beam with an airfoil under steady aerodynamic load

The joined beam with an airfoil shown in Figure 2.1 under static aerodynamic load was considered. A strut was added to the nonlinear Timoshenko beam with an airfoil model investigated in Section 2.4.1. This simple two-dimensional model in Fig. 2.1 has features representative of a three-dimensional joined wing. The two-beam model represents a two-dimensional analog to large spanwise deflection and buckling of the aft wing. The strut was rigidly connected to the sting at the middle point with an 45 degree angle. The strut has membrane rigidity $EA = 1.4e7\ N$, shear rigidity $kGA = 1e7\ N$, bending rigidity $EI = 1.3e6\ N \cdot m^2$, rotary inertia $\rho I = 18\ kg \cdot m$ and mass per unit length $\rho A = 135\ kg/m$. The inflow velocity U_∞ is 105 m/s. The other aerodynamic properties of the potential flow are the same as those listed in Section 2.4.1.

The static FSI response sensitivities with respect to the length of the sting were obtained. The design velocity was parameterized linearly for the sting using Eq. (2.17) with $\delta L = 0.01$ as

$$V_x = \frac{x}{L}\delta L; \quad V_y = 0, \tag{2.72}$$

where V_x is the x direction design velocity and V_y is the y direction design velocity. The length of strut and the angle between sting and strut β change according to the change of sting length with the strut attached to the mid-point of the sting. The perturbed structure can be seen from dashed lines in Figure 2.1. The sensitivity analysis of truss and frame structure with respect to configuration parameters has been investigate by using discrete analytical method (Mroz and Bojczuk, 1996). In this example application, the sensitivity of a joined beam frame under aeroelastic loads with respect to the shape and configuration changes was investigated by using local CSE method. The design velocity of the subdomain

of strut is also parameterized linearly and denoted in local coordinates of strut as

$$\bar{V}_x = \frac{\bar{x}}{2L}\delta L; \quad \bar{V}_y = 0. \tag{2.73}$$

The design velocity is zero at the root and $\frac{\sqrt{2}}{4}\delta L$ at the tip of strut. The material derivative of the transformation matrix in (2.20) is given as

$$\dot{T} = \frac{\partial T}{\partial \beta}\dot{\beta}, \tag{2.74}$$

where the rate of angle β change with respect to the design $\dot{\beta}$ is $\frac{\delta L}{2L}$. Hence, the boundary conditions at the roots and the tip of sting can be obtained according to this parametrization. The boundary conditions at the joint were implemented by using the special treatment discussed in Sectioin 2.3.

The FSI can be solved by using the same solver as for the beam with an airfoil model. The static FSI responses for both linear and nonlinear cases plotted in Fig. 2.8 demonstrate that the buckling effect of the nonlinearities in strut was captured. The bending stiffness of the strut for the nonlinear model decreases due to the axial load on the tip of strut. The shortening effect in the sting can be seen clearly in subfigure (d). The spatial first derivatives of the static FSI response of the sting for the nonlinear case are shown in Fig. 2.9. The first derivatives are discontinuous at the joint ($x = 3m$), which means the convective terms in Eq. (2.21) don't cancel. Hence, the local sensitivity variables are not continuous at the joint. Following the approach for treating discontinuity at the joint discussed in Section 2.3, the CSE system in terms of local sensitivity variables was solved. The total sensitivities were obtained from Eq. (2.7) by adding the convective terms. As seen from the sensitivity results shown in Fig. 2.10, the CSE total sensitivities with respect to the sting length closely match the finite difference results. The discontinuities can be seen from the sensitivities results of

the sting in Fig. 2.10 (f). The axial and transverse displacement sensitivity of the sting are also discontinuous at the joint, but cannot be seen easily in Fig. 2.10 (d) and (e), since the discontinuity is small relative to the magnitude of the sensitivity.

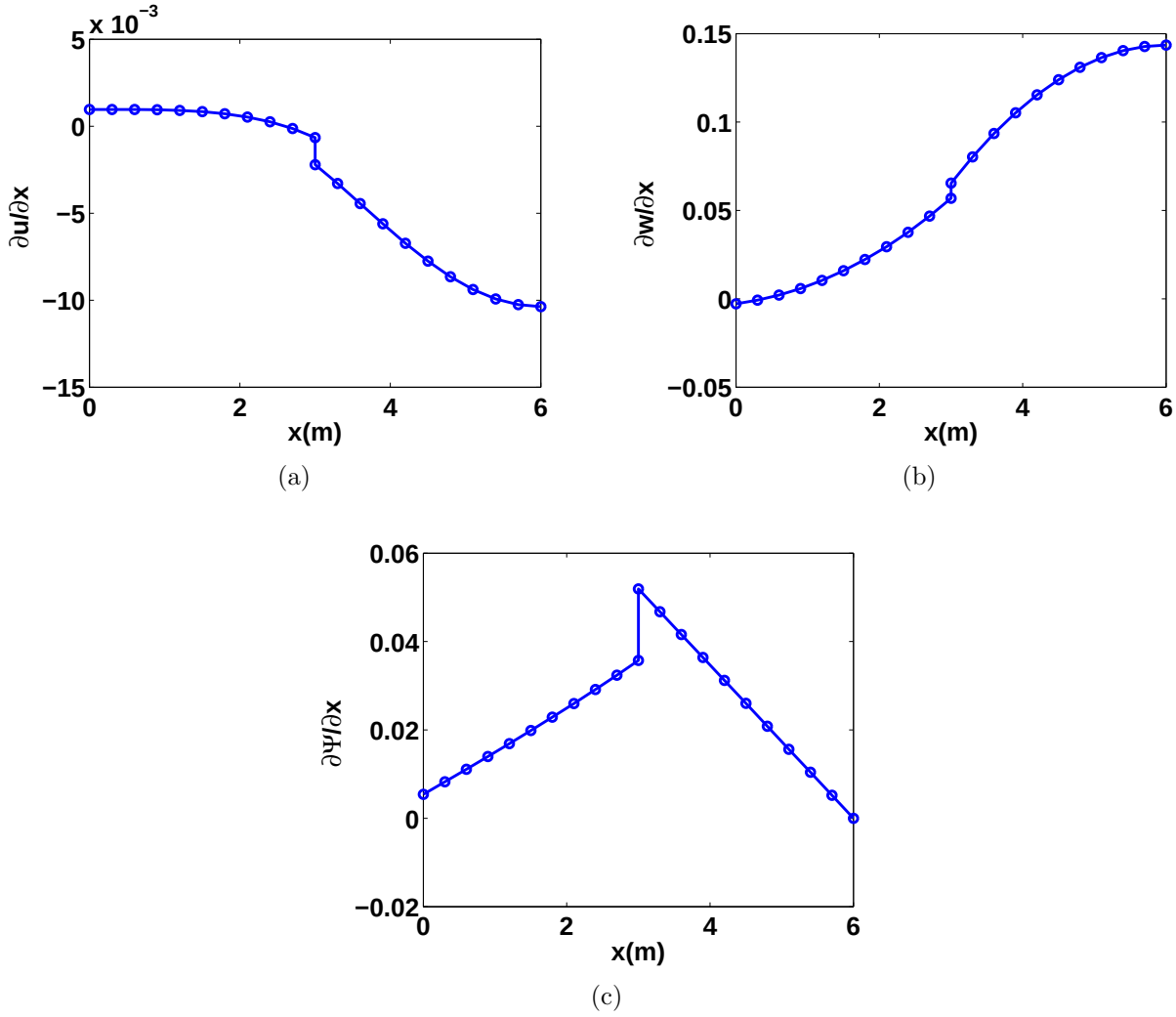

Figure 2.9: Spatial derivatives of nonlinear static FSI deformation of sting.

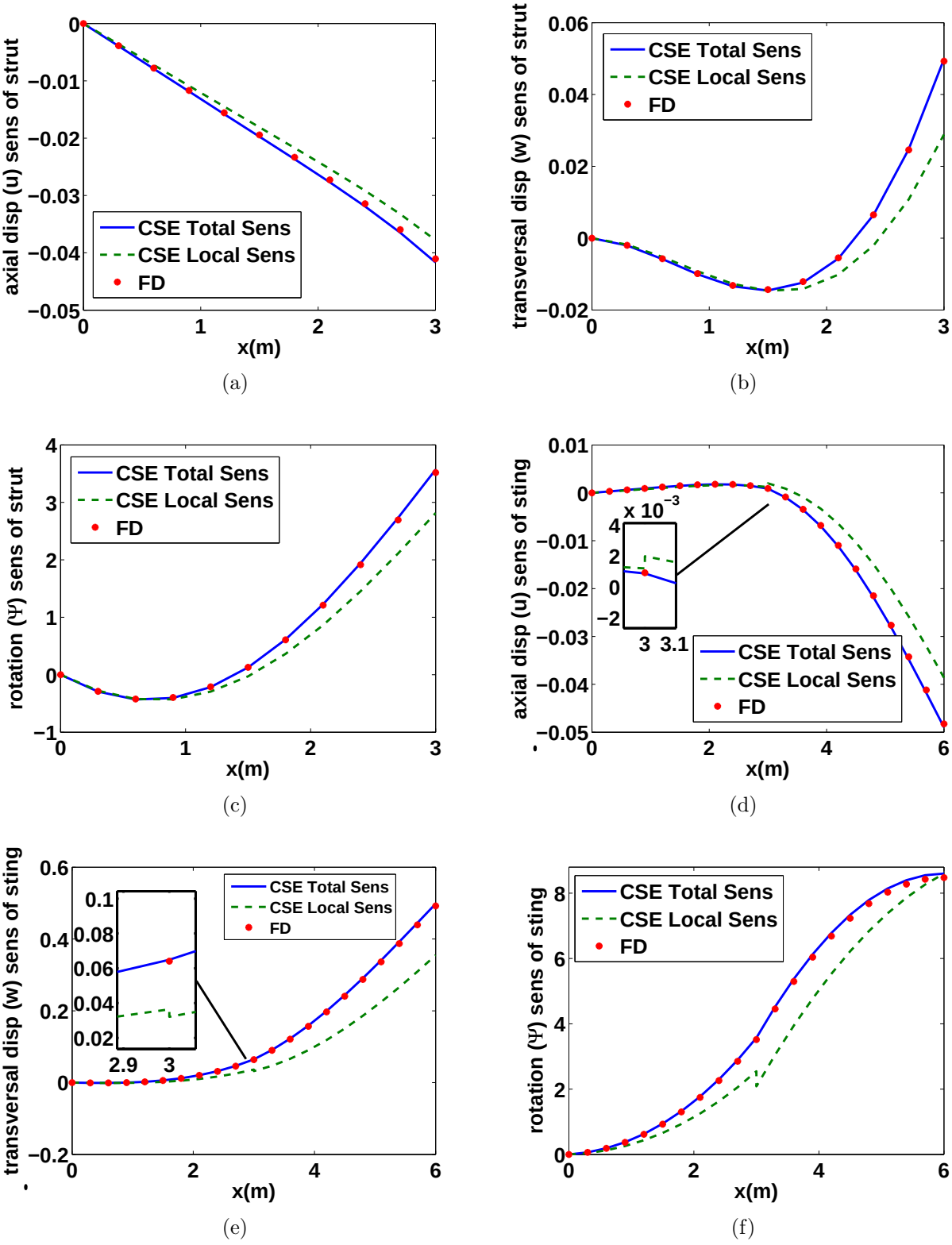

Figure 2.10: Static FSI response sensitivity of the Joined beam with respect to beam length.

2.4.3 Transient joined beam with a typical section airfoil under gust load

A joined beam with a typical section airfoil model under gust load serves as an example for verification of the CSE method for transient aeroelasticity problems. The joined beam has the same properties given in Section 2.4.2. The finite element model and the CSEs for structural domain are the same as discussed in Section 2.4.1. The joined beam deforms under the aerodynamic force, while the tip rotation increases the angle of attack of the airfoil. The flow equations in Section 2.4.1 are for steady state potential flow. For investigating the application of CSE for transient problems, the typical section aerodynamic theory was used to obtain the follower force that exerts on the beam tip (Hodges and Pierce, 2002).

$$L_f = qSC_{l_\alpha}\alpha_{\text{eff}} = qSC_{l_\alpha}\left(\alpha_0 + \psi_{\text{tip}} - \frac{w_{\text{tip},t}}{U_\infty} + \alpha_{\text{gust}}\right), \tag{2.75}$$

where q is the freestream dynamic pressure, S is the planform area, C_{l_α} is the lift-curve slope, α_{eff} is the effective angle of attack, $w_{\text{tip},t}$ is the vertical deflection velocity of the beam tip, and α_{gust} is the change in angle of attack due to vertical gust. Eqs. (2.63)-(2.71) are the CSE boundary conditions for the transient FSI problem. The lift force sensitivity with respect to the angle of attack, $\frac{\partial L_f}{\partial \alpha}$, can be obtained analytically from Eq. (2.75). In Eqs. (2.63)-(2.65), ψ'_{tip} and $w'_{,t}$ are the dependent variables of the CSE system and $\theta_{\text{tip}} = \alpha_0 + \psi_{\text{tip}}$. The derivatives of the initial angle of attack $\dot{\alpha}_0$ and the angle of attack due to gust $\dot{\alpha}_{\text{gust}}$ are equal to zero. Since the external force CSE boundary condition is dependent on the sensitivity variables, the CSE may be solved by forming a single set of fully coupled linear equations.

Gust flow model

The vertical gust is modeled using the usual discrete gust idealization of a one-minus-cosine pulse (Hoblit, 1988), so that

$$V_g(t) = \begin{cases} \frac{1}{2} V_{g,max} \left(1 - \cos \frac{t-\tau_0}{T_g}\right) & \tau_0 \leq t \leq T_g \\ 0 & otherwise, \end{cases} \tag{2.76}$$

where $V_{g,max}$ is the maximum amplitude of the gust, τ_0 is the start of the gust, and T_g is the duration of the gust. Since the NACA0012 is symmetric and the tip of the sting is mounted at the aerodynamic center of the airfoil, the aerodynamic moment is zero.

Numerical results

The typical section has $C_{l\alpha} = 2\pi$ and the same structure and flow properties as in Section 2.4.2. The one-minus-cosine gust described in Section 2.4.3 starts at $t = 3s$ and ends at $t = 4s$ with the maximum amplitude $V_{g,max} = 20\ m/s$. The transient gust response was investigated and the FSI responses at the sting tip are plotted in Fig. 2.11. Before the gust arrives at $t = 3s$, the joined beam structure reached steady state. After the gust arrives, the structure has a large deflection, and the nonlinear model captures the shortening effects as seen in subfigure (a). The transient gust response sensitivities with respect to the sting length were calculated by using the CSE method in local derivative form. The special treatment described in Section 2.3 was implemented for each time step. The transient FSI response sensitivities at the sting tip are shown in Fig. 2.12. As can be seen from the plots, the gust response sensitivity closely matches the finite difference results.

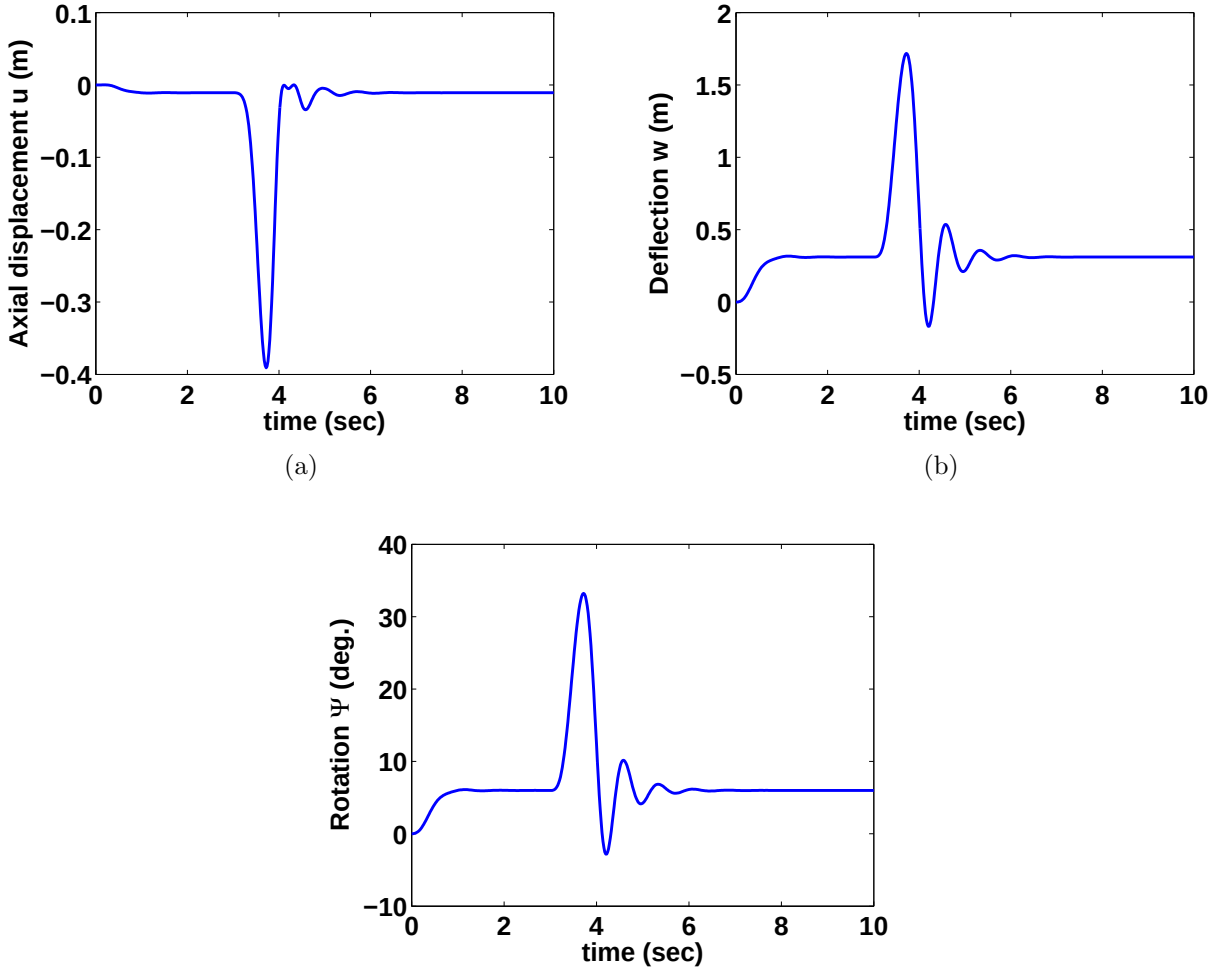

Figure 2.11: Joined beam gust response at sting tip

2.5 Conclusions

In the present work, the CSE method in local derivative form was derived using the boundary velocity method for fluid-structure interaction problems. The order of derivatives in the sensitivity boundary conditions are higher than those in the weak form of the original analysis problem. The p-version Galerkin finite element method was used for solving both the analysis and CSE problem. Higher-order elements facilitated accurate evaluation of the spatial derivatives appearing in the sensitivity boundary conditions. The CSE method solves

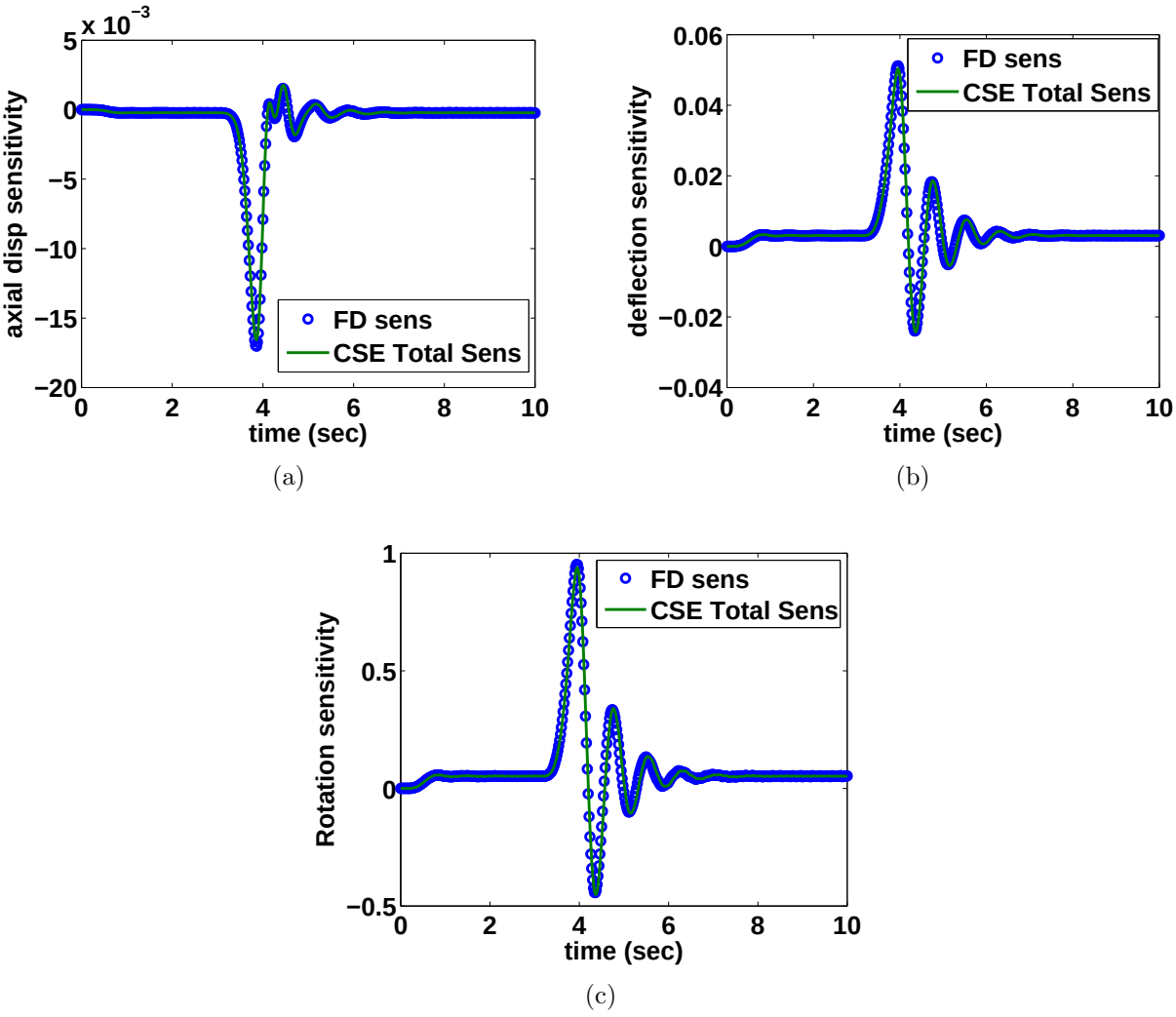

Figure 2.12: Joined beam gust response sensitivity with respect to beam length at sting tip

a system of linear equations even for nonlinear problems. If the Newton-Raphson method is used for nonlinear problems, then the tangent stiffness matrix for the analysis problem gives the sensitivity coefficient matrix for solving the linear CSE system. The CSE method in local derivative form requires geometric sensitivity (design velocity) only at the boundary of the domain, which avoids the need to calculate the mesh sensitivity in the whole domain, if the total sensitivities only on the boundary or at a few locations are of interest. Accuracy of the CSE results were verified against finite difference.

The CSE method in local derivative form is widely adopted by authors for fluid sensitivity problems, but rarely used for structural sensitivity problems. The advantages of local form CSE method are apparent for aerodynamic shape optimization, which often requires only sensitivities at the boundaries or local sensitivities within the flow field. CSE in local derivative form also retains the advantages for simple determinate structures without strain discontinuity. In this paper, the local form continuum sensitivity equations and boundary conditions were derived for built-up nonlinear aeroelastic structures and their solution was obtained for the first time. The local sensitivity variables in the CSE system are not continuous at a joint or other points with strain discontinuities. Hence, the elemental sensitivity matrix cannot be assembled directly based on the continuity of the local sensitivity variables. A special treatment was introduced in Section 2.3 by writing the displacements of joined subdomains at the interface in terms of displacements in one of the subdomains and adding a sensitivity force to the generalized force. As a result, in the discretized system, the tangent stiffness matrix may still be used for the sensitivity coefficient matrix and the number of global degrees of freedom for the CSE remains the same as for the FSI analysis problem.

2.6 Acknowledgements

The Air Force Office of Scientific Research sponsored this research under agreement number FA9550-09-1-0354. The authors gratefully acknowledge the support of AFOSR program manager Dr. Fariba Fahroo and the AFRL Senior Aerospace Engineers Dr. Raymond Kolonay, Dr. Phillip Beran, and Dr. Maxwell Blair.

Bibliography

Babuska, I., Aziz, A. K., 1972. Survey lectures on the mathematical foundations of the finite element method. In: The Mathematical Foundations of the Finite Element Method with Applications to Partial Differential Equations. Academic Press, pp. 5–359.

Berci, M., Gaskell, P. H., Hewson, R. W., Toropov, V. V., 2013. A semi-analytical model for the combined aeroelastic behaviour and gust response of a flexible aerofoil. Journal of Fluids and Structures 38, 3–21.

Bhaskaran, R., Berkooz, G., 1997. Optimization of fluid-structure interaction using the sensitivity equation approach. Fluid-Structure Interaction, Aeroelasticity, Flow-Induced Vibrations and Noise. 53 (1), 49–56.

Borggaard, J., Burns, J., 1994. A sensitivity equation approach to shape optimization in fluid flows. Tech. rep., Langley Research Center.

Borggaard, J., Burns, J., 1997. A PDE sensitivity equation method for optimal aerodynamic design. Journal of Computational Physics. 136, 366–384.

Charlot, L., Etienne, S., Pelletier, D., 2009. A continuous lagrangian sensitivity equation method for incompressible flow. In: 47th AIAA Aerospace Sciences Meeting Including The New Horizons Forum and Aerospace Exposition. No. AIAA-2009-369. Orlando, Florida.

Charlot, L., Etienne, S., Pelletier, D., 2012. A continuous lagrangian sensitivity equation method for incompressible flow. Journal of Computational Physics 231, 5989–6011.

Choi, K. K., Kim, N.-H., 2005. Structural sensitivity analysis and optimization. Springer Science+Business Media, New York.

Cross, D. M., Canfield, R. A., September, 17-19 2012a. Continuum shape sensitivity with spatial gradient reconstruction of nonlinear aeroelastic gust response. In: 14th AIAA/ISSMO Multidisciplinary Analysis and Optimization Conference. No. AIAA 2012-55597. Indianapolis, Indiana.

Cross, D. M., Canfield, R. A., April, 23-26 2012b. Solving continuum shape sensitivity with existing tools for nonlinear aeroelastic gust analysis. In: 53st AIAA/ASME/ASCE/AHS/ASC Structures, Structural Dynamics, and Materials Conference. No. AIAA 2012-1923. Honolulu, Hawaii.

Dems, K., Mroz, Z., 1985. Variational approach to first- and second-order sensitivity analysis of elastic structures. International Journal for Numerical Methods in Engineering 21, 637–661.

Etienne, S., Hay, A., Garon, A., 2006. Shape sensitivity analysis of fluid-structure interaction problems. In: 36th AIAA Fluid Dynamics Conference and Exhibit. No. AIAA 2006-3217. San Francisco, California.

Etienne, S., Hay, A., Garon, A., 2007. Sensitivity analysis of unsteady fluid-structure interaction problems. In: 45th AIAA Aerospace Sciences Meeting and Exhibit. No. AIAA-2007-332. Reno, Nevada.

Etienne, S., Pelletier, D., 2005. A general approach to sensitivity analysis of fluid-structure interactions. Journal of Fluids and Structures 21 (2), 169–186.

Haftka, R. T., Gurdal, Z., 1992. Elements of Structural Optimization. Kluwer Academic Publishers.

Haug, E. J., Choi, K. K., Komkov, V., 1986. Design sensitivity analysis of structural systems, Mathematics in Science and Engineering. Vol. 177. Academic Press, Orlando.

Hoblit, F., 1988. Gust loads on aircraft : concepts and applications. AIAA education series. American Institute of Aeronautics and Astronautics., Washington, D.C.

Hodges, D. H., Pierce, G. A., 2002. An Introduction to Structural Dynamics and Aeroelasticity. Vol. 15. Cambridge Aerospace Series.

Jameson, A., 1988. Aerodynamic design via control theory. Journal of Scientific Computing 3, 233–260, 10.1007/BF01061285.
URL http://dx.doi.org/10.1007/BF01061285

Liu, S., Wickert, P. D., Canfield, R. A., 2010. Fluid-structure transient gust response sensitivity for a nonlinear joined wing model. In: 51st AIAA/ASME/ASCE/AHS/ASC Structures, Structural Dynamics, and Materials Conference. No. AIAA 2010-3118. Orlando,Florda.

Marchman, J. F., 1999. Panel: A "smith-hess" type of 2-d panel code combining source panels and vortices for a single-element, lifting airfoil in incompressible flow. Virginia Tech.
URL http://www.dept.aoe.vt.edu/ marchman/software/index.html

Mroz, Z., Bojczuk, D., 1996. Sensitivity analysis of truss and frame structures in critical states. Mechanics of Structures and Machines: An International Journal 24:1, 105–134.

Reddy, J., 2006. An introduction to nonlinear finite element analysis. McGraw-Hill series in mechanical engineering. McGraw-Hill Higher Education, New York,NY.

Stanley, L., Stewart, D., 2002. Design sensitivity analysis : computational issues of sensitivity equation methods. Academic Press, Philadelphia.

Szabo, B. A., Babuska, I., 1991. Finite Element Analysis. Wiley, New York.

Turgeon, E., Pelletier, D., Borggaard, J., 1999. A continuous sensitivity equation approach to optimal design in mixed convection. No. AIAA 99-3625.

Wickert, D. P., Canfield, R. A., Reddy, J. N., 2009. Fluid-structure transient gust sensitivity using least-squares continuous sensitivity analysis. In: 50th AIAA/ASME/ASCE/AHS/ASC Structures, Structural Dynamics, and Materials Conference. No. AIAA-2008-1821. Palm Springs, California.

Wickert, P. D., Aug. 2009. Least-squares, continuous sensitivity analysis for nonlinear fluid-structure interaction problems. Ph.D. thesis, Air Force Institute of Technology, Ohio.

Chapter 3

Two Forms of Continuum Shape Sensitivity Method for Fluid-Structure Interaction Problems[1]

Abstract

A Continuum Sensitivity Equation (CSE) method for shape sensitivity analysis was developed in both local and total form for fluid and structure shape design problems. The local form poses the sensitivity equations in terms of the local derivative of the state variables, while the sensitivity equations in total form are posed in terms of the total derivative. The CSE method is often posed in local form for fluids and total form for solids. This paper compares the local form and the total form CSE. The local form requires design velocity only at the boundaries of the domain, while the design velocity in the whole domain is required by the total form. The local form requires higher order derivative of the analysis solution than the total form, which affects the accuracy of its results. The local sensitivity variables are discontinuous at the interfaces of built-up structures, which complicates the implementation of local form. The accuracy, efficiency and practicality of these two forms are compared based on the implementation and the sensitivity results of a linear Timoshenko beam under tip force model, fluid flow around an airfoil model and the nonlinear joined beam under gust

[1]In preparation for publication in *AIAA Journal* co-authored with Robert A. Canfield

load model.

Keywords: Shape Design Sensitivity, Continuum Sensitivity Method, Local Form, Total form, Fluid-Structure Interaction

---

3.1 Introduction

The continuum sensitivity method, also known as variational shape design (Haug et al., 1986), the variational sensitivity method (Haftka and Gurdal, 1992), and the continuous sensitivity equation method (Borggaard and Burns, 1997) was first introduced for structural problems (Haug and Arora, 1978; Haug and Rousselet, 1980; Dems and Mroz, 1985). Choi and Kim (2005) cites the lion's share of structural elasticity applications that employ continuum sensitivity methods. Jameson (1988) first introduced continuum sensitivity in adjoint equation form for aerodynamic design problems. Borggaard and Burns (1994) introduced the CSE nomenclature in a fluid setting and several fluid flow optimization applications followed (Borggaard and Burns, 1997; Turgeon et al., 1999; Stanley and Stewart, 2002). Bhaskaran and Berkooz (1997) present one of the earliest continuum sensitivity solution for fluid-structure interaction problem, although it involved CSE only for the fluid with respect to structural mode shapes for the purpose of creating an aerodynamic influence coefficient matrix for flutter calculation. Pelletier et al. have employed continuum sensitivity methods for a range of fluid-structure interaction problems with prominent success (Etienne and Pelletier, 2005; Etienne et al., 2006, 2007), although much of their work focuses on flow variable sensitivities. Wickert and Canfield applied the CSE method to the gust sensitivity for an airfoil mounted to an Euler Bernoulli beam (Wickert et al., 2009). They used least-squares finite elements and solved the nonlinear system with successive substitution for which the nonlinear coefficient matrix is different than the sensitivity matrix. Liu and Canfield (2011)

applied the CSE method to transient nonlinear fluid-structure interaction problems, such as a joined beam structure with a typical section airfoil. Recent work by Liu and Canfield (2012) extends this method to a transient nonlinear joined beam with an airfoil under potential flow, using the Galerkin finite elment method for which the tangent stiffness matrix is the sensitivity coefficient matrix.

Since the CSE method differentiates the continuous system before discretization, minimal details of the solver for the original analysis problem are required. The CSEs are often solved by the same black box solver for analysis problem with the CSE boundary conditions (Cross and Canfield, 2012a,b). Further, the sensitivity system is always a linear system of equations, even when the original system is nonlinear. If Newton-Raphson iteration is used for the nonlinear problems, the tangent stiffness matrix gives the stiffness matrix for the linear system of CSE equations (Liu and Canfield, 2011; Wickert, 2009).

Continuum sensitivity systems are often posed in terms of local derivatives (an Eulerian reference frame) for fluids and total derivatives (Lagrangian reference frame) for solids, just as for the analysis frames of reference. For shape optimization of fluid applications, an Eulerian description of the flow sensitivity is often adequate, once accuracy of the spatial derivatives of the solution on the boundary are addressed (Duvigneau and Pelletier, 2006), since often only local sensitivities for flow are of interest. Thus, much of the fluid mechanics literature does not emphasize the distinction between the local and total derivative. For structural optimization problems, however, the design sensitivity at a material point is usually required, which necessitates a means to calculate total sensitivities at a given material point. In this paper, a comparison is made between the total form and the local form CSE. The total form CSE for structural shape sensitivity may be more accurate than the local form if the displacement finite element method (FEM) was used for the analysis problem, since the local form requires higher derivative of the solution on the boundaries where the FEM

tends to give less accurate solutions (Babuska and Aziz, 1972; Zienkiewicz and Zhu, 1992). The total derivative form is more generally applicable for built-up structure with strain discontinuities (Liu and Canfield, 2013a). The local form requires design velocity only at the boundaries of the domain, while the design velocity in the whole domain is required by the total form. An additional linear system may have to be solved for the domain design velocity for use in the total form CSE when the pseudo-solid for domain deformation is used, for example. In this work, the total form continuum sensitivity method for calculating the total derivatives directly is investigated and compared with the local form for fluid-structure interaction problems. The advantages and disadvantages of these two forms for shape sensitivity problems are discussed.

Section 3.2 begins with a derivation of the continuum sensitivity system and its associated boundary conditions. The next section gives the equations and boundary conditions in both fluid and structure domains for solving the joined beam with an airfoil problem. Four sets of results are given for verifying both the local and total form CSE methods. The first set is the sensitivity results for a linear Timoshenko beam with a tip force model, the second set is the sensitivity results for a nonlinear Timoshenko beam with an airfoil model, where the aerodynamic load is obtained by the typical section airfoil theory, the third set is the flow sensitivity of the potential flow field with respect to the angle of attack, and the last set of results is the joined beam with an airfoil under potential flow field with gust load. All the results are compared with results by the complex step method, and the advantages and disadvantages of these two forms of the CSE method are discussed.

3.2 Continuum sensitivity equations

Consider the following general, nonlinear boundary value system defined in a domain Ω with a boundary Γ for which we seek a solution u of the equations

$$\mathcal{A}\left(u, L(u)\right) = f\left(x, t; b\right) \quad \text{on } \Omega \tag{3.1}$$

with geometric and natural boundary conditions

$$\mathcal{B}\left(u, L(u)\right) = g\left(x, t; b\right) \quad \text{on } \Gamma \tag{3.2}$$

where $u = u(x, t; b)$ is dependent on design variable b implicitly, $L(u)$ is a vector of linear differential operators, such as $\left\{\frac{\partial}{\partial t}, \frac{\partial}{\partial x}, \frac{\partial}{\partial y}, \frac{\partial^2}{\partial x^2}, \frac{\partial^2}{\partial y^2} \ldots\right\}$, that appears in the governing differential equations or boundary conditions, $\mathcal{A}$ and $\mathcal{B}$ are vectors of algebraic functions of u and $L(u)$, and $\mathcal{B}\left(u, L(u)\right)$ can be a simple function of u, such as a prescribed boundary condition $u = \bar{u}$ for Dirichlet boundary conditions, or involve a differential operator for von Neumann boundary conditions. The weak form of the governing equations (3.1) can be written as

$$\iint_{\Omega} C(u, \bar{u}) d\Omega = \iint_{\Omega} \bar{u}^T f d\Omega \tag{3.3}$$

where $C(u, \bar{u})$ is the integrand of the weak form and $\bar{u}$ is the test function. It is usually linear with respect to $\bar{u}$ and can be linear or nonlinear with respect to u.

Discrete sensitivity analysis methods differentiates the system after either the strong form (3.1) or the weak form of the governing equations (3.3) are discretized to obtain a system of algebraic equations, such as the static equation,

$$\mathbf{K}\mathbf{u} = \mathbf{f} \tag{3.4}$$

Then, the sensitivity with respect to the design parameters, $\frac{D\mathbf{u}}{Db}$, can be calculated by using the finite difference method, complex step method, or discrete analytical methods.

The total derivative of solution vector $\mathbf{u}$ with respect to design parameter b is $\frac{D\mathbf{u}}{Db}$. The finite difference method can be used for approximating $\frac{D\mathbf{u}}{Db}$. For example, the forward difference approximation is

$$\frac{D\mathbf{u}}{Db} \simeq \frac{\mathbf{u}(b+\Delta b)-\mathbf{u}(b)}{\Delta b} \tag{3.5}$$

A drawback of the finite difference method is the challenge of determining the optimum step size. Large step sizes are dominated by truncation error and small step sizes are dominated by numerical round-off error (Gill and Wright, 1981). Furthermore, it involves solving the original analysis problem $n+1$ times for n design variables, which makes finite difference method inefficient, especially for nonlinear problems.

The complex method can avoid the challenge of determining the step size Squire and Trapp (1998); Martins (2003). The complex step approximation is formulated as

$$\frac{D\mathbf{u}}{Db} \simeq \frac{\mathrm{Im}\left[\mathbf{u}(b+i\Delta b)\right]}{\Delta b} \tag{3.6}$$

The complex step method is not subject to subtractive cancelation error. A very small step size can be used to minimize the truncation error while avoiding the round-off error. But it still involves solving the original analysis problem at least n + 1 times for n design variables, which makes complex step method inefficient, especially for nonlinear problems.

Discrete analytical methods require the derivatives of the stiffness matrix and load vectors with respect to the design variables. The direct method differentiates static equations (3.4) or its transient analogue and solves for

$$\frac{D\mathbf{u}}{Db} = \mathbf{K}^{-1}\left(\frac{D\mathbf{f}}{Db} - \frac{D\mathbf{K}}{Db}\mathbf{u}\right) \tag{3.7}$$

where $\mathbf{K}$ is the stiffness matrix of the discretized equation of Eq. (3.1) or (3.3). If the design parameter is a shape parameter, the mesh sensitivity in the whole domain should be calculated for $\frac{D\mathbf{K}}{Db}$, which involves additional computation.

3.2.1 Local form CSE

The CSE method avoids these shortcomings by directly differentiating the governing equation. Taking the partial derivative of the governing equations (3.1), the CSEs can be obtained in terms of local sensitivity variable $u' = \frac{\partial u}{\partial b}$ as

$$\frac{\partial \mathcal{A}}{\partial u}u' + \frac{\partial \mathcal{A}}{\partial L}L(u') = \frac{\partial f(x,t;b)}{\partial b} \tag{3.8}$$

Henceforth, the prime notation will be used to indicate a local sensitivity variable as an unknown to be solved for. The dot notation is reserved for a total sensitivity variable, such as $\dot{u} = \frac{Du}{Db}$. Spatial and temporal derivatives will be abbreviated using indices with a comma, such as $\frac{\partial(\cdot)}{\partial x} = (\cdot)_{,x}$. The boundary conditions for (3.8) may be derived by taking the material derivative of the boundary condition (3.2) and writing it in terms of the local derivative and convective term as

$$\frac{Du}{Db} = \frac{\partial u}{\partial b} + V(X) \cdot \nabla u \tag{3.9}$$

where ∇u is the gradient of u with respect to the spatial coordinates, $V(x) = \frac{\partial X}{\partial b}$ is the geometric sensitivity or design velocity, which is dependent on the parameterization of the computational domain. $X = x + bV(x)$ is the coordinates of a material point. After taking material derivatives of (3.2) and moving the convective terms to the right hand side, the CSE boundary conditions are given as

$$\frac{\partial \mathcal{B}}{\partial u}u' + \frac{\partial \mathcal{B}}{\partial L}L(u') = \dot{g}\left(x,t;b\right) - V(X) \cdot \left(\frac{\partial \mathcal{B}}{\partial u}\nabla u + \frac{\partial \mathcal{B}}{\partial L}L\left(\nabla u\right)\right) \tag{3.10}$$

where $\dot{g}(x,t;b)$ is the material derivative of the boundary condition. The commutation of derivatives on the left side of Eq. (3.10) is possible when the derivatives are local. The CSE (3.8) with the boundary conditions in (3.10) is a well posed linear system of equations in terms of sensitivity variable u', which often can be solved by the same numerical method used for solving the analysis problem. The solution u can be obtained from the analysis solution of Eq. (3.1) for use in Eq. (3.8) and Eq. (3.10) when $\mathcal{A}$ or $\mathcal{B}$ is nonlinear with respect to u. The CSE in local form only requires the design velocity, $V(X)$, at the boundaries (3.10). The boundary velocity method is more efficient when only sensitivities at boundaries are of interest, since it avoids calculating design velocity inside the whole domain. If the sensitivities inside the whole domain are of interest, the design velocity field in the domain is required and can be obtained by solving a pseudo-solid system, which will be described in Section 3.2.2.

For shape sensitivity, the solution of local form CSE (3.8) yields local sensitivity. After solving for the local derivative, the total derivative can be obtained by using Eq. (3.9), which defines the total derivative of u with respect to design parameter b at a material point as the sum of the local derivative and the convective term. The latter accounts for how u changes as the material point moves in response to design variable changes.

3.2.2 Total form CSE

Another way to calculate the material derivatives is to form the CSE in terms of the total sensitivity variable, $\dot{u} = \frac{Du}{Db}$, and solve these equations directly. The total derivative form CSEs are derived by taking the material derivatives of the governing equations or the weak form (3.3). The material derivative of a domain functional may be used for deriving the

CSEs. Let ψ be a domain functional, defined as an integral over Ω, namely,

$$\psi = \int_{\Omega} f(x)\ d\Omega \tag{3.11}$$

where $f(x)$ is a function defined in Ω. The material derivative of ψ at Ω is (Haug et al., 1986; Arora, 1993)

$$\dot{\psi} = \int_{\Omega} [f'(x) + \nabla \cdot (fV)]\, d\Omega \tag{3.12}$$

The total form CSE can be derived by taking the material derivative of the weak form (3.3) with respect to the design variable using Eq. (3.9) and Eq. (3.12).

$$\iint_{\Omega} [C(u, \dot{\bar{u}} - \nabla \bar{u} V) + C_L(\dot{u} - \nabla u V, \bar{u})] + \nabla \cdot (C(u, \bar{u})V)\, d\Omega \\ = \int_{\Omega} (\dot{\bar{u}} - \nabla \bar{u} V)^T f + \dot{f} \bar{u} d\Omega \tag{3.13}$$

where C_L is the linearized C with respect to u. It is equal to C for linear problems. Since test function $\bar{u}$ is arbitrary, it can be chosen as $\bar{u}(x + bV(x)) = \bar{u}(X)$. That is $\bar{u}$ can be chosen as constant along $X = x + bV(x)$, so that

$$\dot{\bar{u}} = 0 \tag{3.14}$$

Even if it is assumed that $\dot{\bar{u}} \neq 0$, since $\dot{\bar{u}}$ is in the space of kinematically admissible virtual displacements, it satisfies the weak form relation (Choi and Kim, 2005).

After ignoring the terms containing $\dot{\bar{u}}$ and moving the terms containing design velocity to

the right side, the total form sensitivity equation can be obtained from (3.13) as

$$\begin{aligned} \iint_{\Omega} C_L(\dot{u}, \bar{u}) d\Omega &= \iint_{\Omega} \left[C(u, \nabla \bar{u} V) + C_L(\nabla u V, \bar{u}) - (\bar{u} V)^T f \right] d\Omega \\ &+ \iint_{\Omega} \nabla \cdot \left[\bar{u}^T f V - C(u, \bar{u}) V \right] d\Omega \end{aligned} \tag{3.15}$$

The left side of total form sensitivity equation (3.15) has the same form as the bilinear form in Eq. (3.3) for linear problems. The terms on right side of the total form sensitivity equation (3.15) depend on the design velocity inside the domain, which, of course, depends on the design parameterizaton.

The boundary design velocity field can be obtained directly from the relation between the boundary geometry and the shape parameters. Given the design velocity on the boundary $\overline{V}$ as required by the local form CSE, a pseudo solid method may be used for calculating the design velocity inside the domain. In this method, the domain design velocity is governed by the linear equations of elasticity (Johnson and Tezduyar, 1994),

$$\nabla \cdot \boldsymbol{\sigma} + \mathbf{f} = 0 \tag{3.16}$$

where $\mathbf{f}$ is the prescribed body force, which is zero here. The stress σ is related to the strain tensor as

$$\boldsymbol{\sigma} = \lambda (\text{tr } \boldsymbol{\epsilon}) \mathbf{I} + 2\mu \boldsymbol{\epsilon} \tag{3.17}$$

where $\mathbf{I}$ is the identity matrix, λ and μ are the so-called *Lamé* constants. The strain tensor is related to the design velocity gradients by the expression

$$\boldsymbol{\epsilon} = \frac{1}{2} \left(\nabla V + (\nabla V)^T \right) \tag{3.18}$$

The Dirichlet boundary condition for the pseudo-solid is imposed by the design velocity on

the boundary, and represented by

$$V(x) = \overline{V}(x) \quad \text{on } \Gamma \tag{3.19}$$

Solving the linear elasticity equations (3.16)-(3.18), the design velocity throughout the domain can be obtained, and the design velocity field satisfies the linear dependency requirement, which requires that the design velocity field in the domain should depend linearly on the variation of the shape design variable (Haug et al., 1986). The design velocity field should be compatible with the mesh updating in shape optimization. For avoiding large mesh distortion, it is desirable to preserve the element shape in fine mesh areas, and prevent the smaller elements from deforming too much. Also to avoid large strain in sharp corners, which is the required spatial derivative of the design velocity, the small elements at those corners are weighted to have larger stiffness. This can be implemented by refining the mesh at sharp corners and by replacing the Jacobian of the transformation between the physical and the computational domain with its reciprocal or just by dropping the Jacobian (Johnson and Tezduyar, 1994).

Both the local and total form CSE methods can be used for the evaluation of the total derivative of an output functional with respect to the shape parameter. The local form uses only the analysis solution on the boundary. In contrast, the total form CSE requires information from the analysis solution in the domain, where the finite element solution may be more accurate. Higher order derivatives of the analysis solution at boundaries are needed for local form, which tend to be less accurate, since they are obtained by postprocessing of the solution for primary variable finite element methods. For the local form CSE, the weak form is easily obtained, while more mathematical developments are required for the total form. Furthermore, linear elasticity equations to define the design velocity in the domain increases the computations, although the design velocity field may serve directly as the mesh moving

in the optimization. The local form CSE requires the same amount of additional effort to update the mesh according to the boundary perturbation to obtain the convective terms, if needed to transform to material derivative in the domain interior or for optimization.

To summarize, the CSE system is a linear boundary value problem derived by taking the derivatives of the original field equations (3.1) or its equivalent weak form (3.3) and boundary conditions (3.2). The continuum sensitivity equations may be derived in either total or local derivative form. When expressed in local form, only the boundary parameterization needs to be described. In total derivative form, the parameterization or transformation function for the entire domain is necessary, which is equivalent to the mesh Jacobian after discretization. Posing the CSE in local derivative form and parameterizing only the boundary avoids the numerical complexity and expense of the mesh (domain) sensitivity. However, lower order derivatives of the analysis solution are required by total form CSE than the local form CSE, which may lead to more accurate solutions. As pointed out by Liu and Canfield (2013a) that the local sensitivity variables in local form CSE are not continuous at the strain discontinuous points, such as the interfaces of built-up structures, which requires additional discontinuity information at those points and makes the implementation more complex, while the CSE boundary conditions required for total derivative form are trivial. It is shown by Liu and Canfield (2013b) that the total form CSE is equivalent to the discrete analytic method for geometrically nonlinear elastic structures and even for the potential flow problems under the conditions that they use the same: (1) finite element discretization, (2) numerical integration of element matrices, (3) design velocity fields that are linear with respect to the design variable and (4) shape functions for domain transformation and for design velocity field calculations.

3.3 Applications

3.3.1 Timoshenko beam with an airfoil under typical section flow model

The CSE methods were applied to a Timoshenko beam with an airfoil attached at its tip as shown in Fig.3.1. A straight beam is fixed at one end, and a NACA 0012 airfoil is mounted on the other end of this sting. The beam deforms under the aerodynamic load on the airfoil, and the rotation of the beam changes the angle of attack of the airfoil, which changes the load on airfoil. This Timoshenko beam with an airfoil model forms a simple aeroelastic system. The sensitivity of the static response with respect to the beam length L was investigated using different forms of CSE. The aerodynamic force was obtained using the typical section aerodynamic equation.

$$L_f = qcC_{l_\alpha}\left(\alpha_0 + \psi_{\text{tip}}\right) \tag{3.20}$$

where q is the dynamic pressure, C_{l_α} is the lift coefficient and c is the cord length of the airfoil.

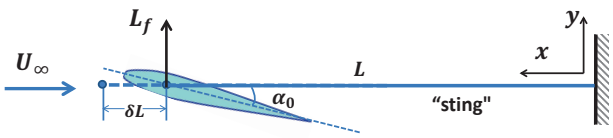

Figure 3.1: Timoshenko beam with an airfoil model.

Finite element model for structure domain

Nonlinear Timoshenko beam theory accounts for moderately large rotations and nonlinear strains (Reddy, 2006). The displacement field can be given as

$$u_x = u(x) - y\psi, \quad u_y = w(x), \quad u_z = 0$$

where ψ is the rotation of the cross section. Using the nonlinear strain-displacement relations

$$\epsilon_{ij} = \frac{1}{2}(u_{i,j} + u_{j,i}) + \frac{1}{2}(u_{m,i}u_{m,j})$$

and retaining only the square of rotation of a transverse normal line in the beam as the only nonlinear strain term, we obtain

$$\epsilon_{xx} = \left[\frac{\partial u}{\partial x} + \frac{1}{2}\left(\frac{\partial w}{\partial x}\right)^2\right] - y\frac{\partial \psi}{\partial x}; \quad \gamma_{xy} = \frac{\partial w}{\partial x} - \psi$$

where w is the vertical deflection, u is the lateral displacement, ψ is the cross section rotation angle. By using extended Hamilton's principle and assuming linear elastic material behavior, the governing equations for the nonlinear Timoshenko beam with the rotational inertia can be derived as

$$\rho A u_{,tt} - \left[EA(u_{,x} + \frac{1}{2}w_{,x}^2)\right]_{,x} - f_1 = 0 \tag{3.21}$$

$$\rho A w_{,tt} - \left[EAw_{,x}(u_{,x} + \frac{1}{2}w_{,x}^2)\right]_{,x} - \left[kGA(w_{,x} - \psi)\right]_{,x} - f_2 = 0 \tag{3.22}$$

$$\rho I \psi_{,tt} - (EI\psi_{,x})_{,x} - kGA(w_{,x} - \psi) = 0 \tag{3.23}$$

where f_1 is the axially distributed load and f_2 is the laterally distributed load. EA, EI and kGA are the flexural rigidity of membrane, bending and shear. E and G are the Young's

and shear modulus, respectively, and k is shear correction factor. ρ, I and A are the material density, the moment of inertia, and the cross-sectional area, respectively. The weak form of the nonlinear Timoshenko beam model is

$$\int_{x_a}^{x_b} \rho A u_{,tt} v_1 dx + \int_{x_a}^{x_b} EA(u_{,x} + \frac{1}{2} w_{,x}^2) v_{1,x} dx = \int_{x_a}^{x_b} v_1 f_1 dx + N_{xx} v_1 |_{x_a}^{x_b} \tag{3.24}$$

$$\int_{x_a}^{x_b} \rho A w_{,tt} v_2 dx + \int_{x_a}^{x_b} EA w_{,x}(u_{,x} + \frac{1}{2} w_{,x}^2) v_{2,x} dx + \int_{x_a}^{x_b} kGA(w_{,x} - \psi) v_{2,x} dx$$
$$= \int_{x_a}^{x_b} v_2 f_2 dx + V_f v_2 |_{x_a}^{x_b} \tag{3.25}$$

$$\int_{x_a}^{x_b} \rho I \psi_{,tt} v_3 dx + \int_{x_a}^{x_b} EI \psi_{,x} v_{3,x} dx - \int_{x_a}^{x_b} kGA(w_{,x} - \psi) v_3 dx = M_{xx} v_3 |_{x_a}^{x_b} \tag{3.26}$$

where v_1, v_2 and v_3 are test functions. The axial force N_{xx}, the moment on the cross section M_{xx}, the shear force on cross section Q_x and the vertical force V_f are given as

$$N_{xx} = EA(u_{,x} + \frac{1}{2} w_{,x}^2); \tag{3.27}$$

$$M_{xx} = EI\psi_{,x} \tag{3.28}$$

$$Q_x = -kGA(w_{,x} - \psi); \tag{3.29}$$

$$V_f = N_{xx} W_{,x} - Q_x \tag{3.30}$$

Local form CSE for structure domain

The CSE in local derivative form can be derived by taking partial derivatives of the governing equations, Eq. (3.21)-(3.23), with respect to the design variable b directly.

$$\rho A u'_{,tt} - \left[EA(u'_{,x} + w_{,x}w'_{,x})\right]_{,x} - f_{1,b} = 0 \tag{3.31}$$

$$\begin{aligned}\rho A w'_{,tt} - \left[EAw'_{,x}(u_{,x} + \frac{1}{2}w^2_{,x})\right]_{,x} - \left[EAw_{,x}(u'_{,x} + w_{,x}w'_{,x})\right]_{,x} \\ - \left[kGA(w'_{,x} - \psi')\right]_{,x} - f_{2,b} = 0\end{aligned} \tag{3.32}$$

$$\rho I \psi'_{,tt} - (EI\psi'_{,x})_{,x} - kGA(w'_{,x} - \psi') = 0 \tag{3.33}$$

where u', w' and ψ' are the local sensitivity variables with respect to b. Essential sensitivity boundary conditions at the root for the cantilevered beam case in Fig. 3.10 are found by differentiating the homogeneous boundary condition for the analysis problem.

$$u' = \dot{u} - u_{,x}V(x)|_{x=0} \tag{3.34}$$

$$w' = \dot{w} - w_{,x}V(x)|_{x=0} \tag{3.35}$$

$$\psi' = \dot{\psi} - \psi_{,x}V(x)|_{x=0} \tag{3.36}$$

The sensitivity natural boundary conditions at the tip of the beam are found by taking the material derivative of Eqs. (3.27)-(3.30) evaluated at the sting tip and solving for the local derivatives

$$N'_{xx} = \dot{N}_{xx} - EA\left[u_{,xx} + w_{,x}w_{,xx}\right]V(x)|_{x=L} \tag{3.37}$$

$$M'_{xx} = \dot{M}_{xx} - EI\psi_{,xx}v(x)|_{x=L} \tag{3.38}$$

$$V'_f = \dot{V}_f - \left[N_{xx,x}w_{,x} + N_{xx}w_{,xx} - Q_{x,x}\right]V(x)|_{x=L} \tag{3.39}$$

where

$$N_{xx,x} = EA\left[u_{,xx} + w_{,x}w_{,xx}\right] \tag{3.40}$$

$$Q_{x,x} = -kGA(w_{,xx} - \psi_{,x}) \tag{3.41}$$

Then a set of new equations, Eqs. (3.31)-(3.33), with boundary conditions, Eqs. (3.34) - (3.39), in terms of the local sensitivity variables can be solved for the local sensitivities. If needed, the total sensitivities can be obtained by the conversion, Eq. (3.9), given in Section 3.2. The design velocity $V(x)$ used in Eq. (3.10) is parameterized linearly for the sting

$$V(x) = \frac{x}{L}\delta L \tag{3.42}$$

where δL is the tip perturbation of the sting and x is the axial coordinate of the sting. The design velocity is required only on the boundary, Eq. (3.37)-(3.39).

Total form CSE for structure domain

For deriving the total form CSE, firstly, we write the weak form Eq. (3.24) as

$$\int_{x_a}^{x_b} C_1(u, w, v_1)dx - N_{xx}v_1|_{x_a}^{x_b} = 0 \tag{3.43}$$

where $C_1(u, w, v_1)$ is the integrand of the weak form of Eq. (3.24). Taking the total derivative of the weak form with respect to the design variable by using Eq. (3.9) and Eq. (3.12), we have

$$\int_{x_a}^{x_b} C_1'(u, w, v_1) + \nabla \cdot \left[C_1(u, w, v_1)V(x)\right] dx = \dot{N}_{xx}v_1|_{x_a}^{x_b} \tag{3.44}$$

which can be expanded as

$$\int_{x_a}^{x_b} \rho A\dot{u}_{,tt}v_1 + \rho A\dot{u}_{,tt}v_1V_{,x} + \left[EA(u'_{,x} + w_{,x}w'_{,x})\right] v_{1,x} + EA[u_{,x} + \frac{1}{2}w_{,x}^2]v'_{1,x}$$
$$+V\left[EA(u_{,xx} + w_{,x}w_{,xx})v_{1,x} + EA[u_{,x} + \frac{1}{2}w_{,x}^2]v_{1,xx} - v_{1,x}f - v_1f_{,x}\right] +$$
$$V_{,x}\left[EA(u_{,x} + \frac{1}{2}w_{,x}^2)v_{1,x} - v_1f\right] - v'_1f - v_1f'dx = \dot{N}_{xx}v_1|_{x_a}^{x_b} \tag{3.45}$$

where

$$\begin{aligned} u'_{,x} &= \dot{u}_{,x} - u_{,xx}V - u_{,x}V_{,x} \\ w'_{,x} &= \dot{w}_{,x} - w_{,xx}V - w_{,x}V_{,x} \\ v'_{1,x} &= \dot{v}_{1,x} - v_{1,xx}V - v_{1,x}V_{,x} \end{aligned} \tag{3.46}$$

Simplifying equation (3.45) using the partial derivatives in Eq. (3.46) and Eq. (3.14), we obtain the weak form of the CSE for Eq. (3.24) as

$$\int_{x_a}^{x_b} \rho A\dot{u}_{,tt}v_1dx + \int_{x_a}^{x_b} EA\left[\dot{u}_{,x} + \dot{w}_{,x}w_{,x}\right] v_{1,x} - v_1\dot{f}dx =$$
$$\int_{x_a}^{x_b} \left[EA(u_{,x} + w_{,x}^2)v_{1,x} + v_1f\right] V_{,x}dx - \int_{x_a}^{x_b} \rho Au_{,tt}v_1V_{,x}dx + \dot{N}_{xx}v_1|_{x_a}^{x_b} \tag{3.47}$$

Similarly, we can derive the CSE weak form of Eq. (3.25) and Eq. (3.26) as

$$\int_{x_a}^{x_b} \left[EA\dot{w}_{,x}(u_{,x} + \frac{1}{2}w_{,x}^2) + EAw_{,x}(\dot{u}_{,x} + w_{,x}\dot{w}_{,x}) + kGA(\dot{w}_{,x} - \dot{\psi})\right] v_{2,x}dx$$
$$+ \int_{x_a}^{x_b} \rho A\dot{w}_{,tt}v_2dx - \int_{x_a}^{x_b} \dot{q}v_2dx = -\int_{x_a}^{x_b} \rho Aw_{,tt}v_2V_{,x}dx + \dot{V}_fv_2|_{x_a}^{x_b}$$
$$+ \int_{x_a}^{x_b} \left[\left(EAw_{,x}(2u_{,x} + \frac{3}{2}w_{,x}^2) + kGAw_{,x}\right) v_{2,x} + qv_2\right] V_{,x}dx \tag{3.48}$$

and

$$\int_{x_a}^{x_b} \rho I\dot{\psi}_{,tt}v_3 + EI\dot{\psi}_{,x}v_{3,x} - kGA(\dot{w}_{,x} - \dot{\psi})v_3 dx = \int_{x_a}^{x_b} \left(EI\psi_{,x}v_{3,x} - kGA\psi v_3 - \rho I\psi_{,tt}v_3\right) V_{,x} dx + \dot{M}_{xx}v_3|_{x_a}^{x_b} \quad (3.49)$$

Equations (3.47)-(3.49) are the weak form of the CSE in total derivative form. The right side of the equations are explicitly dependent on the design velocity $V(x)$ and the analysis solution. The total sensitivity can be obtained by solving this set of equations for the total sensitivity variables $\dot{u}, \dot{w}$, and $\dot{\psi}$, using the same method for solving the analysis problem. In contrast to the local derivative form, only first-order derivatives of the analysis solution are required, but the first derivative of design velocity is needed throughout the domain for the domain integration method.

Linear Timoshenko beam with a tip force results

For verification, a linear Timoshenko beam with a static tip force, which is the Timshenko beam in Fig. 3.1 without the airfoil, was first investigated. The linear static case of the dynamic equations in Section 3.3.1 were used. The numerical results were obtained for a sting with length $L = 10\ m$, membrane rigidity $EA = 1e7\ N$, shear rigidity $kGA = 1e7\ N$, bending rigidity $EI = 5e6\ N \cdot m^2$, rotary inertia $\rho I = 35\ kg \cdot m$ and mass per unit length $\rho A = 80\ kg/m$. A $6000N$ vertical force was exerted on the tip of the beam. The sensitivity of the static response with respect to the beam length L was calculated using the complex step, the local form CSE and the total form CSE. The design velocity was parameterized linearly using Eq. (3.42) with $\delta L = 1$. The static structural problem was implemented by using p-version Galerkin finite element method. The sensitivities and their error relative to the exact solution are plotted in Fig. 3.2. For results in subfigure (a) and (b), 2 elements

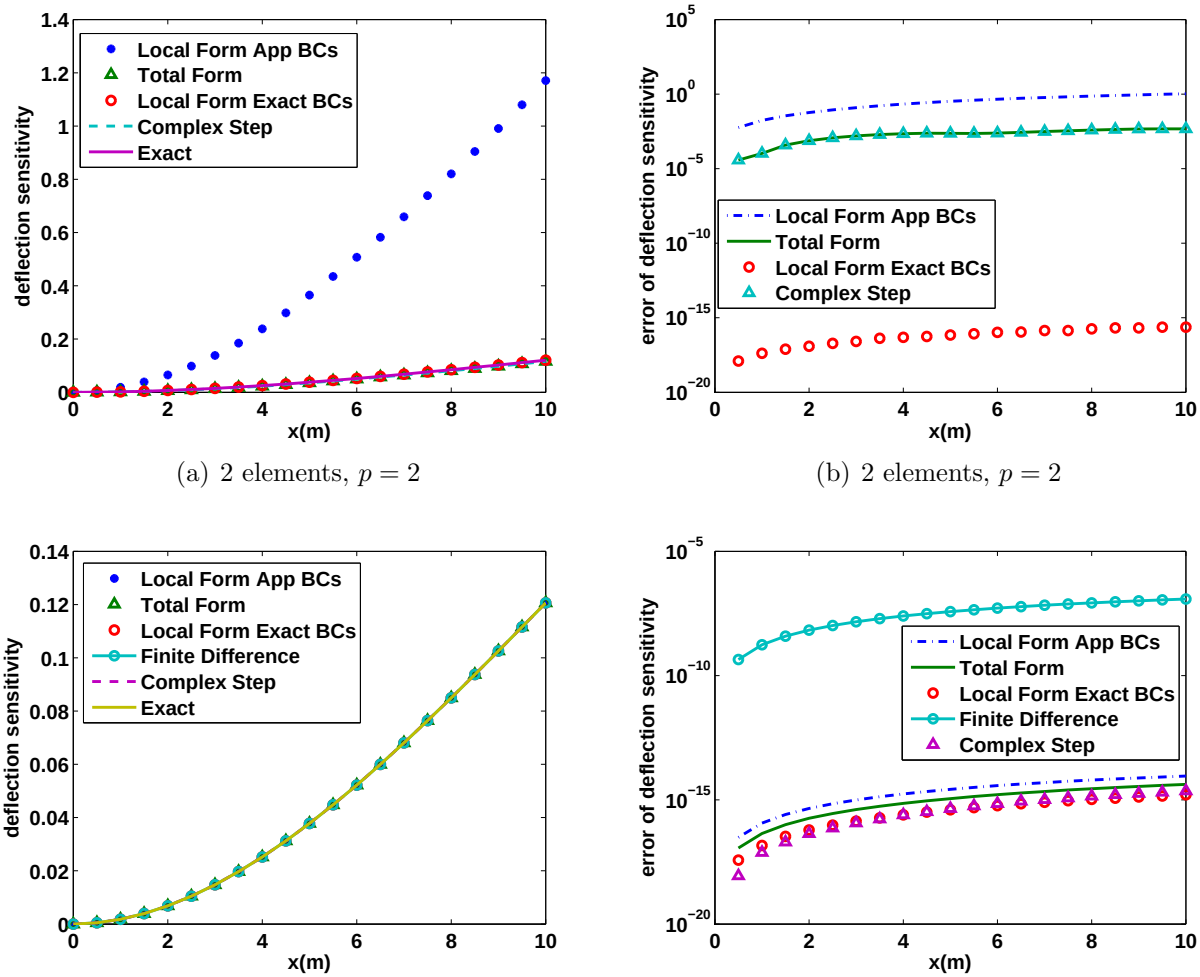

(a) 2 elements, $p = 2$

(b) 2 elements, $p = 2$

(c) 2 elements, $p = 3$

(d) 2 elements, $p = 3$

Figure 3.2: Linear Timoshenko beam sensitivities and error to exact solution.

were used with elemental order $p = 2$. As seem from (a) and (b), the results using the total form CSE and the complex step method closely match the exact solution with small error, while the local form results has larger error. As seen from the local form CSE boundary conditions Eq. (3.37)-(3.39), the second derivatives of displacement are required by the local form. These derivatives of the analysis solution, which were approximated by differentiating the shape functions, are not accurate for the low order elements ($p = 2$) used. If the exact derivatives from the analytical solution were used in the local form CSE boundary conditions

(3.37)-(3.39), the local form CSE gives much more accurate results, as seen in subfigure (b). When the order of elements p was increased to be 3, as seen in subfigure (c) and (d), the accuracy for all the sensitivity solutions closely match the exact solution with very small error. However, the local form still has larger error compared to the exact solution than the total form. The step size of the complex step method in this case was given a very small number ($\delta b = 10^{-15}$) to minimize the truncation error. As seen from the results, the complex method can give very accurate results.

Nonlinear Timoshenko beam with an airfoil results

The nonlinear Timoshenko beam with an airfoil model was then implemented using Newton-Raphson iteration methods and p-version finite elements for two different mesh resolutions. The geometrical and material properties of the sting are the same as those given in Section 3.3.1. A nonlinear static aeroelastic problem with a constant inflow velocity was solved. The magnitude of the flow is 155 m/s with air density $\rho_a = 1.2\ kg/m^3$. The chord length of the airfoil is 1 m with initial angle of attack $\alpha_0 = 3°$. The lift coefficient C_{l_α} in (3.20) is 2π. The lift force L_f serves as the shear force V_f in (3.25). In the CSE boundary conditions (3.39) and (3.48), the material derivative of the shear force $\dot{V}_f$ can be obtained from the sensitivity of aerodynamic force, and can be posed in terms of total sensitivity variables for total form CSE boundary condition (3.48) as

$$\dot{V}_f = \dot{L}_f = \frac{DL_f}{D\alpha}\frac{D\alpha}{Db} = \frac{DL_f}{D\alpha}\dot{\psi}_{\text{tip}} \tag{3.50}$$

and in terms of local sensitivity variables for local form CSE boundary condition (3.39) as

$$\dot{V}_f = \frac{DL_f}{D\alpha}\left(\psi'_{\text{tip}} + \psi_{\text{tip},x}V(x)\right) \tag{3.51}$$

where $\frac{DL_f}{D\alpha} = qcC_{l_\alpha}$. The sensitivities of the static fluid-structure response with respect to the beam length L were calculated using both local and total form CSE. The static case of the dynamic equations for the structural domain in Section 3.3.1 were used. Three elements with shape functions of order $p = 3$ were used for results in Fig. 3.3. As can be seen, the sensitivities results using total form CSE closely match the complex step solution, whereas the sensitivities using local form have large differences compared to the complex step results. After refining the mesh to 20 elements, results using total form and local form closely match the complex step results and the errors are much smaller than the coarse mesh case, as can be seen in Fig. 3.4. Still, local form errors are larger.

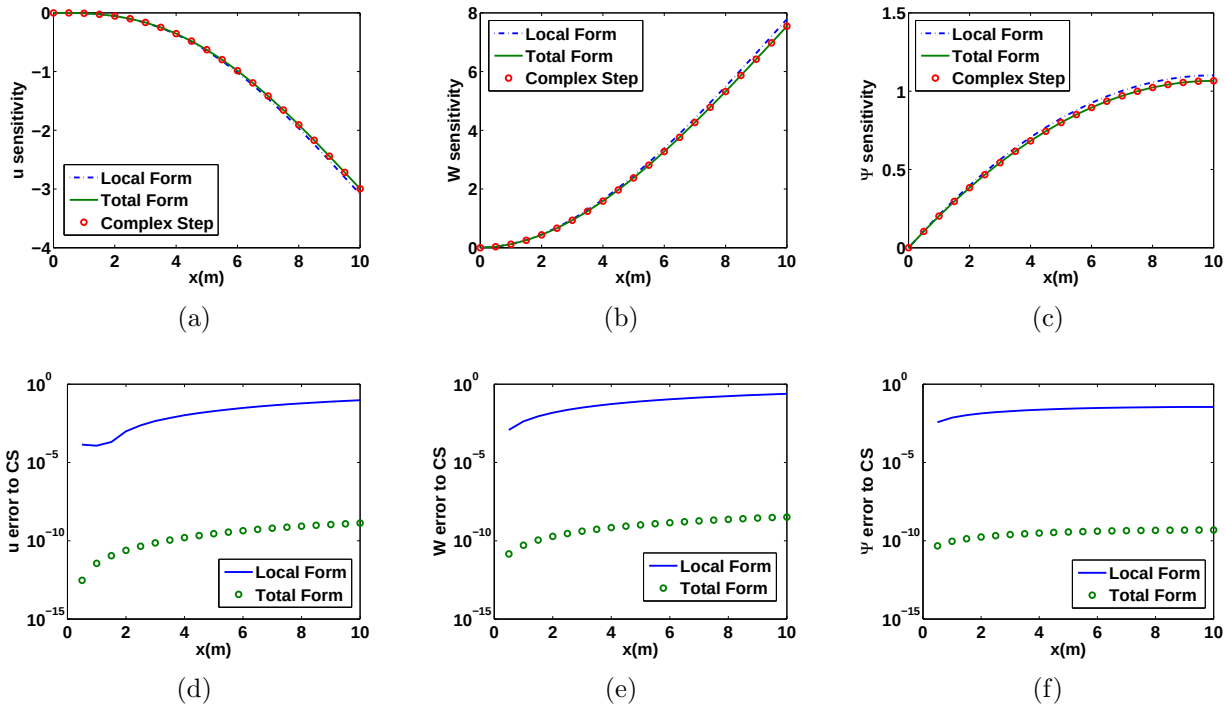

Figure 3.3: Nonlinear Timoshenko beam FSI sensitivities and error to complex step (CS) solution (three elements of order $p = 3$)

From the results for the linear beam with a tip force and the nonlinear Timoshenko beam FSI problems, it can be seen that the local form CSE is not as accurate as the total form when displacement finite elements are used for solving the analysis problem. The local

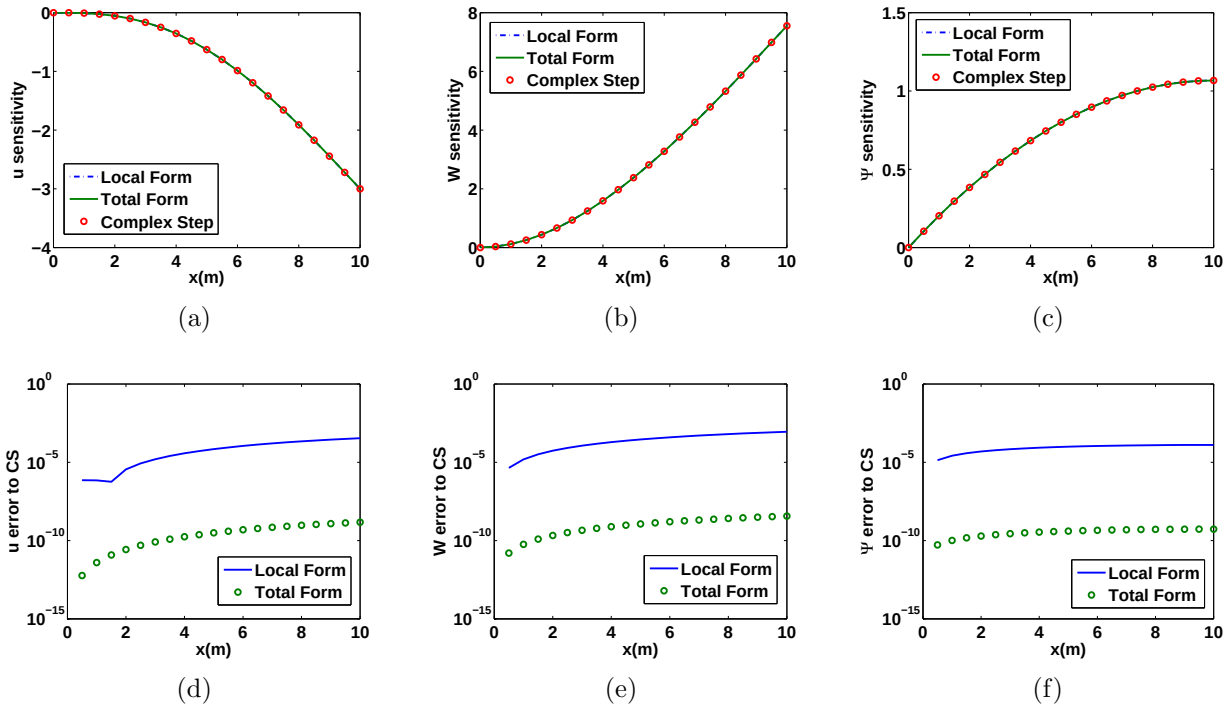

Figure 3.4: Nonlinear Timoshenko beam FSI sensitivities and error to complex step (CS) solution (20 elements of order $p = 3$)

form CSE requires higher order derivatives of the analysis solution than the total form, which is not as accurate, because derivatives of solution are obtained by differentiating the shape functions. By increasing the number of elements, the analysis solution becomes more accurate and so do the derivatives of the solutions at the boundaries. Hence the accuracy of the sensitivities is improved. Other methods to improve the accuracy of the spatial derivatives of the approximate analysis solution are possible, such as spatial gradient reconstruction (Cross and Canfield, 2012a).

3.3.2 Potential flow around an airfoil problem

Finite element model for fluid domain

The flow around the airfoil is modeled as linear potential flow, which is used to demonstrate the application of continuum sensitivity method to two dimensional flow (Fig. 3.5). In irrotational flow, the stream function Ψ satisfies Laplace's equation

$$\nabla^2 \Psi = 0 \tag{3.52}$$

The x and y-component of flow velocity, v_x and v_y, can be found from the streamfunction, Ψ, in two dimensional flows,

$$v_x = \frac{\partial \Psi}{\partial y}, \qquad v_y = -\frac{\partial \Psi}{\partial x} \tag{3.53}$$

The essential boundary conditions on the perimeter boundary of the domain are given as

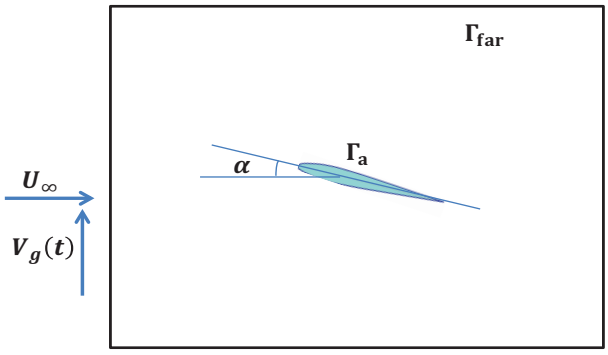

Figure 3.5: Potential flow Around an airfoil model.

$$\Psi = U_\infty y - V_g(t) x \tag{3.54}$$

where U_∞ is the inflow velocity and $V_g(t)$ is a gust velocity profile. The wall boundary condition on the airfoil is the no-penetration condition. Since the airfoil boundary is a streamline, the flow is always tangential to the airfoil. Thus, the no-penetration condition becomes an essential boundary condition on the airfoil, which is

$$\Psi|_{\Gamma_a} = \Psi_a \tag{3.55}$$

where Ψ_a is a constant along the airfoil, but it's not known prior to the simulation. The Kutta condition was used as another constraint. It requires the flow to leave the trailing edge smoothly. To enforce this condition, we require that flow at the trailing edge be aligned along the bisector of the trailing edge, $\hat{t}_{TE}$. The geometry of the trailing edge is shown in Fig. 3.6. For the flow to be aligned to $\hat{t}_{TE}$, the velocity normal to the bisector $\hat{t}_{TE}$ should be zero. Thus, at the trailing edge, the Kutta condition becomes,

$$\nabla\Psi \cdot \hat{t}_{TE} = 0 \tag{3.56}$$

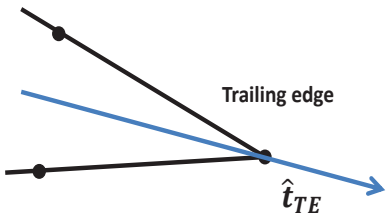

Figure 3.6: Trailing edge geometry.

The finite element method was used for solving the analysis problem. The weak form of Eq. (3.52) is

$$\iint_\Omega \nabla\bar{w} \cdot \nabla\Psi dA = \oint_\Gamma \bar{w} q_n ds \tag{3.57}$$

where $\bar{w}$ is the test function, Ω is the fluid domain, Γ is the boundary of the domain and $q_n = \frac{\partial \Psi}{\partial x} n_x + \frac{\partial \Psi}{\partial y} n_y$ is the flux through the boundaries.

Local form CSE for fluid domain

The CSE method was used for evaluating the steady pressure coefficient sensitivity to the angle of attack. The fluid mesh deforms according to the angle of attack change. The angle of attack α is a shape parameter, since a change in α changes the shape of fluid domain. In other words, the design velocity is not zero in the domain. Taking the partial derivative of the governing equation (3.52) with respect to the design parameter α, we have the CSE for fluid in terms of local sensitivity variable Ψ',

$$\nabla^2 \Psi' = 0 \tag{3.58}$$

The boundary conditions for CSE on the far field boundaries are all homogeneous, because the far field boundary nodes don't change as the airfoil shape changes,

$$\Psi'|_{\Gamma_{\text{far}}} = 0 \tag{3.59}$$

The sensitivity constraint derived from the Kutta condition is found by taking the material derivative of (3.56) and re-arranging

$$\nabla \Psi' \cdot \hat{t}_{TE} = -V \cdot \nabla \left(\nabla \Psi \right) \cdot \hat{t}_{TE} - \nabla \Psi \cdot \frac{D \hat{t}_{TE}}{Db} \tag{3.60}$$

The sensitivity boundary condition on the airfoil can be obtained by taking the material derivative of the essential boundary condition (3.55).

$$\Psi'|_{\Gamma_a} = \Psi'_a + \nabla\Psi_a \cdot V - \nabla\Psi|_{\Gamma_a} \cdot V \tag{3.61}$$

where V is the design velocity vector on the airfoil boundary. As seen from equation (3.61), the local sensitivity of the streamfunction on the airfoil is not equal to a constant. For implementation of theis conditions, a right hand side term should be added to the nodal degree of freedom of all the nodes on the airfoil boundary. However, it's not the case for the total form CSE, as we will see in the next subsection. Comparing with the analysis equations (3.52), the CSE (3.58) has the same form. The CSE can be solved by using the same solver as for the original analysis problem, except for the change of boundary conditions (3.59)-(3.61). The velocity sensitivity can be evaluated by differentiating Eq. (3.53) with respect to the coordinates and commuting the order of differentiation.

$$v'_x = \frac{\partial\Psi'}{\partial y}, \qquad v'_y = -\frac{\partial\Psi'}{\partial x}$$

The pressure coefficient in an inviscid, incompressible flow can be found using Bernoulli's equation,

$$C_p = \frac{p - p_\infty}{\frac{1}{2}\rho_a U_\infty^2} = 1 - \left(\frac{\bar{v}}{U_\infty}\right)^2 \tag{3.62}$$

where $\bar{v} = \sqrt{v_x^2 + v_y^2}$ is the local flow speed. The sensitivity of C_p with respect the design variable α can be obtained

$$\dot{C}_p = \frac{2(v_x v'_x + v_y v'_y)}{U_\infty^2} + \frac{2\left[v_x(V(x)\cdot\nabla v_x) + v_y(V(x)\cdot\nabla v_y)\right]}{U_\infty^2} \tag{3.63}$$

The lift force sensitivity with respect to the angle of attack is given as

$$\frac{DL_f}{D\alpha} = \oint_{\Gamma_a} \frac{1}{2}\rho_a c U_\infty^2 \dot{C}_p \, ds + \oint_{\Gamma_a} \frac{1}{2}\rho_a c U_\infty^2 C_p \, \dot{\overline{ds}} \tag{3.64}$$

Total form CSE for fluid domain

For total form CSE, the weak form of the governing equation (3.57) is differentiated using equations (3.9) and (3.12) for material derivatives in Section 3.2. We obtain the weak form of the CSE system in terms of the total sensitivity variable $\dot{\Psi}$ as

$$\iint_\Omega \nabla\dot{\Psi} \cdot \nabla\bar{w} dA = \iint_\Omega \left(\left(\nabla V\right)^T \nabla\bar{w} \right) \cdot \nabla\Psi + \nabla\bar{w} \cdot \left(\left(\nabla V\right)^T \nabla\Psi \right) + \left(\nabla\bar{w} \cdot \nabla\Psi\right)\left(\nabla \cdot V\right) dA \tag{3.65}$$

The material derivative of the boundary term in (3.57) vanishes, since the boundary integral is constant over the far field boundary. The CSE boundary constraint for the Kutta condition can be derived by taking the total derivative of Eq. (3.56) and moving the convective terms to the right hand side as

$$\nabla\dot{\Psi} \cdot \hat{t}_{TE} = \left(\nabla V\right)^T \nabla\Psi - \nabla\Psi \cdot \frac{D\hat{t}_{TE}}{Db} \tag{3.66}$$

The CSE boundary conditions on the outer boundary of the domain vanish as the boundary condition for the local form CSE system, since these boundaries do not change with the shape design valuables. The essential boundary conditions on the airfoil can be derived by taking the total derivative of Eq. (3.55).

$$\dot{\Psi}|_{\Gamma_a} = \dot{\Psi}_a \tag{3.67}$$

Equation (3.67) has the same form of the essential boundary condition of the original analysis problem. The way we implement this condition is the same as solving the analysis problem. The variable $\dot{\Psi}_a$ is treated as an unknown to be found for all nodes on the airfoil in the same way as for analysis problem.

The material derivative of the flow velocity can be obtained by taking the total derivative of Eq. (3.53) as

$$\dot{u} = -\dot{\Psi}_{,x} + \nabla\Psi \cdot V_{,x} \tag{3.68}$$

$$\dot{v} = \dot{\Psi}_{,y} - \nabla\Psi \cdot V_{,y} \tag{3.69}$$

where $V_{,x}$ and $V_{,y}$ are the spatial derivatives of the design velocity. The material derivative of the pressure coefficient can be calculated from the material derivatives of the flow velocities.

$$\dot{C}_p = \frac{2(u\dot{u} + v\dot{v})}{U_\infty^2} \tag{3.70}$$

The total sensitivity of the stream function $\dot{\Psi}$ can be obtained by solving the total form CSE (3.65) subject to boundary conditions (3.66)-(3.67) and the homogeneous essential boundary conditions in the far field. As seen from (3.65), the total form CSE requires only first spatial derivatives of the dependent variable Ψ throughout the domain, while second spatial derivatives of the stream function are required by local form CSE on the boundary in Eqs. (3.60) and (3.63). The accuracy of the pressure coefficient sensitivity by total form CSE (3.70) is not degraded as the local form CSE (3.63), since the second spatial derivatives of the stream function are not needed. Therefore, the total form CSE tends to obtain more accurate sensitivity results than the local form CSE, especially at the flow field boundaries where the displacement based finite element method tends to give less accurate spatial derivatives. In the total form CSE (3.65) and its boundary condition (3.66), the spatial derivatives of the

design velocity are required throughout the domain, while in the boundary conditions for local form CSE (3.60) and (3.61), only the design velocity itself is required. Hence, the smoothness requirement of the design velocity field is higher for total form CSE than the local form.

Results

The finite element solver for potential flow around a NACA 0012 airfoil was implemented with bilinear rectangular elements. The number of elements used was 3574 and the number of nodes associated was 3714. The angle of attack α was 10 degrees. The numerical results for the fluid analysis are shown in Fig. 3.7, which are non-dimensionalized by the inflow velocity U_∞. The velocity in x direction in subfigure (a) increases on the upper airfoil surface and decreases on the lower airfoil surface. The velocity in y direction increases rapidly at the upper leading edge. Hence, the pressure coefficient has positive values at the upper leading edge and has negative values at the lower leading edge. As seen in subfigure (d), the pressure coefficient on the airfoil closely matches a vortex panel code solution (Marchman, 1999).

The flow sensitivities with respect to the angle of attack are calculated by using both total and local form CSE. The sensitivity results are shown in Fig. 3.8. As the angle of attack increases, the velocities at the upper airfoil surface increase and the velocities at the lower airfoil surface decrease. Hence, the velocity sensitivities are positive on the upper surface and negative on the lower surface, while the pressure coefficient sensitivity is negative on the upper surface and positive on the lower surface. As seen from subfigure (d), the pressure coefficient sensitivity on the airfoil surface by total form closely matches the complex step solution. The sensitivity results by local form CSE has large error at the leading edge of the airfoil, where the flow velocity gradients are large. The local form requires those flow velocity gradients (second derivative of the streamline function), but linear elements were

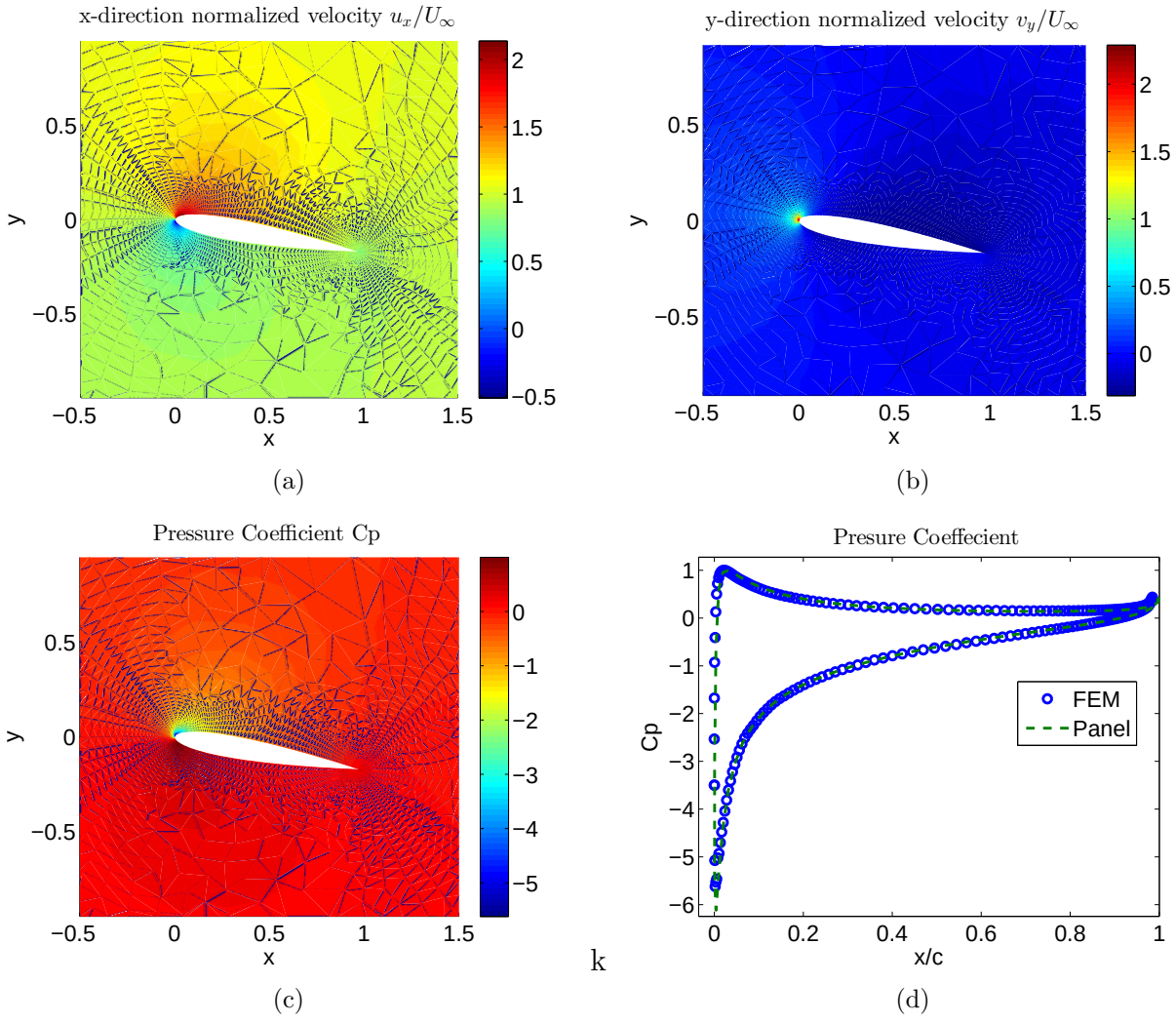

k

Figure 3.7: Finite element solutions for flow around NACA 0012

used for flow analysis. For calculating the second derivative of the streamline function Ψ, the nodal values of the first derivatives (velocities) were first obtained by averaging the velocities from the surrounding elements, then the spatial gradients of the velocities for each element are reconstructed by differentiating the shape functions and the nodal velocity gradients are averages of the velocity gradients from all the related elements. The accuracy of the velocity gradient was degraded.

The accuracy of local form sensitivity solution may be improved by refining the mesh near

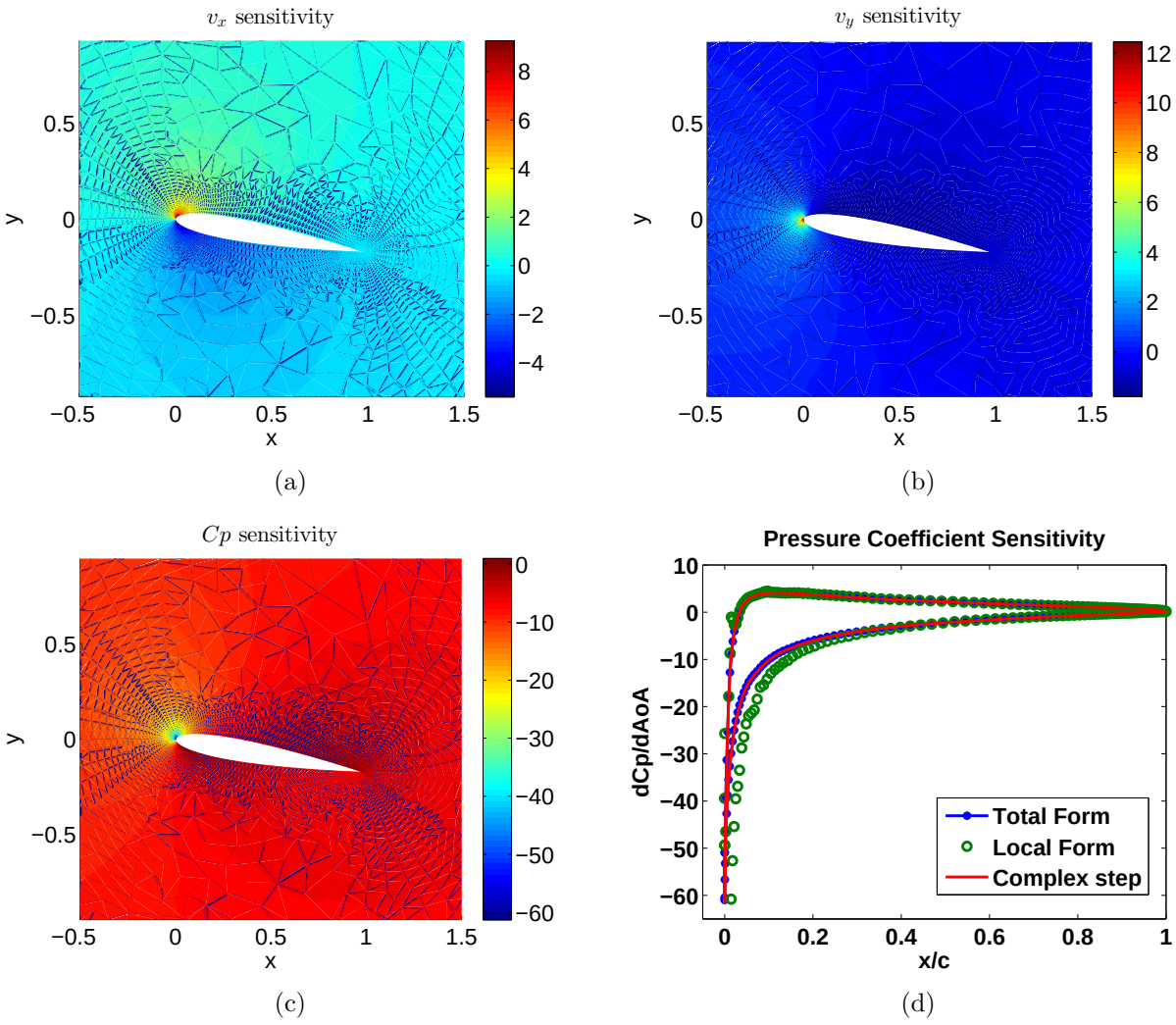

Figure 3.8: Sensitivity of flow around NACA 0012 with respect to angle of attack.

boundaries as can be seen from the results in Section 3.3.1. Another way of improving the accuracy of higher derivatives of the analysis solution required by the CSE boundary conditions is by using the p-version finite elements for the analysis problem. The hierarchic shape functions for quadrilaterals (Szabo and Babuska, 1991) were implemented for this potential flow around an airfoil problem. The mesh used here is coarser than the mesh used for the bilinear elements with 1096 elements and 1176 nodes associated. As seen form Fig. 3.9, after using p elements with element order $p = 2$, the accuracy of the sensitivity results

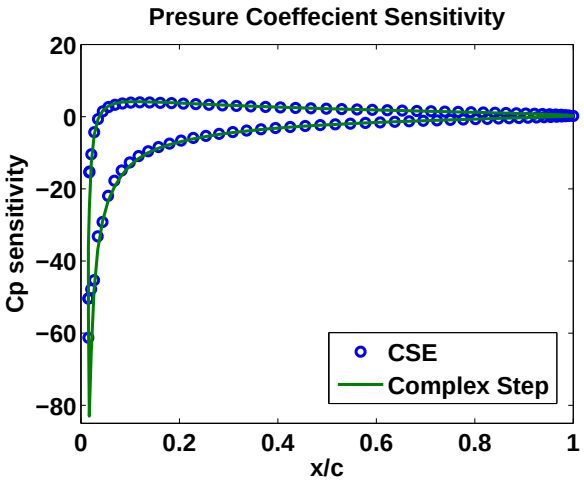

Figure 3.9: Flow sensitivity to angle of attack using local form CSE and p-elements, $p = 2$

using local form CSE was increased. The pressure coefficient sensitivity results using local form CSE method closely match the results by complex step method.

Although the total form CSE requires calculating the design velocity field throughout the domain, the design velocity field for the total form CSE is consistent with mesh update during the shape optimization. For more than one design parameter, the total form needs to calculate the design velocity field by solving a linear system (3.16)-(3.18) of the pseudo-solid for each design parameter during every design iteration, whereas the local form CSE requires no solution of the pseudo-solid. However, the stiffness matrix of the pseudo-solid is the same for all the design parameters. After solving the design velocity field for one of the design parameters, the factorized stiffness matrix can be saved and used for calculating the design velocity for other shape design parameters. If the sensitivity is being calculated for shape optimization, then the mesh updating is necessary even for the local form CSE, which perhaps requires at least one (more) pseudo-solid solution.

3.3.3 Transient joined beam with an airfoil under gust load

Joined beam with an airfoil

A NACA 0012 airfoil is mounted on a sting with a supporting strut. This simple two-dimensional model in Fig. 3.10 has features representative of a three-dimensional joined wing. The two-beam model represents a two-dimensional analog to large spanwise deflection and buckling of the aft wing. The sting and strut are modeled as nonlinear Timoshenko beams capable of large deflections as described in subsection 3.3.1. At a positive angle of attack, the airfoil generates lift, deflecting the beam in the fluid, resulting in an increased angle of attack. The equilibrium deflection of the sting occurs when the force and moments generated by the lifting airfoil balance the internal sting force and moments resisting the bending. The strut is subject to buckling due to the deflection of the sting. Since the NACA0012 is symmetric and the tip of the sting is mounted at the aerodynamic center of the airfoil, the aerodynamic moment is zero.

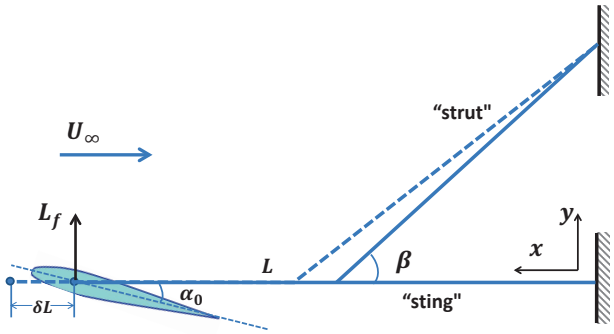

Figure 3.10: Joined beam with an airfoil model.

For shape sensitivity analysis, the sting length L is taken as a shape design parameter. The

length of strut and the angle between sting and strut β change according to the change of sting length with the strut attached to the mid-point of the sting. The perturbed structure can be seen from dashed lines in Figure 3.10. The design velocity was parameterized linearly for the sting using Eq. (3.42) as

$$V_x = \frac{x}{L}\delta L; \quad V_y = 0 \tag{3.71}$$

where V_x is the x direction design velocity and V_y is the y direction design velocity. In this example application, the sensitivity of a joined beam frame under aeroelastic loads with respect to the shape and configuration changes was investigated by using total form CSE method. The design velocity of the subdomain of strut is also parameterized linearly and denoted in local coordinates of the strut as

$$\bar{V}_x = \frac{\bar{x}}{2L}\delta L; \quad \bar{V}_y = 0 \tag{3.72}$$

The design velocity is zero at the root and $\frac{\sqrt{2}}{4}\delta L$ at the tip of strut.

Gust model

The vertical gust is modeled using the usual discrete gust idealization of a one-minus-cosine pulse (Hoblit, 1988), so that

$$V_g(t) = \begin{cases} \frac{1}{2}V_{g,max}\left(1 - \cos\frac{t-\tau_0}{T_g}\right) & \tau_0 \le t \le T_g \\ 0 & \text{otherwise} \end{cases} \tag{3.73}$$

where $V_{g,max}$ is the maximum amplitude of the gust, τ_0 is the start of the gust, and T_g is the duration of the gust.

Fluid-structure boundary conditions

In the joined beam with an airfoil model, the airfoil is mounted on the tip of the sting at the aerodynamic center. The aerodynamic force, L_f, calculated by solving the potential flow problem discussed in Section 3.3.2 serves as a shear force V_f on the tip of the sting. As seen in Eq. (3.37) and Eqs. (3.47)-(3.49), the CSE boundary conditions for local form, as well as the total form, require the total derivative of the external forces. If the external forces are constants or independent of the design variables, the total derivatives are zero. If the external forces are dependent on the design parameters explicitly or implicitly, the force boundary conditions should be given in terms of the sensitivity variables. Hence, the shear force sensitivity boundary condition is given by the total derivative of the lift force from the airfoil as given by the first equation in (3.51). The effective angle of attack α for the transient case here is determined by the initial airfoil incidence angle, tip rotation and the effective angle of attack change due to gust flow and the vertical velocity of the sting tip.

$$\alpha = \alpha_0 + \psi_{\text{tip}} - \frac{w_{\text{tip},t}}{U_\infty} + \alpha_{\text{gust}} \tag{3.74}$$

Hence, substituting Eq. (3.74) to Eq. (3.51), the shear force sensitivity boundary condition for total form CSE is given as

$$\dot{V}_f = \frac{DL_f}{D\alpha}\left(\dot{\psi}_{\text{tip}} - \frac{\dot{w}_{\text{tip},t}}{U_\infty}\right) \tag{3.75}$$

where $\dot{w}_{\text{tip},t}$ is the total derivative of the velocity of the beam tip. The design derivatives of initial angle of attack $\dot{\alpha}_0$ and the angle of attack due to gust $\dot{\alpha}_{\text{gust}}$ are equal to zero, since they are independent of the shape design variable. By using Eq. (3.9), the CSE boundary

condition in Eq. (3.75) can be written in terms of the local sensitivity variable as

$$\dot{V}_f = \frac{DL_f}{D\alpha}\left(\psi'_{\text{tip}} - \frac{w'_{\text{tip},t}}{U_\infty} + \left(\psi_{\text{tip},x} + \frac{w_{\text{tip},xt}}{U_\infty}\right)V(x)\right) \tag{3.76}$$

Eq. (3.76) serves the force sensitivity boundary condition for the local form CSE. The force sensitivity boundary conditions for total form (3.75) and local form (3.76) CSE are similar to (3.50) and (3.51) except only $\alpha = \alpha_0 + \psi_{\text{tip}}$ was used in (3.50) and (3.51). The sensitivity of the lift force with respect to the angle of attack $\frac{DL_f}{D\alpha}$ here can be obtained by solving the potential flow sensitivity and using Eq. (3.64). In contrast, the example in Section 3.3.1 assumed $\frac{DL_f}{D\alpha} = qcC_{l_\alpha}$ for a typical section airfoil. Here, since the external force CSE boundary conditions in Eq. (3.75) and (3.76) are dependent on the sensitivity variables, the CSE equations may be solved iteratively by loosely coupled equations.

Results

The joined beam with an airfoil model shown in Fig. 3.10 subject to a gust load serves as an example for verification of the CSE method for transient aeroelasticity problems. A strut was added to the nonlinear Timoshenko beam with an airfoil model investigated in Section 3.3.1. The strut was rigidly connected to the sting at the middle point with an 45 degree angle. The sting has the same properties of the nonlinear Timoshenko beam in Section 3.3.1. The strut has membrane rigidity $EA = 1.0e5\ N$, shear rigidity $kGA = 1e6\ N$, bending rigidity $EI = 5.0e6\ N \cdot m^2$, rotary inertia $\rho I = 10\ kg \cdot m$ and mass per unit length $\rho A = 40\ kg/m$. The magnitude of inflow velocity is 135 m/s with air density $\rho_a = 1.2\ kg/m^3$. The chord length of the airfoil is 1 m with initial angle of attack $\alpha_0 = 3°$. The one-minus-cosine gust described in Section 3.3.3 starts at $t = 2s$ and ends at $t = 3s$ with the maximum amplitude $V_{g,max} = 9.5\ m/s$.

As seen in Fig. 3.11, the joined beam deforms under the aerodynamic force, while the tip rotation increases the angle of attack of the airfoil, and then further increases the aerodynamic forces. The aerodynamic forces were obtained by solving the potential as described in Section 3.3.2. This flow model is actually a quasi-steady flow, since the inertia and compressibility effects of the flow are not considered. A loosely coupled algorithm was adopted for solving the aeroelastic system. The fluid mesh moves according to the deformation of the airfoil attached to the sting. A mesh moving algorithm based on the pseudo-solid method was implemented. By adjusting the Young's modulus and the Poisson's ratio, this algorithm was able to deal with fairly large mesh deflection.

The transient gust response was investigated and the FSI responses at the sting tip are plotted in Fig. 3.11. Before the gust arrives at $t = 2s$, the joined beam structure reached steady state. When the gust arrives, the structure has a large deflection, and the nonlinear model captures the shortening effects as seen in subfigure (a). After the gust leaves at $t = 3$, the vibration is damped out due to the aerodynamic damping and the response goes back to state steady.

The transient gust response sensitivities with respect to the sting length are calculated by using the total form CSE method. The total form CSE was easier to implement than the local form, since no special treatment is needed at the joint node (Liu and Canfield, 2013a). As can be seen in Fig. 3.12, the nonlinear joined beam gust response sensitivity by total form CSE method matches the complex step results. As far as author's knowledge, this is the first implementation of total form CSE for aeroelastic shape sensitivity problems.

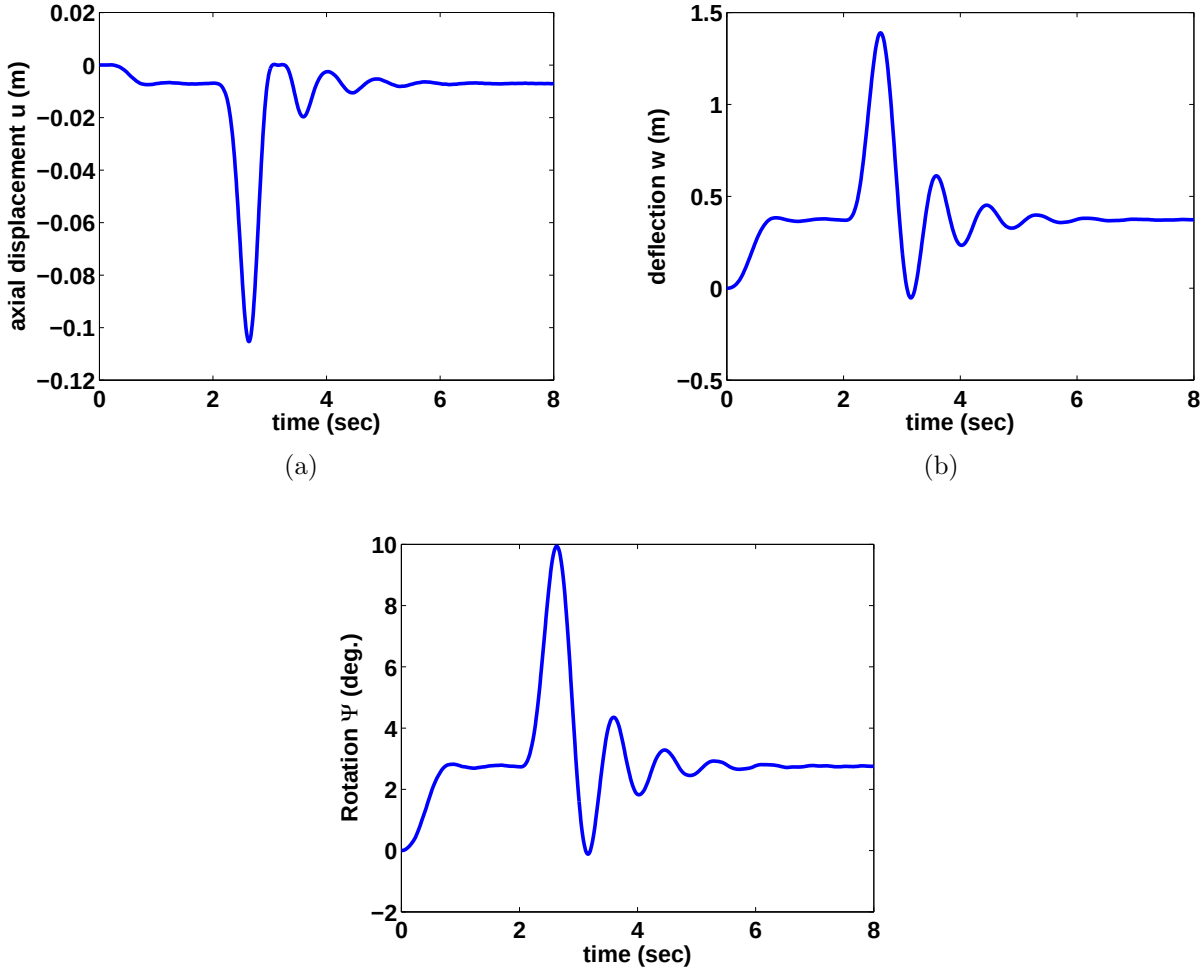

(a) (b) (c)

Figure 3.11: Joined beam gust response at sting tip

3.4 Conclusions

In the present work, the CSE method was derived in both the local form and the total form for the shape sensitivity of fluid-structure interaction problems. The detailed finite element model and the CSEs were derived for a joined beam with an airfoil model. The accuracy, efficiency and implementation of the two forms of CSE method for structures and fluids were compared, based on numerical shape sensitivity results for structural, fluid and fluid-structure interaction problems. The pseudo-solid method was used for calculating domain

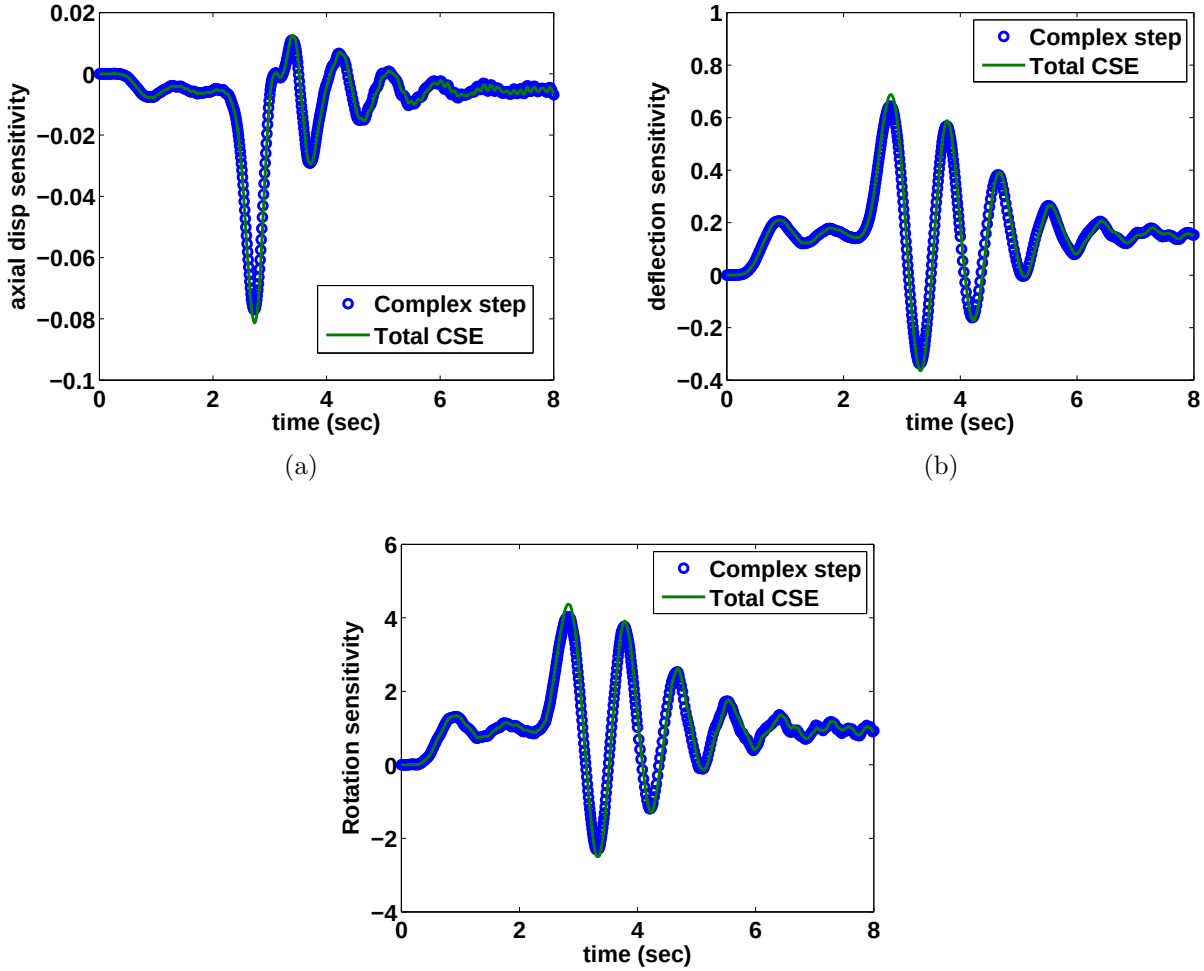

Figure 3.12: Joined beam gust response sensitivity with respect to beam length at sting tip

design velocity needed for the total form CSE and for mesh movement of the FSI solver.

The derivation of total form CSE is complex than the local form CSE, since the material derivatives do not commute with the spatial differentiation. Besides, the smoothness requirement on design velocity for the total form CSE is higher, which makes the parametrization of the domain more difficult. However, the implementation of the total form CSE for build-up structures is easier, since it needs not the special treatment at the strain discontinuous points as required by local form CSE due to the discontinuity of the local sensitivity variable (Liu

and Canfield, 2013a).

The total form CSE was shown to be more accurate than the local form CSE for the numerical models in this study. The local form CSE requires higher order derivatives of the analysis solution only at the boundaries, which tend to be less accurate if displacement-based finite element method is used for solving the analysis problems. On the other hand, the total derivative form CSE makes use of the gradient of the analysis solution in the domain, where the order of derivative of the solution required is lower than the local form. The accuracy of local form CSE method was demonstrated to be improved by using higher order finite element for the analysis problem.

The local form CSE needs design velocity only at boundaries without solving the linear pseudo-solid system for domain design velocity as required by total form, if only the sensitivities at boundaries are of interest, which makes local form CSE more efficient. However, for accurate sensitivity results, the local form CSE needs additional effort for calculating higher order derivatives of the analysis solution on the moving boundary by increasing the order of elements or by adapting the mesh to obtain finer mesh at boundaries.

3.5 Acknowledgements

The Air Force Office of Scientific Research sponsored this research under agreement number FA9550-09-1-0354. The authors gratefully acknowledge the support of AFOSR program manager Dr. Fariba Fahroo and the AFRL Senior Aerospace Engineers Dr. Raymond Kolonay, Dr. Phillip Beran, and Dr. Maxwell Blair.

Bibliography

Arora, J. S., 1993. An exposition of the material derivatives approach for structural shape sensitivity analysis. Computer Methods in Applied Mechanics and Engineering 105, 41–62.

Babuska, I., Aziz, A. K., 1972. Survey lectures on the mathematical foundations of the finite element method. In: The mathematical foundations of the finite element method with applications to partial differential equations. Academic Press, pp. 5–359.

Bhaskaran, R., Berkooz, G., 1997. Optimization of fluid-structure interaction using the sensitivity equation approach. Fluid-Structure Interaction, Aeroelasticity, Flow-Induced Vibrations and Noise. 53 (1), 49–56.

Borggaard, J., Burns, J., 1994. A sensitivity equation approach to shape optimization in fluid flows. Tech. rep., Langley Research Center.

Borggaard, J., Burns, J., 1997. A pde sensitivity equation method for optimal aerodynamic design. Journal of Computational Physics. 136, 366–384.

Choi, K. K., Kim, N.-H., 2005. Structural sensitivity analysis and optimization. Springer Science+Business media, New York.

Cross, D. M., Canfield, R. A., September, 17-19 2012a. Continuum shape sensitivity with spatial gradient reconstruction of nonlinear aeroelastic gust response. In: 14th AIAA/ISSMO Multidisciplinary Analysis and Optimization Conference. No. AIAA 2012-55597. Indianapolis, Indiana.

Cross, D. M., Canfield, R. A., April, 23-26 2012b. Solving continuum shape sensitivity with existing tools for nonlinear aeroelastic gust analysis. In: 53st AIAA/ASME/ASCE/AHS/ASC Structures, Structural Dynamics, and Materials Conference. No. AIAA 2012-1923. Honolulu, Hawaii.

Dems, K., Mroz, Z., 1985. Variational approach to first- and second-order sensitivity analysis of elastic structures. International Journal for Numerical Methods in Engineering 21, 637–661.

Duvigneau, R., Pelletier, D., 2006. On accurate boundary conditions for a shape sensitivity equation method. International Journal for Numerical Methods in Fluids 50, 147–164.

Etienne, S., Hay, A., Garon, A., 2006. Shape sensitivity analysis of fluid-structure interaction problems. No. AIAA 2006-3217.

Etienne, S., Hay, A., Garon, A., 2007. Sensitivity analysis of unsteady fluid-structure interaction problems. No. AIAA-2007-332.

Etienne, S., Pelletier, D., 2005. A general approach to sensitivity analysis of fluid-structure interactions. Journal of Fluids and Structures 21 (2), 169–186.

Gill, P. E., a. M. W., Wright, M. H., 1981. Practical Optimization. Vol. 177. Academic Press, San Diego, CA.

Haftka, R. T., Gurdal, Z., 1992. Elements of Structural Optimization. Kluwer Academic Publishers.

Haug, E. J., Arora, J. S., 1978. Design sensitivity analysis of elastic mechanical systems. Computer Methods in Applied Mechanics and Engineering 15 (1), 35–62.

Haug, E. J., Choi, K. K., Komkov, V., 1986. Design sensitivity analysis of structural systems, Mathematics in science and engineering. Vol. 177. Academic Press, Orlando.

Haug, E. J., Rousselet, B., 1980. Design sensitivity analysis in structural mechanics, I. static response variations. Journal of Structural Mechanics 8 (1), 17–41.

Hoblit, F., 1988. Gust loads on aircraft : concepts and applications. AIAA education series. American Institute of Aeronautics and Astronautics., Washington, D.C.

Jameson, A., 1988. Aerodynamic design via control theory. Journal of Scientific Computing 3, 233–260, 10.1007/BF01061285.
URL http://dx.doi.org/10.1007/BF01061285

Johnson, A. A., Tezduyar, T. E., 1994. Mesh update strategies in parallel finite element computations of flow problems with moving boundaries and interfaces. Computer Methods in Applied Mechanics and Engineering 119, 73–94.

Liu, S., Canfield, R. A., April, 4-7 2011. Continuum shape sensitivity for nonlinear transient aeroelastic gust response. In: 52nd AIAA/ASME/ASCE/AHS/ASC Structures, Structural Dynamics, and Materials Conference. No. AIAA 2011-1971. Denver, Colorado.

Liu, S., Canfield, R. A., September, 17-19 2012. Continuum sensitivity method for aeroelastic shape design problems. In: 14th AIAA/ISSMO Multidisciplinary Analysis and Optimization Conference. No. AIAA 2012-5480. Indianapolis, Indiana.

Liu, S., Canfield, R. A., 2013a. Boundary velocity method for continuum shape sensitivity of nonlinear fluid–structure interaction problems. Journal of Fluids and Structures.
URL http://dx.doi.org/10.1016/j.jfluidstructs.2013.05.003

Liu, S., Canfield, R. A., 2013b. Equivalence of discrete analytic and continuum sensitivity methods for nonlinear differential equations. Accepted for publication in Structural and Multidisciplinary Optimization.

Marchman, J. F., 1999. Panel: A “smith-hess” type of 2-d panel code combining source panels and vortices for a single-element, lifting airfoil in incompressible flow. Virginia

Tech.

URL `http://www.dept.aoe.vt.edu/ marchman/software/index.html`

Martins, J. R. R. A., 2003. The complex-step derivative approximation. ACM Transactions on Mathematical Software. 29 (3), 245–262.

Reddy, J., 2006. An introduction to nonlinear finite element analysis. McGraw-Hill series in mechanical engineering. McGraw-Hill Higher Education, New York,NY.

Squire, W., Trapp, G., 1998. Using complex variables to estimate derivatives of real functions. SIAM Review 40 (1), 110–112.

Stanley, L., Stewart, D., 2002. Design sensitivity analysis : computational issues of sensitivity equation methods. Academic Press, Philadelphia.

Szabo, B. A., Babuska, I., 1991. Finite element analysis. Wiley, New York.

Turgeon, E., Pelletier, D., Borggaard, J., 1999. A continuous sensitivity equation approach to optimal design in mixed convection. No. AIAA 99-3625.

Wickert, D. P., Canfield, R. A., Reddy, J. N., 2009. Fluid-structure transient gust sensitivity using least-squares continuous sensitivity analysis. In: 50th AIAA/ASME/ASCE/AHS/ASC Structures, Structural Dynamics, and Materials Conference. No. AIAA-2008-1821. Palm Springs, California.

Wickert, P. D., Aug. 2009. Least-squares, continuous sensitivity analysis for nonlinear fluid-structure interaction problems. Ph.D. thesis, Air Force Institute of Technology, Ohio.

Zienkiewicz, O. C., Zhu, J. Z., 1992. The superconvergent patch recovery and a posteriori error estimates. part 1: The recovery technique. International Journal of Numerical Methods in Engineering 33, 1331–1364.

Chapter 4

Equivalence of Continuum and Discrete Analytic Sensitivity Methods for Nonlinear Differential Equations[1]

Abstract

This paper presents results for the study of equivalence between the total form continuum sensitivity equation (CSE) method and the discrete analytic method of shape design sensitivity analysis. For the discrete analytic method, the sensitivity equations are obtained by taking analytic derivatives of the discretized equilibrium equations with respect to the shape design parameters. For the CSE method, the equilibrium equations are firstly differentiated to form a set of linear continuous sensitivity equations and then discretized for solving the shape sensitivities. The sensitivity equations can be derived by taking the material derivatives (total form) or the partial derivatives (local form) of the equilibrium equations. The total form CSE method is shown for the first time to be equivalent, after finite element discretization, to the discrete analytic method for nonlinear second-order differential equations of a particular form with design dependent loads when they use the same: (1) finite element discretization, (2) numerical integration of element matrices, (3) design velocity fields that are linear with respect to the design variable and (4) shape functions for domain

[1]Accepted for publication in *Structural and Multidisciplinary Optimization* co-authored with Robert A. Canfield

transformation and for design velocity field calculations. The shape sensitivity equations for three-dimensional geometric nonlinear elastic structures and linear potential flow are derived by using both total form CSE and discrete analytic method to show the equivalence of the two methods for these specific examples. The accuracy of shape sensitivity analysis is verified by potential flow around an airfoil and a joined beam with an airfoil under gust load. The results show that analytic sensitivity results are consistent with the complex step results.

Keywords: Shape sensitivity, Continuum sensitivity equations, Discrete analytic sensitivity, Geometric nonlinear structure, Fluid-structure interaction

---

4.1 Introduction

In a gradient-based optimization procedure, the design sensitivity analysis (DSA), which calculates the gradients of performance measures with respect to the design variables, is a key step. Sensitivity analysis often becomes the determining factor of the efficiency and accuracy of the optimal design procedure, especially for shape design of structures and fluid boundaries. The developments in DSA have led to the emergence of three fundamentally different approaches: (1) the discrete method, (2) the continuum method, and (3) automatic differentiation. In the discrete approach, the governing equations are first discretized and then used to carry out the DSA. There are four different methods in the discrete DSA approach: finite difference method, complex step method, discrete analytic method, and discrete semi-analytic method. In the continuum method, the continuum equations are first differentiated, then discretized. The continuum sensitivity equations can be posed in the total form or the local form. The comparison of these two forms has been investigated by Liu and Canfield (2012).

The finite difference (FD) method is widely used due to its simplicity of implementation, but a drawback of the finite difference method is the challenge of determining the optimum step size. Large step sizes are dominated by truncation error and small step sizes are dominated by numerical round-off error. The complex step method is not subject to subtractive cancelation error (Squire and Trapp, 1998), which is a tremendous advantage over the finite difference method. A very small step size can be used to minimize the truncation error while avoiding the round-off error. Both methods involve solving the original analysis problem at least $n + 1$ times for n design variables, which makes these methods inefficient, especially for nonlinear problems. An advantage of the FD and complex step methods is that they do not require much knowledge of governing equations and the analysis procedures. However the analytic and discrete semi-analytic methods require understanding the details of the analysis procedure, since they need the derivatives of the system matrices. In the semi-analytic method, the derivatives of the system matrices are computed by finite difference, hence, it shares some drawbacks of the FD method. Moreover, it has been shown that the semi-analytic method can have serious accuracy problems for shape design variables (Barthelemy and Haftka, 1988). In the analytic method, the derivatives of the system matrices are obtained analytically, which is more accurate, but somewhat costly because of the mesh sensitivity. For an extensive list of references for DSA methods in general see Olhoff and Taylor (1983), Haug et al (1986), Haftka and Grandhi (1986), Haftka and Adelman (1989), Tortorelli and Michaleris (1994), and van Keulen et al (2005).

The continuum sensitivity method, also known as the variational sensitivity method (Haftka and Gurdal, 1992), variational shape design (Haug et al, 1986), and the continuous sensitivity equation method (Borggaard and Burns, 1997), was first introduced for structural problems (Haug and Arora, 1978; Haug and Rousselet, 1980; Dems and Mroz, 1985; Dems and Haftka, 1988). Choi and Kim (2005) cite the lion's share of structural elasticity applications that

employ continuum sensitivity methods. Jameson (1988) first introduced continuum sensitivity concept in adjoint equation form for aerodynamic design problems. Borggaard and Burns (1994) introduced the CSE nomenclature in a fluid setting and several fluid flow optimization applications followed (Borggaard and Burns, 1997; Turgeon et al, 1999; Stanley and Stewart, 2002). Bhaskaran and Berkooz (1997) present the earliest continuum sensitivity solution for fluid-structure interaction, albeit for one-way structure to fluid coupling. Pelletier et al. have employed continuum sensitivity methods for a range of fluid-structure interaction problems (Etienne and Pelletier, 2005; Etienne et al, 2006, 2007) with prominent success; their work primarily focuses on flow variable sensitivities. Wickert et al (2009) recently applied the CSE method to the gust sensitivity for a simple airfoil mounted to a 1D Euler-Bernoulli beam. Recent work applied the CSE method to transient nonlinear fluid-structure interaction problems such as a joined beam structure with a typical section airfoil (Liu et al, 2010; Liu and Canfield, 2011, 2012).

Continuum sensitivity systems are often posed in terms of the local derivative (an Eulerian reference frame) for fluids (Borggaard and Burns, 1997; Etienne and Pelletier, 2005) and the material derivative (Lagrangian reference frame) for solids (Haug et al, 1986; Choi and Kim, 2005). For shape optimization of fluid applications, an Eulerian description of the flow sensitivity is often adequate. Thus, much of the fluid mechanics literature does not emphasize the distinction between the local and total derivative. For structural optimization problems, however, the design sensitivity at a material point is usually required, which necessitates means to calculate total sensitivities at a given material point. Liu and Canfield (2012) compared local and total form CSE and showed that the total derivative form of CSE for shape sensitivity may be more accurate than the local derivative form, if the displacement finite element method (FEM) is used for the analysis problem, due to less accuracy of FEM at the boundaries. As a result, higher order finite elements are recommended for local form

CSE. The total derivative form is more generally applicable for built-up structures with strain discontinuities, since the material derivative remains continuous (Liu and Canfield, 2011). However, as we will show in this paper, the total form CSE is identical to the discrete analytic method under certain conditions.

Several comparisons between the discrete methods and the continuum methods have been made in the literature. Yang and Botkin (1986) gave a comparison between the discrete semi-analytic method and the continuum method. Haftka and Adelman (1989) state that the continuum methods require only minimal knowledge of the structural analysis code, which is often inaccessible and very complex. The equivalence of total form CSE (continuum) and discrete methods have been investigated by several authors (Choi and Twu, 1988; Akbari et al, 2010). Akbari et al (2010) showed that both methods are equivalent for linear elasticity when the same discretization, numerical integration and linear design velocity fields are used. These conditions are more general than previously observed by Choi and Twu (1988) in which exact integration and exact analytical solutions were required to demonstrate equivalence. In both papers, equivalence was established only for linear static elasticity problems. The purpose of this paper is to generalize this comparison for transient nonlinear differential equations of a certain form, including the nonlinear elastic structures and fluid flow problems. In fact, this is the first proof that shows the equivalence of the two methods for transient nonlinear field problems. Another requirement for the equivalence is added to the previous study by Akbari et al (2010), which is that the shape functions for domain transformation of a finite element's geometry to a master element for numeric integration must be the same as used for design velocity field calculation of the discretized total form CSE.

4.2 Material derivatives

In this section, some material derivative identities are introduced (Haug et al, 1986; Arora, 1993; Choi and Kim, 2005). They are important, because the derivation of sensitivity equations in total form is a direct application of these material derivative expressions. In shape design, the shape of the physical domain is parameterized by the design variable. Suppose that the initial domain Ω with boundary S is changed to the perturbed domain Ω_b with boundary S_b due to the change of design variable b as shown in Fig.4.1. Thus, when $b = 0$, it is the current domain. Let $\boldsymbol{x}_b(\boldsymbol{x}, b)$ to be the independent variable in the perturbed domain Ω_b. The transformation $\boldsymbol{x}_b(\boldsymbol{x}, b)$ is a one to one mapping from domain Ω to Ω_b. Using a linear Taylor's expansion at $b = 0$, the coordinates in perturbed domain $\boldsymbol{x}_b(\boldsymbol{x}, b)$ can be given as

$$\boldsymbol{x}_b(\boldsymbol{x}, b) = \boldsymbol{x} + b\,\boldsymbol{V}(\boldsymbol{x}) \tag{4.1}$$

where $\boldsymbol{x}_b(\boldsymbol{x}, 0) = \boldsymbol{x}$ and $\boldsymbol{V}(\boldsymbol{x}) = \frac{\partial \boldsymbol{x}}{\partial b}$ have been used. The quantity $\boldsymbol{V}(\boldsymbol{x})$ is called the design velocity. The total derivative of a scalar field $u(x; b)$ with respect to b at $b = 0$ is a directional derivative in the direction of $\boldsymbol{V}$, which can be obtained as (Arora, 1993; Choi and Kim, 2005)

$$\dot{u}(\boldsymbol{x}) = u' + \boldsymbol{V}(\boldsymbol{x}) \cdot \nabla u \tag{4.2}$$

where ∇ is the spatial gradient operator. From here on, the over-dot represents a material derivative and the prime represents a local derivative. The material (total) derivative defined in (4.2) consists of the local design derivative u', plus the convective term involving the design velocity. Equation (4.2) is the basic material derivative identity. With this identity, the following useful identities can be derived.

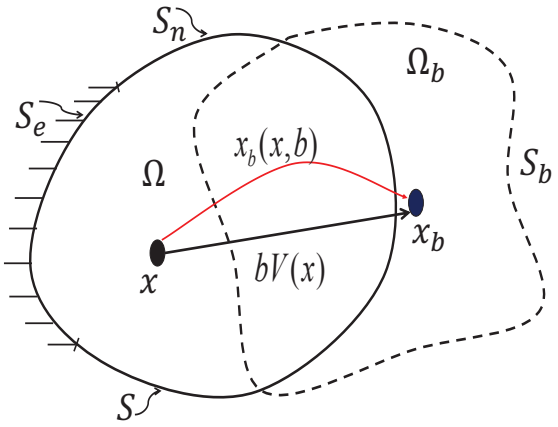

Figure 4.1: Variation of domain due to shape change.

Let u be a scalar field and $\boldsymbol{A}$ be a vector of spatial differential operators. Then

$$\overline{\dot{\boldsymbol{A}u}} = \boldsymbol{A}\dot{u} - (\boldsymbol{A}\,\boldsymbol{V})^T \nabla u \tag{4.3}$$

For instance, if $\boldsymbol{A} = \nabla$, then we have

$$\overline{\dot{\nabla u}} = \nabla\dot{u} - (\nabla\,\boldsymbol{V})^T \nabla u \tag{4.4}$$

Let $\boldsymbol{u}$ be a vector field, $\boldsymbol{A}$ be a matrix of spatial differential operators and $\boldsymbol{A} = [\boldsymbol{A}_1, \boldsymbol{A}_2, \cdots, \boldsymbol{A}_j, \cdots]$. Then

$$\overline{\dot{\boldsymbol{A}\boldsymbol{u}}} = \boldsymbol{A}\dot{\boldsymbol{u}} - (\boldsymbol{A}_j\,\boldsymbol{V})^T \nabla \boldsymbol{u}_j \tag{4.5}$$

Here implied summation is assumed over the repeated index $j = 1, 2, \cdots$. If

$$\boldsymbol{A} = \boldsymbol{\nabla} = \begin{pmatrix} \nabla & 0 & 0 \\ 0 & \nabla & 0 \\ 0 & 0 & \nabla \end{pmatrix} \tag{4.6}$$

then we have

$$\overline{\dot{\boldsymbol{\nabla}\boldsymbol{u}}} = \boldsymbol{\nabla}\dot{\boldsymbol{u}} - (\boldsymbol{\nabla}_j \boldsymbol{V})^T \nabla \boldsymbol{u}_j = \boldsymbol{\nabla}\dot{\boldsymbol{u}} - \boldsymbol{\Lambda}^T \boldsymbol{\nabla}\boldsymbol{u} \tag{4.7}$$

where

$$\boldsymbol{\Lambda} = \begin{pmatrix} \nabla \boldsymbol{V} & 0 & 0 \\ 0 & \nabla \boldsymbol{V} & 0 \\ 0 & 0 & \nabla \boldsymbol{V} \end{pmatrix} \tag{4.8}$$

4.3 Shape sensitivity for a general field problem

4.3.1 Equations for a general field problem

The governing equations of many field problems, such as structural and fluid problems, are second-order partial differential equations in terms of dependent variables $\boldsymbol{u}(\boldsymbol{x}, t; b)$ and can be written in a general form as

$$\boldsymbol{L}_t(\boldsymbol{u}) + \boldsymbol{A}_x\left(\boldsymbol{u}, \boldsymbol{L}_x(\boldsymbol{u})\right) = \boldsymbol{f}_b(\boldsymbol{x}, t) \tag{4.9}$$

where $\boldsymbol{L}_t(\boldsymbol{u})$ is a vector of linear time derivatives of $\boldsymbol{u}$, $\boldsymbol{A}_x\left(\boldsymbol{u}, \boldsymbol{L}_x(\boldsymbol{u})\right)$ can be a vector of linear or nonlinear functions of $\boldsymbol{u}$ and spatial derivatives $\boldsymbol{L}_x(\boldsymbol{u})$. The highest derivatives of $\boldsymbol{u}$ in $\boldsymbol{L}_x(\boldsymbol{u})$ are assumed to be second derivatives and the operator is linear with respect to second derivatives. The particular nonlinear form of (4.9) can represent many second-order field problems of physics, such as structural and fluid problems. For example, (4.9) may represent geometric nonlinearity in elasticity, however, it may not represent all models of material nonlinearity, such as elasto-plasticity.

The weak form of a second-order field problem can be written as

$$\int_{\Omega} \delta \boldsymbol{u} \cdot \boldsymbol{L}_t(\boldsymbol{u}) + \boldsymbol{D}(\delta \boldsymbol{u}, \boldsymbol{u}) \cdot \boldsymbol{A}(\boldsymbol{u})\, dV = \int_{\Omega} \delta \boldsymbol{u} \cdot \boldsymbol{f}_b\, dV + \int_{S} \delta \boldsymbol{u} \cdot \boldsymbol{T}\, dS \tag{4.10}$$

with the essential and natural boundary conditions,

$$\boldsymbol{u} = \boldsymbol{u}_0 \quad \text{on} \quad S_e \tag{4.11}$$

$$\boldsymbol{T} = \boldsymbol{T}_0 \quad \text{on} \quad S_n \tag{4.12}$$

where $\boldsymbol{A}(\boldsymbol{u})$ can be a vector of linear or nonlinear functions of $\boldsymbol{u}$ and first spatial derivatives of $\boldsymbol{u}$, since the linear second derivative terms in (4.9) have been transformed to the first derivatives by integrating by parts. The spatially weak form is used here to maintain lower differentiability requirements on the spatial derivatives and to develop the finite element model from an integral form. $\delta \boldsymbol{u}$ is the test function or the perturbation that satisfies the homogeneous essential boundary conditions, and it should satisfy the continuity requirements of the weak form. $\boldsymbol{D}(\delta \boldsymbol{u}, \boldsymbol{u})$ can be written as a mapping from $\boldsymbol{\nabla} \delta \boldsymbol{u}$ and $\delta \boldsymbol{u}$ as

$$\boldsymbol{D}(\delta \boldsymbol{u}, \boldsymbol{u}) = \boldsymbol{S}^D \boldsymbol{\nabla} \delta \boldsymbol{u} + \boldsymbol{S}^u \delta \boldsymbol{u} \tag{4.13}$$

where the mapping matrices $\boldsymbol{S}^D$ and $\boldsymbol{S}^u$ are functions of dependent variable $\boldsymbol{u}$ and the first spatial derivatives of $\boldsymbol{u}$.

In order to solve the field problems numerically, the weak form (4.10) can be discretized by the finite element method and integrated in the computational domain with coordinates $\boldsymbol{\xi}$. In the Galerkin finite element method, the dependent variables and the test function can be

approximated using the same shape functions $\boldsymbol{N}(\boldsymbol{\xi})$ as

$$\delta \boldsymbol{u} \doteq \delta \overline{\boldsymbol{u}} = \boldsymbol{N}(\boldsymbol{\xi}) \delta \boldsymbol{u}^e \tag{4.14}$$

$$\boldsymbol{u} \doteq \overline{\boldsymbol{u}} = \boldsymbol{N}(\boldsymbol{\xi}) \boldsymbol{u}^e \tag{4.15}$$

where the over-bar denotes the approximated values in an element. Substituting the approximation in Eq. (4.14)-(4.15), the discretized equations of the weak form (4.10) for a single element can be obtained as

$$\begin{aligned} &\int_{\bar{\Omega}} \left[\delta \overline{\boldsymbol{u}} \cdot \boldsymbol{L}_t(\overline{\boldsymbol{u}}) + \boldsymbol{D}(\delta \overline{\boldsymbol{u}}, \overline{\boldsymbol{u}}) \cdot \boldsymbol{A}(\overline{\boldsymbol{u}}) \right] |\boldsymbol{J}| d\bar{V} = \\ &\delta \boldsymbol{u}^e \cdot \int_{\bar{\Omega}} \left[\boldsymbol{N}^T \boldsymbol{f}_b \right] |\boldsymbol{J}| \; d\bar{V} + \int_{\bar{S}} \boldsymbol{N}^T \boldsymbol{T} |\boldsymbol{J}| \| \boldsymbol{J}^{-T} \boldsymbol{k} \| \; d\bar{S} \end{aligned} \tag{4.16}$$

where $\bar{\Omega}$ is the computational domain or master element expressed in natural coordinates that map to an element in Ω, $\boldsymbol{J}$ is the Jacobian for the transformation and $\boldsymbol{J}^{-T} = (\boldsymbol{J}^{-1})^T$. $d\bar{V}$ and $d\bar{S}$ are differential volume and surface of the computational domain. Unit vector $\boldsymbol{k}$ is the normal vector of the differential surface in the computational domain.

4.3.2 Total form CSE for a general field problem

Derivation of the CSE

The total form CSE can be derived by taking the material derivative of the weak form (4.10) and forming a new set of equations in terms of the total sensitivity variables $\dot{\boldsymbol{u}}$. Using an over-dot to represent the material derivative, the total form CSE of the general field problem

can be derived by taking material derivative of (4.10) as

$$\begin{aligned}
&\int_\Omega \delta \boldsymbol{u} \cdot \dot{\overline{\boldsymbol{L}_t(\boldsymbol{u})}} + \dot{\overline{\boldsymbol{D}(\delta \boldsymbol{u}, \boldsymbol{u})}} \cdot \boldsymbol{A}(\boldsymbol{u}) + \boldsymbol{D}(\delta \boldsymbol{u}, \boldsymbol{u}) \cdot \dot{\overline{\boldsymbol{A}(\boldsymbol{u})}} dV \\
&= \int_\Omega \delta \boldsymbol{u} \cdot \dot{\boldsymbol{f}}_b \, dV + \int_S \delta \boldsymbol{u} \cdot \dot{\boldsymbol{T}} \, dS + \int_S \delta \boldsymbol{u} \cdot \boldsymbol{T} \, \dot{\overline{dS}} \\
&+ \int_\Omega \left[\delta \boldsymbol{u} \cdot \boldsymbol{f}_b - \delta \boldsymbol{u} \cdot \boldsymbol{L}_t(u) - \boldsymbol{D}(\delta \boldsymbol{u}, \boldsymbol{u}) \cdot \boldsymbol{A}(\boldsymbol{u}) \right] \, \dot{\overline{dV}}
\end{aligned} \tag{4.17}$$

The material derivatives of the differential volume and surface area can be found in several references (Haug et al, 1986; Arora, 1993; Choi and Kim, 2005)

$$\dot{\overline{dV}} = (\nabla \cdot \boldsymbol{V}) dV \tag{4.18}$$

$$\dot{\overline{dS}} = \left[\nabla \cdot \boldsymbol{V} - (\nabla \boldsymbol{V})^T \boldsymbol{n} \cdot \boldsymbol{n} \right] dS \tag{4.19}$$

where $\boldsymbol{n}$ is the unit vector normal to the surface of physical domain.

For material derivative of the time derivative term $\boldsymbol{L}_t(u)$, the order of differentiation commutes, since the shape design parameter is not a function of time.

$$\dot{\overline{\boldsymbol{L}_t(\boldsymbol{u})}} = \boldsymbol{L}_t(\dot{\boldsymbol{u}}) \tag{4.20}$$

The material derivative of $\boldsymbol{A}(\boldsymbol{u})$ can be derived by using the chain rule. Since all the entries of $\boldsymbol{A}(\boldsymbol{u})$ are functions of $\boldsymbol{u}$ and first spatial derivatives of $\boldsymbol{u}$, the derivatives can be carried out as a mapping of the material derivatives of the dependent variable gradients. Using the material identity in Eq. (4.7), we have

$$\dot{\overline{\boldsymbol{A}(\boldsymbol{u})}} = \boldsymbol{S}_1^A \dot{\overline{\boldsymbol{\nabla} \boldsymbol{u}}} + \boldsymbol{S}_2^A \dot{\boldsymbol{u}} = \boldsymbol{S}_1^A \left(\boldsymbol{\nabla} \dot{\boldsymbol{u}} - \boldsymbol{\Lambda}^T \boldsymbol{\nabla} \boldsymbol{u} \right) + \boldsymbol{S}_2^A \dot{\boldsymbol{u}} \tag{4.21}$$

where the mapping matrices $\boldsymbol{S}_1^A$ and $\boldsymbol{S}_2^A$ can be constant matrices for linear problems or

functions of the dependent variables $\boldsymbol{u}$ or its spatial derivatives for nonlinear problems.

The following lemma is given to evaluate the second integrand term of (4.17) in terms of the total sensitivity variable $\dot{\boldsymbol{u}}$.

Lemma 3.1 Given a vector $\boldsymbol{A}(\boldsymbol{u})$, the elements of which are functions of the dependent variables $\boldsymbol{u}$ or its first spatial derivatives, the material derivative of the perturbation term $\boldsymbol{D}(\delta\boldsymbol{u}, \boldsymbol{u})$ vector product by $\boldsymbol{A}(\boldsymbol{u})$ can be represented in matrix form as

$$\begin{aligned}
&\mathbb{D}\left\{\boldsymbol{D}(\delta\boldsymbol{u}, \boldsymbol{u})\right\} \cdot \boldsymbol{A}(\boldsymbol{u}) = \boldsymbol{\nabla}\delta\boldsymbol{u} \cdot \left(\boldsymbol{M}_1^D \mathbb{D}\{\boldsymbol{\nabla}\boldsymbol{u}\} + \boldsymbol{M}_2^D \mathbb{D}\{\boldsymbol{u}\}\right) \\
&+ \delta\boldsymbol{u} \cdot \left(\boldsymbol{M}_1^u \mathbb{D}\{\boldsymbol{\nabla}\boldsymbol{u}\} + \boldsymbol{M}_2^u \mathbb{D}\{\boldsymbol{u}\}\right) \\
&+ \mathbb{D}\left\{\boldsymbol{\nabla}\delta\boldsymbol{u}\right\} \cdot (\boldsymbol{S}^D)^T \boldsymbol{A}(\boldsymbol{u}) + \mathbb{D}\left\{\delta\boldsymbol{u}\right\} \cdot (\boldsymbol{S}^u)^T \boldsymbol{A}(\boldsymbol{u})
\end{aligned} \tag{4.22}$$

where $\mathbb{D}\{\ \}$ can be material derivatives, partial derivatives or any other derivatives that satisfy the chain rule and product rule. The entries of the mapping matrices $\boldsymbol{M}_i^D$ and $\boldsymbol{M}_i^u$ are functions of entries of $\boldsymbol{\nabla}\boldsymbol{u}$ or $\boldsymbol{u}$.

Applying *Lemma 3.1* to the second term of (4.17), we have

$$\begin{aligned}
&\overline{\boldsymbol{D}(\delta\boldsymbol{u}, \boldsymbol{u})}^{\cdot} \cdot \boldsymbol{A}(\boldsymbol{u}) = -\left(\boldsymbol{\Lambda}^T \boldsymbol{\nabla}\delta\boldsymbol{u}\right) \cdot (\boldsymbol{S}^D)^T \boldsymbol{A}(\boldsymbol{u}) \\
&+ \boldsymbol{\nabla}\delta\boldsymbol{u} \cdot \left(\boldsymbol{M}_1^D \left(\boldsymbol{\nabla}\dot{\boldsymbol{u}} - \boldsymbol{\Lambda}^T \boldsymbol{\nabla}\boldsymbol{u}\right) + \boldsymbol{M}_2^D \dot{\boldsymbol{u}}\right) \\
&+ \delta\boldsymbol{u} \cdot \left(\boldsymbol{M}_1^u \left(\boldsymbol{\nabla}\dot{\boldsymbol{u}} - \boldsymbol{\Lambda}^T \boldsymbol{\nabla}\boldsymbol{u}\right) + \boldsymbol{M}_2^u \dot{\boldsymbol{u}}\right)
\end{aligned} \tag{4.23}$$

Since $\delta\boldsymbol{u}$ is the perturbation of the dependent variable, if we assume that $\delta\boldsymbol{u}$ is independent of the design, then we have $\dot{\delta\boldsymbol{u}} = 0$. However, even this assumption is not necessary. Since $\dot{\delta\boldsymbol{u}}$ is a kinematically admissible field, all the terms contain $\dot{\delta\boldsymbol{u}}$ satisfy the governing equations and will cancel out in the CSE (4.24). Nevertheless, $\dot{\delta\boldsymbol{u}} = 0$ has been applied to (4.23).

Substituting Eqs. (4.18)-(4.21) and (4.23) into (4.17) and applying (4.13) for $\boldsymbol{D}(\delta\boldsymbol{u},\boldsymbol{u})$, the total form CSE of a general field problem can be obtained as

$$
\begin{aligned}
&\int_\Omega \big[\delta\boldsymbol{u}\cdot\boldsymbol{L}_t(\dot{\boldsymbol{u}}) + (\boldsymbol{\nabla}\delta\boldsymbol{u})^T\left((\boldsymbol{S}^D)^T\boldsymbol{S}_1^A + \boldsymbol{M}_1^D\right)\boldsymbol{\nabla}\dot{\boldsymbol{u}}\\
&+ (\delta\boldsymbol{u})^T\left((\boldsymbol{S}^u)^T\boldsymbol{S}_1^A + \boldsymbol{M}_1^u\right)\boldsymbol{\nabla}\dot{\boldsymbol{u}}\\
&+ (\boldsymbol{\nabla}\delta\boldsymbol{u})^T\left((\boldsymbol{S}^D)^T\boldsymbol{S}_2^A + \boldsymbol{M}_2^D\right)\dot{\boldsymbol{u}}\\
&+ (\delta\boldsymbol{u})^T\left((\boldsymbol{S}^u)^T\boldsymbol{S}_2^A + \boldsymbol{M}_2^u\right)\dot{\boldsymbol{u}}\big]\ dV\\
&= \int_\Omega \delta\boldsymbol{u}\cdot\dot{\boldsymbol{f}}_b\ dV + \int_S \delta\boldsymbol{u}\cdot\dot{\boldsymbol{T}}\ dS\\
&+ \int_\Omega (\boldsymbol{\nabla}\delta\boldsymbol{u})^T\boldsymbol{\Lambda}(\boldsymbol{S}^D)^T\boldsymbol{A}(\boldsymbol{u})\ dV\\
&+ \int_\Omega (\boldsymbol{\nabla}\delta\boldsymbol{u})^T\left((\boldsymbol{S}^D)^T\boldsymbol{S}_1^A + \boldsymbol{M}_1^D\right)\left(\boldsymbol{\Lambda}^T\boldsymbol{\nabla}\boldsymbol{u}\right)\ dV\\
&+ \int_\Omega (\delta\boldsymbol{u})^T\left((\boldsymbol{S}^u)^T\boldsymbol{S}_1^A + \boldsymbol{M}_1^u\right)\left(\boldsymbol{\Lambda}^T\boldsymbol{\nabla}\boldsymbol{u}\right)\ dV\\
&+ \int_\Omega \big[\delta\boldsymbol{u}\cdot\boldsymbol{f}_b - \delta\boldsymbol{u}\cdot\boldsymbol{L}_t(\boldsymbol{u})\\
&- (\boldsymbol{\nabla}\delta\boldsymbol{u})^T(\boldsymbol{S}^D)^T\boldsymbol{A}(\boldsymbol{u}) - (\delta\boldsymbol{u})^T(\boldsymbol{S}^u)^T\boldsymbol{A}(\boldsymbol{u})\big](\nabla\cdot\boldsymbol{V})dV\\
&+ \int_S \delta\boldsymbol{u}\cdot\boldsymbol{T}\big[\nabla\cdot\boldsymbol{V} - (\nabla\boldsymbol{V})^T\boldsymbol{n}\cdot\boldsymbol{n}\big]\ dS
\end{aligned}
\tag{4.24}
$$

The left-hand side of design sensitivity equation (4.24) is expressed in terms of the total sensitivity variable $\dot{\boldsymbol{u}}$, which, for linear problems, takes the same form as that of the analysis in (4.10). Even for nonlinear problems, the CSE is still a linear system with respect to $\dot{\boldsymbol{u}}$. All the nonlinear terms of $\boldsymbol{u}$ are obtained from the analysis solution. The right-hand side of Eq. (4.24) is comprised of the fictitious load terms. The material derivative of external load $\dot{\boldsymbol{f}}_b$ and $\dot{\boldsymbol{T}}$ vanish for design independent external loads. For design dependent loads, the material derivative of external loads can be obtained by solving the sensitivity of another field problem that generates the loads, for instance the pressure sensitivity for fluid-structure interaction problems.

Discretization of the CSE

The CSE (4.24) is continuous. To solve for the sensitivities, $\dot{\boldsymbol{u}}$, it can be discretized using the finite element method as for the analysis field problem. The same set of shape functions in (4.14) can be used to approximate the sensitivity variables,

$$\dot{\boldsymbol{u}} \doteq \dot{\overline{\boldsymbol{u}}} = \boldsymbol{N}(\boldsymbol{\xi})\dot{\boldsymbol{u}}^e \tag{4.25}$$

The gradient matrix of the design velocity can be obtained as (Akbari et al, 2010)

$$\begin{aligned}(\nabla V) &= \begin{pmatrix} \frac{\partial V_1}{\partial x_1} & \frac{\partial V_1}{\partial x_2} & \frac{\partial V_1}{\partial x_3} \\ \frac{\partial V_2}{\partial x_1} & \frac{\partial V_2}{\partial x_2} & \frac{\partial V_2}{\partial x_3} \\ \frac{\partial V_3}{\partial x_1} & \frac{\partial V_3}{\partial x_2} & \frac{\partial V_3}{\partial x_3} \end{pmatrix} \\ &= \begin{pmatrix} \frac{\partial V_1}{\partial \xi} & \frac{\partial V_1}{\partial \eta} & \frac{\partial V_1}{\partial \zeta} \\ \frac{\partial V_2}{\partial \xi} & \frac{\partial V_2}{\partial \eta} & \frac{\partial V_2}{\partial \zeta} \\ \frac{\partial V_3}{\partial \xi} & \frac{\partial V_3}{\partial \eta} & \frac{\partial V_3}{\partial \zeta} \end{pmatrix} \begin{pmatrix} \frac{\partial \xi}{\partial x_1} & \frac{\partial \xi}{\partial x_2} & \frac{\partial \xi}{\partial x_3} \\ \frac{\partial \eta}{\partial x_1} & \frac{\partial \eta}{\partial x_2} & \frac{\partial \eta}{\partial x_3} \\ \frac{\partial \zeta}{\partial x_1} & \frac{\partial \zeta}{\partial x_2} & \frac{\partial \zeta}{\partial x_3} \end{pmatrix} = \dot{\boldsymbol{J}}\boldsymbol{J}^{-1} \end{aligned} \tag{4.26}$$

For satisfying Eq. (4.26), we assume

$$\begin{pmatrix} \frac{\partial V_1}{\partial \xi} & \frac{\partial V_1}{\partial \eta} & \frac{\partial V_1}{\partial \zeta} \\ \frac{\partial V_2}{\partial \xi} & \frac{\partial V_2}{\partial \eta} & \frac{\partial V_2}{\partial \zeta} \\ \frac{\partial V_3}{\partial \xi} & \frac{\partial V_3}{\partial \eta} & \frac{\partial V_3}{\partial \zeta} \end{pmatrix} = \dot{\boldsymbol{J}} = \hat{\mathbf{T}} \begin{pmatrix} V_{11} & V_{21} & V_{31} \\ \vdots & \vdots & \vdots \\ V_{1k} & V_{2k} & V_{3k} \end{pmatrix} \tag{4.27}$$

where $\hat{\mathbf{T}}$ is a set of gradients of shape functions that transform the physical domain to the computational domain, and V_{ik} denotes the design velocity in the x_i direction at the kth node. For Eq. (4.27) to hold, it requires that the shape functions for approximating the design velocity field should be the same as the shape functions used for domain transformation. The

divergence of the design velocity can be obtained as

$$\nabla \cdot V = \mathrm{tr}\left(\nabla V\right) = \mathrm{tr}\left(\dot{\boldsymbol{J}}\boldsymbol{J}^{-1}\right) \tag{4.28}$$

For numerical integration in the computational domain, the physical differential volume dV and the physical differential surface dS should be transformed to the computational domain. An infinitesimal surface area with unit normal vector can be transformed into the reference domain as

$$\boldsymbol{n}dS = |\boldsymbol{J}|\boldsymbol{J}^{-T}\boldsymbol{k}d\bar{S} \tag{4.29}$$

Thus, $\boldsymbol{n}$ is parallel to $\boldsymbol{J}^{-T}\boldsymbol{k}$. The unit normal vector $\boldsymbol{n}$ can be written explicitly as

$$\boldsymbol{n} = \frac{\boldsymbol{J}^{-T}\boldsymbol{k}}{\|\boldsymbol{J}^{-T}\boldsymbol{k}\|} \tag{4.30}$$

where $\|\cdot\|$ is the Euclidean norm. By applying (4.30) to (4.29), the relation between dS and $d\bar{S}$ can be obtained as

$$dS = |\boldsymbol{J}|\|\boldsymbol{J}^{-T}\boldsymbol{k}\|d\bar{S} \tag{4.31}$$

By transforming the infinitesimal volume in the physical domain to the computational domain, we have

$$dV = |\boldsymbol{J}|d\bar{V} \tag{4.32}$$

Substituting Eqs. (4.14)-(4.15), (4.25)-(4.26), (4.28) and (4.30)-(4.32) into (4.24), the discretized CSE can be obtained as

$$
\begin{aligned}
&\delta \boldsymbol{u}^e \cdot \int_{\bar{\Omega}} \left[\boldsymbol{N}^T \boldsymbol{L}_t(\dot{\overline{\boldsymbol{u}}}) + \boldsymbol{G}^T \left((\boldsymbol{S}^D)^T \boldsymbol{S}_1^A + \boldsymbol{M}_1^D \right) \boldsymbol{G} \right. \\
&+ \boldsymbol{N}^T \left((\boldsymbol{S}^u)^T \boldsymbol{S}_1^A + \boldsymbol{M}_1^u \right) \boldsymbol{G} + \boldsymbol{G}^T \left((\boldsymbol{S}^D)^T \boldsymbol{S}_2^A + \boldsymbol{M}_2^D \right) \boldsymbol{N} \\
&\left. + \boldsymbol{N}^T \left((\boldsymbol{S}^u)^T \boldsymbol{S}_2^A + \boldsymbol{M}_2^u \right) \boldsymbol{N} \right] |\boldsymbol{J}| \, d\bar{V} \dot{\boldsymbol{u}}^e \\
&= \delta \boldsymbol{u}^e \cdot \left[\int_{\bar{\Omega}} \boldsymbol{N}^T \dot{\boldsymbol{f}}_b |\boldsymbol{J}| \, d\bar{V} + \int_S \boldsymbol{N}^T \dot{\boldsymbol{T}} |\boldsymbol{J}| \|\boldsymbol{J}^{-T} \boldsymbol{k}\| \, d\bar{S} \right] \\
&+ \delta \boldsymbol{u}^e \cdot \int_{\bar{\Omega}} \boldsymbol{G}^T \bar{\boldsymbol{\Lambda}} (\boldsymbol{S}^D)^T \boldsymbol{A}(\boldsymbol{u}) |\boldsymbol{J}| \, d\bar{V} \\
&+ \delta \boldsymbol{u}^e \cdot \int_{\bar{\Omega}} \boldsymbol{G}^T \left((\boldsymbol{S}^D)^T \boldsymbol{S}_1^A + \boldsymbol{M}_1^D \right) \left(\bar{\boldsymbol{\Lambda}}^T \boldsymbol{G} \right) |\boldsymbol{J}| \, d\bar{V} \boldsymbol{u}^e \\
&+ \delta \boldsymbol{u}^e \cdot \int_{\bar{\Omega}} \boldsymbol{N}^T \left((\boldsymbol{S}^u)^T \boldsymbol{S}_1^A + \boldsymbol{M}_1^u \right) \left(\bar{\boldsymbol{\Lambda}}^T \boldsymbol{G} \right) |\boldsymbol{J}| \, d\bar{V} \boldsymbol{u}^e \\
&+ \delta \boldsymbol{u}^e \cdot \int_{\bar{\Omega}} \left[\left(\boldsymbol{N}^T \boldsymbol{f}_b - \boldsymbol{N}^T \boldsymbol{L}_t(\overline{\boldsymbol{u}}) \right) \right. \\
&\left. - \boldsymbol{G}^T (\boldsymbol{S}^D)^T \boldsymbol{A}(\boldsymbol{u}) - \boldsymbol{N}^T (\boldsymbol{S}^u)^T \boldsymbol{A}(\boldsymbol{u}) \right] \mathrm{tr}(\dot{\boldsymbol{J}} \boldsymbol{J}^{-1}) |\boldsymbol{J}| d\bar{V} \\
&+ \delta \boldsymbol{u}^e \cdot \int_S \boldsymbol{N}^T \boldsymbol{T} \left[\mathrm{tr} \left(\dot{\boldsymbol{J}} \boldsymbol{J}^{-1} \right) \|\boldsymbol{J}^{-T} \boldsymbol{k}\| \right. \\
&\left. - \frac{(\boldsymbol{J}^{-T} \boldsymbol{k})^T (\dot{\boldsymbol{J}} \boldsymbol{J}^{-1}) \boldsymbol{J}^{-T} \boldsymbol{k}}{\|\boldsymbol{J}^{-T} \boldsymbol{k}\|} \right] |\boldsymbol{J}| d\bar{S}
\end{aligned}
\tag{4.33}
$$

where

$$
\bar{\boldsymbol{\Lambda}} = \begin{pmatrix} \dot{\boldsymbol{J}} \boldsymbol{J}^{-1} & 0 & 0 \\ 0 & \dot{\boldsymbol{J}} \boldsymbol{J}^{-1} & 0 \\ 0 & 0 & \dot{\boldsymbol{J}} \boldsymbol{J}^{-1} \end{pmatrix} \tag{4.34}
$$

and

$$\boldsymbol{G} = [\boldsymbol{N}_1, \boldsymbol{N}_2, \cdots, \boldsymbol{N}_n], \quad \boldsymbol{N}_i = \begin{pmatrix} N_{i,1} & 0 & 0 \\ N_{i,2} & 0 & 0 \\ N_{i,3} & 0 & 0 \\ 0 & N_{i,1} & 0 \\ 0 & N_{i,2} & 0 \\ 0 & N_{i,3} & 0 \\ 0 & 0 & N_{i,1} \\ 0 & 0 & N_{i,2} \\ 0 & 0 & N_{i,3} \end{pmatrix} \tag{4.35}$$

The dependency of $\boldsymbol{S}^D$, $\boldsymbol{S}^A$, $\boldsymbol{M}^D$, $\boldsymbol{M}^u$ and $\boldsymbol{A}$ on $\overline{\boldsymbol{u}}$ in (4.33) has not been made explicit to simplify the notation. $\boldsymbol{G}$ is the second kind of strain displacement matrix (Akbari et al, 2010).

4.3.3 Discrete analytic method for a general field problem

For the discrete analytic method, the governing equations are first discretized, then the discrete equations are differentiated to obtain the equations for sensitivity. The discrete equation for the field problem in (4.16) can be written in a compact form as

$$R^e = F_b \tag{4.36}$$

where R^e is the left side terms of (4.16) and F_b is the external force terms on the right side of (4.16). Taking the material derivative of Eq. (4.36) with respect to the design parameter

b, the discrete analytic sensitivity equations are given as

$$\frac{\partial R^e}{\partial \boldsymbol{u}_j^e}\dot{\boldsymbol{u}}_j^e = \dot{F}_b - \frac{\partial R^e}{\partial b} \tag{4.37}$$

The tangential terms on the left and the fictitious load terms on the right side of Eq. (4.37) are further expanded in the following sections.

Tangential terms

The tangential terms can be expanded as

$$\begin{aligned}\frac{\partial R^e}{\partial \boldsymbol{u}_j^e}\dot{\boldsymbol{u}}_j^e = \int_\Omega \Bigg[& \delta\overline{\boldsymbol{u}} \cdot \left(\frac{\partial \boldsymbol{L}_t(\overline{\boldsymbol{u}})}{\partial \boldsymbol{u}_j^e}\dot{\boldsymbol{u}}_j^e\right) + \frac{\partial \boldsymbol{D}(\delta\overline{\boldsymbol{u}}, \overline{\boldsymbol{u}})}{\partial \boldsymbol{u}_j^e}\dot{\boldsymbol{u}}_j^e \cdot \boldsymbol{A}(\overline{\boldsymbol{u}}) \\ & + \boldsymbol{D}(\delta\overline{\boldsymbol{u}}, \overline{\boldsymbol{u}}) \cdot \left(\frac{\partial \boldsymbol{A}(\overline{\boldsymbol{u}})}{\partial \boldsymbol{u}_j^e}\dot{\boldsymbol{u}}_j^e\right)\Bigg] |\boldsymbol{J}| d\bar{V}\end{aligned} \tag{4.38}$$

In analogy to (4.20) and (4.21), the partial derivatives with respect to the dependent variables can be carried out as a mapping of the partial derivatives of the dependent variable gradients.

$$\frac{\partial \boldsymbol{L}_t(\overline{\boldsymbol{u}})}{\partial \boldsymbol{u}_j^e}\dot{\boldsymbol{u}}_j^e = \boldsymbol{L}_t(\dot{\overline{\boldsymbol{u}}}) \tag{4.39}$$

$$\begin{aligned}\frac{\partial \boldsymbol{A}(\overline{\boldsymbol{u}})}{\partial \boldsymbol{u}_j^e}\dot{\boldsymbol{u}}_j^e &= \boldsymbol{S}_1^A\left(\frac{\partial \boldsymbol{\nabla}\overline{\boldsymbol{u}}}{\partial \boldsymbol{u}_j^e}\right)\dot{\boldsymbol{u}}_j^e + \boldsymbol{S}_2^A\left(\frac{\partial \overline{\boldsymbol{u}}}{\partial \boldsymbol{u}_j^e}\right)\dot{\boldsymbol{u}}_j^e \\ &= \boldsymbol{S}_1^A \boldsymbol{G}\dot{\boldsymbol{u}}^e + \boldsymbol{S}_2^A \boldsymbol{N}\dot{\boldsymbol{u}}^e\end{aligned} \tag{4.40}$$

Applying *Lemma 3.1* to the second term of the right hand side of (4.38), we have

$$\begin{aligned}\frac{\partial \boldsymbol{D}(\delta\overline{\boldsymbol{u}}, \overline{\boldsymbol{u}})}{\partial \boldsymbol{u}_j^e}\dot{\boldsymbol{u}}_j^e \cdot \boldsymbol{A}(\overline{\boldsymbol{u}}) = {} & \delta\boldsymbol{u}^e \cdot \boldsymbol{G}^T\left(\boldsymbol{M}_1^D \boldsymbol{G} + \boldsymbol{M}_2^D \boldsymbol{N}\right)\dot{\boldsymbol{u}} \\ & + \delta\boldsymbol{u}^e \cdot \boldsymbol{N}^T\left(\boldsymbol{M}_1^u \boldsymbol{G} + \boldsymbol{M}_2^u \boldsymbol{N}\right)\dot{\boldsymbol{u}}\end{aligned} \tag{4.41}$$

Hence, the tangential terms (4.38) are obtained as

$$\begin{aligned}\frac{\partial R^e}{\partial \boldsymbol{u}_j^e}\dot{\boldsymbol{u}}_j^e = \delta\boldsymbol{u}^e \cdot \int_{\bar{\Omega}} \big[& \boldsymbol{N}^T \boldsymbol{L}_t(\dot{\overline{\boldsymbol{u}}}) \\ & + \boldsymbol{G}^T \left((\boldsymbol{S}^D)^T \boldsymbol{S}_1^A + \boldsymbol{M}_1^D \right) \boldsymbol{G} + \boldsymbol{N}^T \left((\boldsymbol{S}^u)^T \boldsymbol{S}_1^A + \boldsymbol{M}_1^u \right) \boldsymbol{G} \\ & + \boldsymbol{G}^T \left((\boldsymbol{S}^D)^T \boldsymbol{S}_2^A + \boldsymbol{M}_2^D \right) \boldsymbol{N} \\ & + \boldsymbol{N}^T \left((\boldsymbol{S}^u)^T \boldsymbol{S}_2^A + \boldsymbol{M}_2^u \right) \boldsymbol{N} \big] \, |\boldsymbol{J}| \, d\bar{V} \, \dot{\boldsymbol{u}}^e \end{aligned} \tag{4.42}$$

Fictitious load terms

The material derivative of the external force, the first term on the right side of (4.37), may be expanded as

$$\begin{aligned}\dot{F}_b = & \delta\boldsymbol{u}^e \cdot \int_{\Omega} \boldsymbol{N}^T \dot{\boldsymbol{f}}_b |\boldsymbol{J}| \, d\bar{V} + \boldsymbol{N}^T \boldsymbol{f}_b |\dot{\boldsymbol{J}}| \, d\bar{V} \\ & + \delta\boldsymbol{u}^e \cdot \int_{\bar{S}} \boldsymbol{N}^T \dot{\boldsymbol{T}} |\boldsymbol{J}| \|\boldsymbol{J}^{-T}\boldsymbol{k}\| + \boldsymbol{N}^T \boldsymbol{T} \dot{\overline{|\boldsymbol{J}| \|\boldsymbol{J}^{-T}\boldsymbol{k}\|}} \, d\bar{S} \end{aligned} \tag{4.43}$$

The second term of the fictitious load in (4.37) can be expanded as

$$\begin{aligned}\frac{\partial R^e}{\partial b} = & \int_{\bar{\Omega}} \left[\frac{\partial \boldsymbol{D}(\delta\overline{\boldsymbol{u}}, \overline{\boldsymbol{u}})}{\partial b} \cdot \boldsymbol{A}(\overline{\boldsymbol{u}}) \right. \\ & \left. + \boldsymbol{D}(\delta\overline{\boldsymbol{u}}, \overline{\boldsymbol{u}}) \cdot \frac{\partial \boldsymbol{A}(\overline{\boldsymbol{u}})}{\partial b} \right] |\boldsymbol{J}| d\bar{V} \\ & + \int_{\bar{\Omega}} \left[\delta\boldsymbol{u}^e \cdot \boldsymbol{L}_t(\overline{\boldsymbol{u}}) + \boldsymbol{D}(\delta\overline{\boldsymbol{u}}, \overline{\boldsymbol{u}}) \cdot \boldsymbol{A}(\overline{\boldsymbol{u}}) \right] |\dot{\boldsymbol{J}}| d\bar{V} \end{aligned} \tag{4.44}$$

In analogy to (4.21), the partial derivatives of $\boldsymbol{A}(\overline{\boldsymbol{u}})$ with respect to the design parameter can be carried out as a mapping of the partial derivatives of the dependent variable gradients.

$$\frac{\partial \boldsymbol{A}(\overline{\boldsymbol{u}})}{\partial b} = \boldsymbol{S}_1^A \left(\frac{\partial \boldsymbol{\nabla}\overline{\boldsymbol{u}}}{\partial b} \right) = \boldsymbol{S}_1^A \dot{\boldsymbol{G}} \boldsymbol{u}^e \tag{4.45}$$

Applying *Lemma 3.1* to the first term of right side of (4.44), we have

$$\frac{\partial \boldsymbol{D}(\delta\overline{\boldsymbol{u}},\overline{\boldsymbol{u}})}{\partial b}\cdot\boldsymbol{A}(\overline{\boldsymbol{u}}) = \delta\boldsymbol{u}^e\cdot\left(\boldsymbol{G}^T\boldsymbol{M}_1^D+\boldsymbol{N}^T\boldsymbol{M}_1^u\right)\dot{\boldsymbol{G}}\boldsymbol{u}^e + \delta\boldsymbol{u}^e\cdot\dot{\boldsymbol{G}}^T(\boldsymbol{S}^D)^T\boldsymbol{A}(\overline{\boldsymbol{u}}) \tag{4.46}$$

The derivative of the determinant of the Jacobian can be obtained by making use of a simple result from linear algebra (Christensen and Klarbring, 2009),

$$|\dot{\boldsymbol{J}}| = |\boldsymbol{J}|\mathrm{tr}\left(\dot{\boldsymbol{J}}\boldsymbol{J}^{-1}\right) \tag{4.47}$$

Thus, we have

$$\overline{|\boldsymbol{J}|\|\dot{\boldsymbol{J}^{-T}}\boldsymbol{k}\|} = \left[\mathrm{tr}\left(\dot{\boldsymbol{J}}\boldsymbol{J}^{-1}\right)\|\boldsymbol{J}^{-T}\boldsymbol{k}\| - \frac{(\boldsymbol{J}^{-T}\boldsymbol{k})^T(\dot{\boldsymbol{J}}\boldsymbol{J}^{-1})\boldsymbol{J}^{-T}\boldsymbol{k}}{\|\boldsymbol{J}^{-T}\boldsymbol{k}\|}\right]|\boldsymbol{J}| \tag{4.48}$$

For obtaining the derivative of the second strain displacement matrix, $\dot{\boldsymbol{G}}$, we first define the gradient matrix of shape functions with respect to the physical spatial coordinates

$$\mathbf{B} = \begin{pmatrix} \frac{\partial N_1}{\partial x_1} & \frac{\partial N_2}{\partial x_1} & \dots & \frac{\partial N_k}{\partial x_1} \\ \frac{\partial N_1}{\partial x_2} & \frac{\partial N_2}{\partial x_2} & \dots & \frac{\partial N_k}{\partial x_2} \\ \frac{\partial N_1}{\partial x_3} & \frac{\partial N_2}{\partial x_3} & \dots & \frac{\partial N_k}{\partial x_3} \end{pmatrix} \tag{4.49}$$

and the gradient matrix of shape functions with respect to computational coordinates is also defined as

$$\hat{\mathbf{B}} = \begin{pmatrix} \frac{\partial N_1}{\partial \xi} & \frac{\partial N_2}{\partial \xi} & \dots & \frac{\partial N_k}{\partial \xi} \\ \frac{\partial N_1}{\partial \eta} & \frac{\partial N_2}{\partial \eta} & \dots & \frac{\partial N_k}{\partial \eta} \\ \frac{\partial N_1}{\partial \zeta} & \frac{\partial N_2}{\partial \zeta} & \dots & \frac{\partial N_k}{\partial \zeta} \end{pmatrix} \tag{4.50}$$

By the chain rule we have

$$\hat{\mathbf{B}} = \boldsymbol{J}^T \mathbf{B} \tag{4.51}$$

Since $\hat{\mathbf{B}}$ is independent of the design, the derivative of $\mathbf{B}$ can be obtained by differentiating (4.51) as

$$\dot{\mathbf{B}} = -(\dot{\boldsymbol{J}}\boldsymbol{J}^{-1})^T \mathbf{B} \tag{4.52}$$

From (4.34), (4.35), and (4.52), the derivative of the second strain displacement matrix needed in (4.46) can be obtained as

$$\dot{\boldsymbol{G}} = -\bar{\boldsymbol{\Lambda}}^T \boldsymbol{G} \tag{4.53}$$

Substituting Eqns. (4.45)-(4.48) and (4.53) into (4.43) and (4.44), the fictitious load terms can be obtained as

$$\begin{aligned}
&\dot{F}_b - \frac{\partial R^e}{\partial b} \\
&= \delta \boldsymbol{u}^e \cdot \left[\int_{\bar{\Omega}} \boldsymbol{N}^T \dot{\boldsymbol{f}}_b |\boldsymbol{J}| \; d\bar{V} + \int_S \boldsymbol{N}^T \dot{\boldsymbol{T}} |\boldsymbol{J}| \|\boldsymbol{J}^{-T}\boldsymbol{k}\| \; d\bar{S} \right] \\
&+ \delta \boldsymbol{u}^e \cdot \int_{\bar{\Omega}} \boldsymbol{G}^T \bar{\boldsymbol{\Lambda}} (\boldsymbol{S}^D)^T \boldsymbol{A}(\boldsymbol{u}) |\boldsymbol{J}| \; d\bar{V} \\
&+ \delta \boldsymbol{u}^e \cdot \int_{\bar{\Omega}} \boldsymbol{G}^T \left((\boldsymbol{S}^D)^T \boldsymbol{S}_1^A + \boldsymbol{M}_1^D \right) \left(\bar{\boldsymbol{\Lambda}}^T \boldsymbol{G} \right) |\boldsymbol{J}| \; d\bar{V} \boldsymbol{u}^e \\
&+ \delta \boldsymbol{u}^e \cdot \int_{\bar{\Omega}} \boldsymbol{N}^T \left((\boldsymbol{S}^u)^T \boldsymbol{S}_1^A + \boldsymbol{M}_1^u \right) \left(\bar{\boldsymbol{\Lambda}}^T \boldsymbol{G} \right) |\boldsymbol{J}| \; d\bar{V} \boldsymbol{u}^e \\
&+ \delta \boldsymbol{u}^e \cdot \int_{\bar{\Omega}} \left[\left(\boldsymbol{N}^T \boldsymbol{f}_b - \boldsymbol{N}^T \boldsymbol{L}_t(\overline{\boldsymbol{u}}) \right) \right. \\
&\left. - \boldsymbol{G}^T (\boldsymbol{S}^D)^T \boldsymbol{A} - \boldsymbol{N}^T (\boldsymbol{S}^u)^T \boldsymbol{A} \right] \mathrm{tr}(\dot{\boldsymbol{J}}\boldsymbol{J}^{-1}) |\boldsymbol{J}| d\bar{V} \\
&+ \delta \boldsymbol{u}^e \cdot \int_S \boldsymbol{N}^T \boldsymbol{T} \left[\mathrm{tr} \left(\dot{\boldsymbol{J}}\boldsymbol{J}^{-1} \right) \|\boldsymbol{J}^{-T}\boldsymbol{k}\| \right. \\
&\left. - \frac{(\boldsymbol{J}^{-T}\boldsymbol{k})^T (\dot{\boldsymbol{J}}\boldsymbol{J}^{-1}) \boldsymbol{J}^{-T}\boldsymbol{k}}{\|\boldsymbol{J}^{-T}\boldsymbol{k}\|} \right] |\boldsymbol{J}| d\bar{S}
\end{aligned} \tag{4.54}$$

By replacing the tangential terms and the fictitious load terms in (4.37) with (4.42) and (4.54) respectively, the discrete analytic sensitivity equation can be obtained, which is identical to the discretized CSE (4.33). In the derivations, we assumed that the finite element discretization for the analysis problem in (4.14)-(4.15) is the same as that for the sensitivity equations in (4.25). In equation (4.1), the shape deformation mapping is assumed to be linear with respect to the design variable b. For Eq. (4.27) to hold, it requires that the shape functions for approximating the design velocity field should be the same as the shape functions used for domain transformation. If the integrals in (4.33) are integrated by the same numerical integration method for these two different sensitivity methods, and time integration is carried out by using the same time integration method, they can result in exact the same numerical solution for the sensitivities. Thus, we have proved the following theorem.

Theorem 3.1 Given a field problem governed by the second-order differential equation described in (4.9), the sensitivity equations derived by the total form CSE and by the discrete analytic method are identical in discrete form (4.33) when they have the same [1] finite element discretization, [2] numerical integration method of element matrices, [3] shape deformation mapping that is linear with respect to the design parameter and [4] shape functions for finite element domain transformation as for the design velocity field representation in the finite elements for CSE.

Although *Theorem 3.1* indicates that the discrete analytic method is identical to the discretized total form CSE method, the advantage of the CSE method is that the discrete analytic method requires the knowledge of the implementation details of the original analysis code, which are often inaccessible or very complex. In contrast, if equivalence is not required, then the continuum method needs minimal information about the source code.

The continuum method need only know the governing equations, the numerical solutions and the gradients of the solutions for the governing equations.

4.4 Shape sensitivity for linear potential flow

The equivalence between continuum and discrete analytic methods is demonstrated for potential flow. The flow sensitivity equation with respect to the shape parameter is derived by total form CSE method and discrete analytic method for inviscid, incompressible flow. In an irrotational flow, the governing equation for the stream function Ψ is

$$\nabla^2 \Psi = 0 \tag{4.55}$$

The x- and y-components of velocity, v_x and v_y, can be found from the streamfunction, Ψ, in two dimensional flows

$$v_x = \frac{\partial \Psi}{\partial y}, \qquad v_y = -\frac{\partial \Psi}{\partial x} \tag{4.56}$$

The weak form of Eq. (4.55) is

$$\int_\Omega \nabla \delta\Psi \cdot \nabla \Psi dA = \oint_\Gamma \delta\Psi q_n ds \tag{4.57}$$

where $\delta\Psi$ is the test function, Ω is the fluid domain, Γ is the boundary of the domain and q_n is the flux through the boundaries.

4.4.1 Sensitivity using total form CSE method

For this linear potential flow problem, the weak form equation (4.57) is a special case of the weak form of the general field problem (4.10). The same procedures can be used to derive

the sensitivity equations either by using total form CSE or discrete analytic. By comparing (4.57) with (4.10), we do not have the transient terms and body force terms here, and the other terms are all linear where

$$\boldsymbol{D}(\delta\boldsymbol{u},\boldsymbol{u}) = \nabla\delta\Psi = \boldsymbol{S}^D\boldsymbol{\nabla}\delta\Psi \tag{4.58}$$

$$\boldsymbol{A}(\boldsymbol{u}) = \nabla\Psi \tag{4.59}$$

$$\boldsymbol{T} = q_n \tag{4.60}$$

$$\boldsymbol{S}^D = \begin{pmatrix} 1 & 0 \\ 0 & 1 \end{pmatrix} \tag{4.61}$$

and $\boldsymbol{\nabla} = \nabla$. According to (4.21) and by applying *Lemma 3.1* to $\overline{\dot{\nabla\delta\Psi}} \cdot \nabla\Psi$, we have

$$\overline{\dot{\nabla\Psi}} = \boldsymbol{S}_1^A\left(\nabla\dot{\Psi} - (\nabla\boldsymbol{V})^T\nabla\Psi\right) \tag{4.62}$$

$$\overline{\dot{\nabla\delta\Psi}} \cdot \nabla\Psi = -\left(\boldsymbol{\Lambda}^T\nabla\delta\Psi\right)\cdot(\boldsymbol{S}^D)^T\nabla\Psi \tag{4.63}$$

where

$$\boldsymbol{S}_1^A = \boldsymbol{S}^D \tag{4.64}$$

and

$$\boldsymbol{\Lambda}^T = (\nabla\boldsymbol{V})^T \tag{4.65}$$

Substituting (4.61) and (4.64)-(4.65) into (4.33) and leaving out all the nonlinear terms and the transient term, the discrete CSE equation for linear potential flow can be obtained as

$$\begin{aligned}
&\delta\boldsymbol{\Psi}^e \cdot \int_{\bar{A}} \boldsymbol{G}^T \boldsymbol{G}|\boldsymbol{J}|\ d\bar{A}\dot{\boldsymbol{\Psi}}^e = \delta\boldsymbol{\Psi}^e \cdot \oint_{\bar{\Gamma}} \boldsymbol{N}^T \dot{\boldsymbol{q}}_n |\boldsymbol{J}| \|\boldsymbol{J}^{-T}\boldsymbol{k}\|\ d\bar{s} \\
&+ \delta\boldsymbol{\Psi}^e \cdot \left[\int_{\bar{A}} \boldsymbol{G}^T \bar{\boldsymbol{\Lambda}} \boldsymbol{G}|\boldsymbol{J}|\ d\bar{A} + \int_{\bar{A}} \boldsymbol{G}^T \bar{\boldsymbol{\Lambda}}^T \boldsymbol{G}|\boldsymbol{J}|\ d\bar{V} \right] \boldsymbol{\Psi}^e \\
&+ \delta\boldsymbol{\Psi}^e \cdot \int_{\bar{A}} \boldsymbol{G}^T \boldsymbol{G} \mathrm{tr}(\dot{\boldsymbol{J}}\boldsymbol{J}^{-1}) |\boldsymbol{J}| d\bar{A}\ \boldsymbol{\Psi}^e \\
&+ \delta\boldsymbol{\Psi}^e \cdot \oint_{\bar{\Gamma}} \boldsymbol{N}^T q_n \left[\mathrm{tr}\left(\dot{\boldsymbol{J}}\boldsymbol{J}^{-1}\right) \|\boldsymbol{J}^{-T}\boldsymbol{k}\| \right. \\
&\left. - \frac{(\boldsymbol{J}^{-T}\boldsymbol{k})^T (\dot{\boldsymbol{J}}\boldsymbol{J}^{-1}) \boldsymbol{J}^{-T}\boldsymbol{k}}{\|\boldsymbol{J}^{-T}\boldsymbol{k}\|} \right] |\boldsymbol{J}| d\bar{s}
\end{aligned} \tag{4.66}$$

where

$$\boldsymbol{G} = \begin{pmatrix} \frac{\partial N_1}{\partial x_1} & \frac{\partial N_2}{\partial x_1} & \cdots & \frac{\partial N_k}{\partial x_1} \\ \frac{\partial N_1}{\partial x_2} & \frac{\partial N_2}{\partial x_2} & \cdots & \frac{\partial N_k}{\partial x_2} \end{pmatrix} \tag{4.67}$$

and

$$\bar{\boldsymbol{\Lambda}} = \dot{\boldsymbol{J}}\boldsymbol{J}^{-1} \tag{4.68}$$

4.4.2 Sensitivity using discrete analytic Method

The weak form of the linear potential flow equation (4.57) can be discretized by the finite element method. The stream function and the test function can be approximated as

$$\delta\Psi = \delta\overline{\Psi} = \boldsymbol{N}\delta\boldsymbol{\Psi}^e \tag{4.69}$$

$$\Psi = \overline{\Psi} = \boldsymbol{N}\boldsymbol{\Psi}^e \tag{4.70}$$

Substituting (4.69)-(4.70) into (4.57), the discrete weak form of the potential flow equation can be obtained as

$$\int_{\bar{A}} \nabla\delta\overline{\Psi} \cdot \nabla\overline{\Psi}|\boldsymbol{J}| \; d\bar{A} \; \boldsymbol{\Psi}^e = \oint_{\bar{\Gamma}} \boldsymbol{N}^T q_n |\boldsymbol{J}| \|\boldsymbol{J}^{-T}\boldsymbol{k}\| d\bar{s} \tag{4.71}$$

The discrete sensitivity equations can be derived according to the same procedure as that for the general field problem in Section 4.3.3. Applying (4.61) and (4.64)-(4.65) to the tangential terms (4.42) and the fictitious load terms (4.54), and leaving out all the nonlinear terms and the transient term, the sensitivity equations by discrete analytic method can be obtained, which are identical to the discrete CSE (4.66).

4.5 Shape sensitivity for geometrically nonlinear elasticity

In this section, the shape sensitivity equations for a three-dimensional, geometrically nonlinear elastic structure are derived by using both the total form CSE method and the discrete analytic method, which serves a nonlinear example of the equivalence between total form CSE and discrete analytic method for transient nonlinear field problems. This extends the equivalency proof for linear elasticity found in (Akbari et al, 2010) to nonlinear elasticity.

4.5.1 Geometric nonlinearity

In this derivation, the structure under large deformation with moderately small strain is considered. The the nonlinear strain and stress are given in the Lagrangian reference frame.

The Green-Lagrange strain tensor is given as

$$E_{ij} = \frac{1}{2}\left[\frac{\partial u_i}{\partial x_j} + \frac{\partial u_j}{\partial x_i} + \frac{\partial u_k}{\partial x_i}\frac{\partial u_k}{\partial x_j}\right] \tag{4.72}$$

The Green-Lagrange strain tensor of geometrically nonlinear deformation is obtained by addition of the linear part and the nonlinear part in vector form as

$$\boldsymbol{E}(\boldsymbol{u}) = \begin{pmatrix} E_{11} \\ E_{22} \\ E_{33} \\ 2E_{12} \\ 2E_{23} \\ 2E_{13} \end{pmatrix} = \boldsymbol{S}^{l}\boldsymbol{\nabla}\boldsymbol{u} + \boldsymbol{E}^{nl}(\boldsymbol{u}) \tag{4.73}$$

where

$$\boldsymbol{S}^{l} = \begin{pmatrix} 1 & 0 & 0 & 0 & 0 & 0 & 0 & 0 & 0 \\ 0 & 0 & 0 & 0 & 1 & 0 & 0 & 0 & 0 \\ 0 & 0 & 0 & 0 & 0 & 0 & 0 & 0 & 1 \\ 0 & 1 & 0 & 1 & 0 & 0 & 0 & 0 & 0 \\ 0 & 0 & 0 & 0 & 0 & 1 & 0 & 1 & 0 \\ 0 & 0 & 1 & 0 & 0 & 0 & 1 & 0 & 0 \end{pmatrix} \tag{4.74}$$

and

$$\boldsymbol{E}^{nl}(\boldsymbol{u}) = \begin{pmatrix} 1/2u_{k,1}u_{k,1} \\ 1/2u_{k,2}u_{k,2} \\ 1/2u_{k,3}u_{k,3} \\ u_{k,1}u_{k,2} \\ u_{k,2}u_{k,3} \\ u_{k,1}u_{k,3} \end{pmatrix} \tag{4.75}$$

For structures with isotropic, elastic material and moderate strain, to which we shall limit ourselves here, the Saint Venant Kirchhoff material model is introduced to project the Green-Lagrange strains onto second Piola Kirchhoff stress vector $\boldsymbol{S}$ in matrix notation.

$$\boldsymbol{S} = \boldsymbol{C}\boldsymbol{E} \tag{4.76}$$

where $\boldsymbol{C}$ is the constitutive matrix, which can be determined by the elastic modulus and the Poisson's ratio for isotropic materials. The stress vector $\boldsymbol{S}$ is defined as

$$\boldsymbol{S} = \begin{pmatrix} S_{11} & S_{22} & S_{33} & S_{12} & S_{23} & S_{13} \end{pmatrix}^T \tag{4.77}$$

4.5.2 Weak form of nonlinear elasticity equations

Using the principle of virtual work, the weak form of geometrically nonlinear elastic equations is given as

$$\int_\Omega \delta\boldsymbol{u} \cdot \boldsymbol{u}_{,tt}\rho dV + \int_\Omega \delta\boldsymbol{E} \cdot \boldsymbol{S} dV = \int_\Omega \delta\boldsymbol{u} \cdot \boldsymbol{f}_b dV + \int_S \delta\boldsymbol{u} \cdot \boldsymbol{T}\, dS \tag{4.78}$$

where ρ is the density of the structure and $\boldsymbol{f}_b$ is the body force, and $\boldsymbol{T}$ is the traction force vector. The variation of Green-Lagrange strain in tensor notation is given as

$$\delta E_{ij} = \frac{1}{2}\left[\frac{\partial \delta u_i}{\partial x_j} + \frac{\partial \delta u_j}{\partial x_i} + \frac{\partial u_k}{\partial x_i}\frac{\partial \delta u_k}{\partial x_j} + \frac{\partial u_k}{\partial x_j}\frac{\partial \delta u_k}{\partial x_i}\right] \tag{4.79}$$

For the convenience of numerical discretization, the variation of Green-Lagrange strain in vector form is expressed as

$$\delta \boldsymbol{E}(\boldsymbol{u}) = \left(\boldsymbol{S}^l + \boldsymbol{S}^{nl}\right)\boldsymbol{\nabla}\delta\boldsymbol{u} = \boldsymbol{S}^D\boldsymbol{\nabla}\delta\boldsymbol{u} \tag{4.80}$$

where

$$\boldsymbol{S}^{nl} = \begin{pmatrix} u_{1,1} & 0 & 0 & u_{2,1} & 0 & 0 & u_{3,1} & 0 & 0 \\ 0 & u_{1,2} & 0 & 0 & u_{2,2} & 0 & 0 & u_{3,2} & 0 \\ 0 & 0 & u_{1,3} & 0 & 0 & u_{2,3} & 0 & 0 & u_{3,3} \\ u_{1,2} & u_{1,1} & 0 & u_{2,3} & u_{2,1} & 0 & u_{3,2} & u_{3,1} & 0 \\ 0 & u_{1,3} & u_{1,2} & 0 & u_{2,3} & u_{2,2} & 0 & u_{3,3} & u_{3,2} \\ u_{1,3} & 0 & u_{1,1} & u_{2,3} & 0 & u_{2,1} & u_{3,3} & 0 & u_{3,1} \end{pmatrix} \tag{4.81}$$

and the weak form of nonlinear elastic equations in matrix notation is given as

$$\begin{aligned} &\int_\Omega \delta\boldsymbol{u}\cdot\boldsymbol{u}_{,tt}\rho dV + \int_\Omega \left(\boldsymbol{S}^D\boldsymbol{\nabla}\delta\boldsymbol{u}\right)\cdot\boldsymbol{C}\left(\boldsymbol{S}^l\boldsymbol{\nabla}\boldsymbol{u} + \boldsymbol{E}^{nl}(\boldsymbol{u})\right)dV \\ &= \int_\Omega \delta\boldsymbol{u}\cdot\boldsymbol{f}_b dV + \int_S \delta\boldsymbol{u}\cdot\boldsymbol{T}\,dS \end{aligned} \tag{4.82}$$

4.5.3 Sensitivity using total form CSE method

The total form CSE for the nonlinear elastic structure can be derived by following the same procedure as that for the general field problem. By comparing (4.78) with (4.10), we find that the nonlinear elastic structure problem is a specific example of the general field problem. Here, we have

$$\boldsymbol{L}_t(\boldsymbol{u}) = \rho \boldsymbol{u}_{,tt} \tag{4.83}$$

$$\boldsymbol{D}(\delta \boldsymbol{u}, \boldsymbol{u}) = \delta \boldsymbol{E}(\boldsymbol{u}) \tag{4.84}$$

$$\boldsymbol{A}(\boldsymbol{u}) = \boldsymbol{C}\boldsymbol{E}(\boldsymbol{u}) \tag{4.85}$$

According to (4.20), (4.21) and applying *Lemma 3.1* to $\overline{\delta \boldsymbol{E}(\boldsymbol{u})} \cdot \boldsymbol{S}$, the material derivatives of the terms in (4.83)-(4.85) can be obtained as

$$\overline{\rho \dot{\boldsymbol{u}}_{,tt}} = \rho \dot{\boldsymbol{u}}_{,tt} \tag{4.86}$$

$$\overline{\boldsymbol{C}\boldsymbol{E}} = \boldsymbol{S}_1^A \overline{\boldsymbol{\nabla} \boldsymbol{u}} = \boldsymbol{S}_1^A \left(\boldsymbol{\nabla} \dot{\boldsymbol{u}} - \boldsymbol{\Lambda}^T \boldsymbol{\nabla} \boldsymbol{u} \right) \tag{4.87}$$

$$\begin{aligned} \overline{\delta \boldsymbol{E}(\boldsymbol{u})} \cdot \boldsymbol{S} &= -\left(\boldsymbol{\Lambda}^T \boldsymbol{\nabla} \delta \boldsymbol{u} \right) \cdot (\boldsymbol{S}^D)^T \boldsymbol{C}\boldsymbol{E} \\ &+ \boldsymbol{\nabla} \delta \boldsymbol{u} \cdot \boldsymbol{M}_1^D \left(\boldsymbol{\nabla} \dot{\boldsymbol{u}} - \boldsymbol{\Lambda}^T \boldsymbol{\nabla} \boldsymbol{u} \right) \end{aligned} \tag{4.88}$$

The mapping matrices in (4.87) and (4.88) are given explicitly as

$$\boldsymbol{S}_1^A = \boldsymbol{C}\boldsymbol{S}^D \tag{4.89}$$

$$\boldsymbol{M}_1^D = \hat{\boldsymbol{S}} \tag{4.90}$$

where

$$\hat{\boldsymbol{S}} = \begin{pmatrix} \boldsymbol{S}^t & 0 & 0 \\ 0 & \boldsymbol{S}^t & 0 \\ 0 & 0 & \boldsymbol{S}^t \end{pmatrix}, \quad \boldsymbol{S}^t = \begin{pmatrix} S_{11} & S_{12} & S_{13} \\ S_{12} & S_{22} & S_{23} \\ S_{13} & S_{23} & S_{33} \end{pmatrix} \tag{4.91}$$

By applying (4.86) and (4.89)-(4.90) to (4.33) and letting the other mapping matrices be zeros, the discretized CSE for geometrically nonlinear elastic structures can be obtained as

$$\begin{aligned}
&\delta \boldsymbol{u}^e \cdot \int_{\bar{\Omega}} \left[\rho \boldsymbol{N}^T \boldsymbol{N} \ddot{\boldsymbol{u}}^e_{,tt} + \boldsymbol{G}^T \left((\boldsymbol{S}^D)^T \boldsymbol{C} \boldsymbol{S}^D + \hat{\boldsymbol{S}} \right) \boldsymbol{G} \dot{\boldsymbol{u}}^e \right] \\
&|\boldsymbol{J}| \; d\bar{V} \\
&= \delta \boldsymbol{u}^e \cdot \left[\int_{\bar{\Omega}} \boldsymbol{N}^T \dot{\boldsymbol{f}}_b |\boldsymbol{J}| \; d\bar{V} + \int_S \boldsymbol{N}^T \dot{\boldsymbol{T}} |\boldsymbol{J}| \|\boldsymbol{J}^{-T} \boldsymbol{k}\| \; d\bar{S} \right] \\
&+ \delta \boldsymbol{u}^e \cdot \int_{\bar{\Omega}} \boldsymbol{G}^T \bar{\boldsymbol{\Lambda}} (\boldsymbol{S}^D)^T \boldsymbol{C} \boldsymbol{E} |\boldsymbol{J}| \; d\bar{V} \\
&+ \delta \boldsymbol{u}^e \cdot \int_{\bar{\Omega}} \boldsymbol{G}^T \left((\boldsymbol{S}^D)^T \boldsymbol{C} \boldsymbol{S}^D + \hat{\boldsymbol{S}} \right) \left(\bar{\boldsymbol{\Lambda}}^T \boldsymbol{G} \right) |\boldsymbol{J}| \; d\bar{V} \boldsymbol{u}^e \\
&+ \delta \boldsymbol{u}^e \cdot \int_{\bar{\Omega}} \left[\left(\boldsymbol{N}^T \dot{\boldsymbol{f}}_b - \rho \boldsymbol{N}^T \boldsymbol{N} \ddot{\boldsymbol{u}}^e_{,tt} \right) \right. \\
&\left. - \; \boldsymbol{G}^T (\boldsymbol{S}^D)^T \boldsymbol{C} \boldsymbol{E} \right] \mathrm{tr}(\dot{\boldsymbol{J}} \boldsymbol{J}^{-1}) |\boldsymbol{J}| d\bar{V} \\
&+ \delta \boldsymbol{u}^e \cdot \int_S \boldsymbol{N}^T \boldsymbol{T} \left[\mathrm{tr} \left(\dot{\boldsymbol{J}} \boldsymbol{J}^{-1} \right) \|\boldsymbol{J}^{-T} \boldsymbol{k}\| \right. \\
&\left. - \; \frac{(\boldsymbol{J}^{-T} \boldsymbol{k})^T (\dot{\boldsymbol{J}} \boldsymbol{J}^{-1}) \boldsymbol{J}^{-T} \boldsymbol{k}}{\|\boldsymbol{J}^{-T} \boldsymbol{k}\|} \right] |\boldsymbol{J}| d\bar{S}
\end{aligned} \tag{4.92}$$

4.5.4 Sensitivity using discrete analytic method

The weak form (4.78) can be discretized by using the approximation in (4.14)-(4.15) as

$$\begin{aligned}
&\int_{\bar{\Omega}} \left[\delta \boldsymbol{u}^e \cdot \boldsymbol{N}^T \rho \overline{\boldsymbol{u}}_{,tt} + \delta \boldsymbol{E}(\delta \overline{\boldsymbol{u}}, \overline{\boldsymbol{u}}) \cdot \boldsymbol{C} \boldsymbol{E}(\overline{\boldsymbol{u}}) \right] |\boldsymbol{J}| d\bar{V} = \\
&\delta \boldsymbol{u}^e \cdot \int_{\bar{\Omega}} \left[\boldsymbol{N}^T \boldsymbol{f}_b \right] |\boldsymbol{J}| \; d\bar{V} + \int_{\bar{S}} \boldsymbol{N}^T \boldsymbol{T} |\boldsymbol{J}| \|\boldsymbol{J}^{-T} \boldsymbol{k}\| \; d\bar{S}
\end{aligned} \tag{4.93}$$

By comparing (4.93) with (4.16), we have

$$\boldsymbol{L}_t(\overline{\boldsymbol{u}}_{,tt}) = \rho\overline{\boldsymbol{u}}_{,tt} \tag{4.94}$$

$$\boldsymbol{D}(\delta\overline{\boldsymbol{u}}, \overline{\boldsymbol{u}}) = \delta\boldsymbol{E}(\overline{\boldsymbol{u}}) \tag{4.95}$$

$$\boldsymbol{A}(\overline{\boldsymbol{u}}) = \boldsymbol{C}\boldsymbol{E}(\overline{\boldsymbol{u}}) \tag{4.96}$$

The discrete sensitivity equations can be derived by the same procedure as that for the general field problem in Section 4.3.3. The time dependent terms $\boldsymbol{L}_t(\dot{\overline{\boldsymbol{u}}})$ in (4.42) and $\boldsymbol{L}_t(\overline{\boldsymbol{u}})$ in (4.54) can be discretized as $\rho\boldsymbol{N}\boldsymbol{\ddot{u}}^e_{,tt}$ and $\rho\boldsymbol{N}\boldsymbol{u}^e_{,tt}$ respectively. Upon substituting (4.89)-(4.90) into (4.42) and (4.54), a set of discrete sensitivity equations can be obtained, which is identical to the the discretized CSE in (4.92). Hence, we have shown that the proof of equivalence between continuum and discrete analytic method is applicable to shape sensitivity analysis of transient, geometrically nonlinear elastic structures. Dropping all the transient and nonlinear terms throughout the derivation, it reduces to the equivalence proof for linear static elastic structure as shown in Akbari et al (2010).

4.6 Numeric examples

4.6.1 Potential flow around an airfoil

We consider linear potential flow around an airfoil as shown in Fig. 4.2 for verification of the CSE method for two dimensional flow problems. The finite element model and CSE method are developed for inviscid, incompressible flow around an airfoil. In an irrotational flow, the governing equation for the stream function Ψ is given in (4.55).

The inflow velocity magnitude is U_∞ with an angle of attack α. The essential boundary

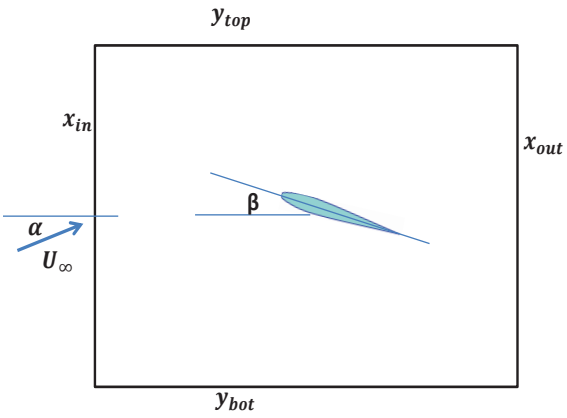

Figure 4.2: Potential flow around an airfoil model.

conditions on the perimeter boundary of the domain are given as

$$\Psi = U_\infty y \cos(\alpha) - U_\infty x \sin(\alpha) \tag{4.97}$$

The boundary condition on the airfoil is the no-penetration condition. If airfoil boundary is a streamline, then the velocity is always tangential to the airfoil. Thus, the no-penetration condition becomes an essential boundary condition on the airfoil,

$$\Psi|_{\Gamma_a} = \Psi_a \tag{4.98}$$

where Ψ_a is a constant along the airfoil, but it's not known *a priori*. For implementation of the essential boundary condition on the airfoil (4.98), the nodal values of the stream function on the airfoil are all given by the single unknown Ψ_a. The Kutta condition was used as a constraint. It requires the flow to leave the trailing edge smoothly. To enforce this condition, we require that flow at the trailing edge be aligned along the bisector of the trailing edge. The geometry of the trailing edge is shown in Fig. 4.3. For the flow to be aligned to $\vec{n}_{te}$,

the velocity normal to the bisector $\vec{n}_{te}$ should be zero. Thus, at the trailing edge, the Kutta condition becomes,

$$\nabla\Psi \cdot \vec{n}_{te} = 0 \tag{4.99}$$

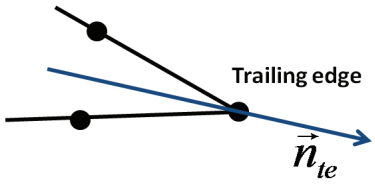

Figure 4.3: Trailing edge geometry.

The CSE method was applied to calculate the shape sensitivity of the potential flow around an airfoil with respect to the angle of attack. For this example, we pose the pressure coefficient sensitivity with respect to the angle of attack to be a shape sensitivity problem by fixing the angle of inflow velocity α and rotating the mesh for an incremental angle of attack change. The sensitivity with respect to the effective angle of attack is the same as the sensitivity with respect to the incidence angle of the airfoil β shown in Fig. 4.2. The angle β is now a shape parameter, since the change of β does change the shape of the fluid domain. The surface of the airfoil can be parameterized by β as

$$\begin{bmatrix} x \\ y \end{bmatrix}_{\Gamma_a} = \begin{bmatrix} \cos(\beta) & \sin(\beta) \\ -\sin(\beta) & \cos(\beta) \end{bmatrix} \begin{bmatrix} x_0 \\ y_0 \end{bmatrix}_{\Gamma_a} \tag{4.100}$$

where $[x\ y]^T$ are the current airfoil surface coordinates, and $[x_0\ y_0]^T$ are the airfoil surface coordinates when $\beta = 0$. The boundary design velocity can be obtained by differentiating (4.100) with respect to the shape parameter β. Given the design velocity on the boundary, a pseudo solid method may be used for calculating the design velocity inside the domain. In this method, the domain design velocity is assumed to be governed by the linear equations

of elasticity (Johnson and Tezduyar, 1994).

The finite element solver for potential flow around a NACA 0012 airfoil problem has been implemented. Linear triangular elements were used. The number of elements used was 1324 and the number of nodes associated was 726. The angle of inflow velocity α is zero and the incidence angle of airfoil β_0 is 10 degrees, which gives the airfoil 10 degrees angle of attack. The numerical results for the fluid analysis are shown in Figure 4.4, which are non-dimensionalized by the inflow velocity U_∞. The velocity in x direction in subfigure 4(a) increases on the upper airfoil surface and decreases on the lower airfoil surface. The velocity in y direction increases rapidly at the upper leading edge. Hence, the pressure coefficient has positive values at the upper leading edge and has negative values at the lower leading edge. As seen in subfigure 4(d), the pressure coefficient on the airfoil closely matches with a vortex panel code solution (Marchman, 1999).

As the angle of attack increases, the velocities at the upper airfoil surface increase and the velocities at the lower airfoil surface decrease. Hence, the velocity sensitivities shown in Fig. 4.5 are positive on the upper surface and negative on the lower surface, while the pressure coefficient sensitivity is negative on the upper surface and positive on the lower surface. As seen from subfigure 5(d), the pressure coefficient sensitivity on the airfoil surface closely matches the complex step solution.

4.6.2 Joined beam with an airfoil under gust load

A NACA 0012 airfoil is mounted on a sting with a supporting strut. This simple two-dimensional model in Fig. 4.6 has features representative of a three-dimensional joined wing. The two-beam model represents a two-dimensional analog to large spanwise deflection and buckling of the aft wing. The sting and strut are modeled as nonlinear Timoshenko beams

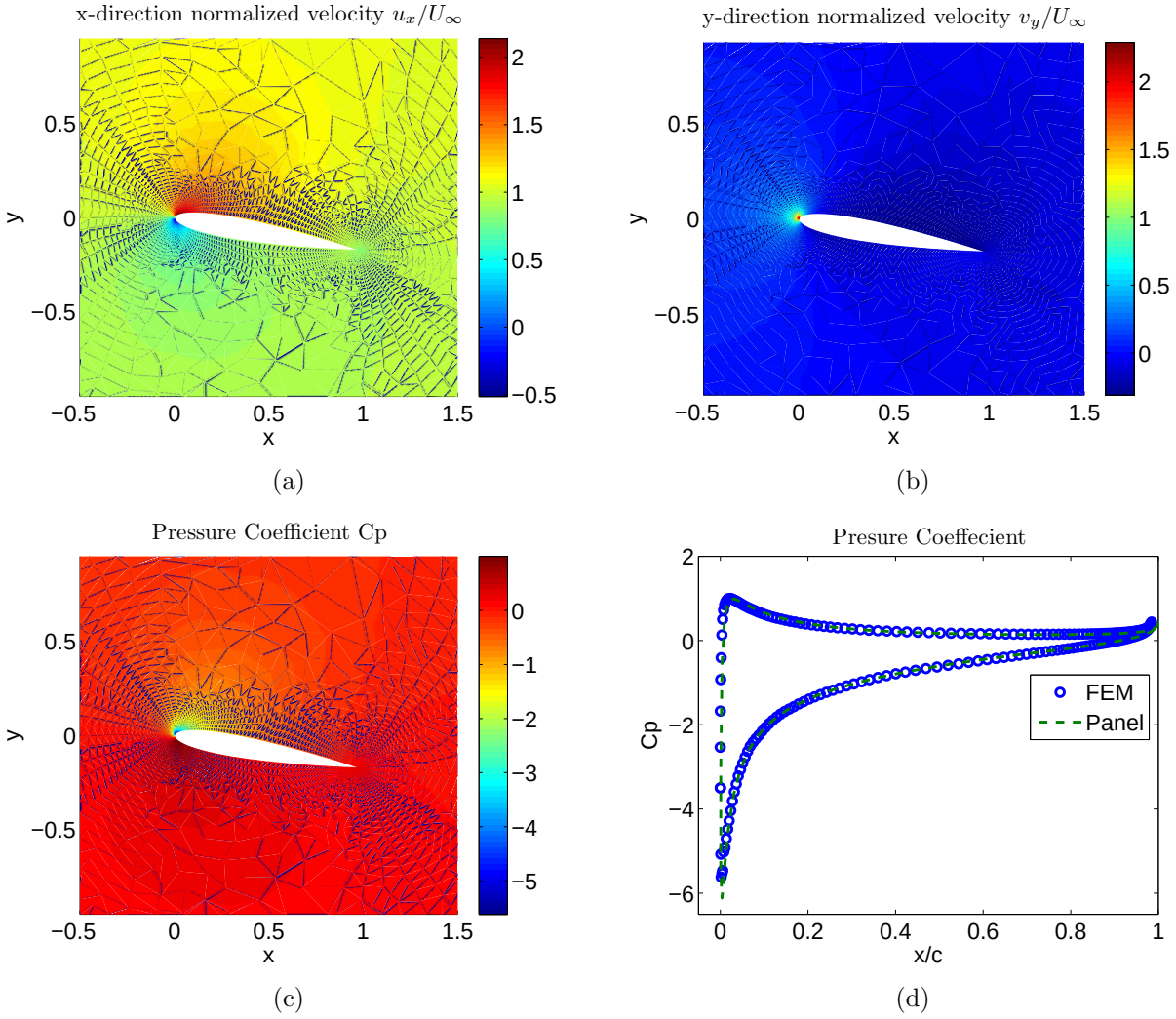

Figure 4.4: Finite element solutions for flow around NACA 0012

capable of large deflections. At a positive angle of attack, the airfoil generates lift, deflecting the beam in the fluid, resulting in an increased angle of attack. Equilibrium deflection of the sting occurs when the force and moments generated by the lifting airfoil balance the internal sting force and moments resisting the bending. The strut is subject to a buckling load due to the deflection of the sting. For shape sensitivity analysis, the sting length L is taken as a shape design parameter. The length of the strut changes according to the change of sting length preserving the angle between sting and strut β.

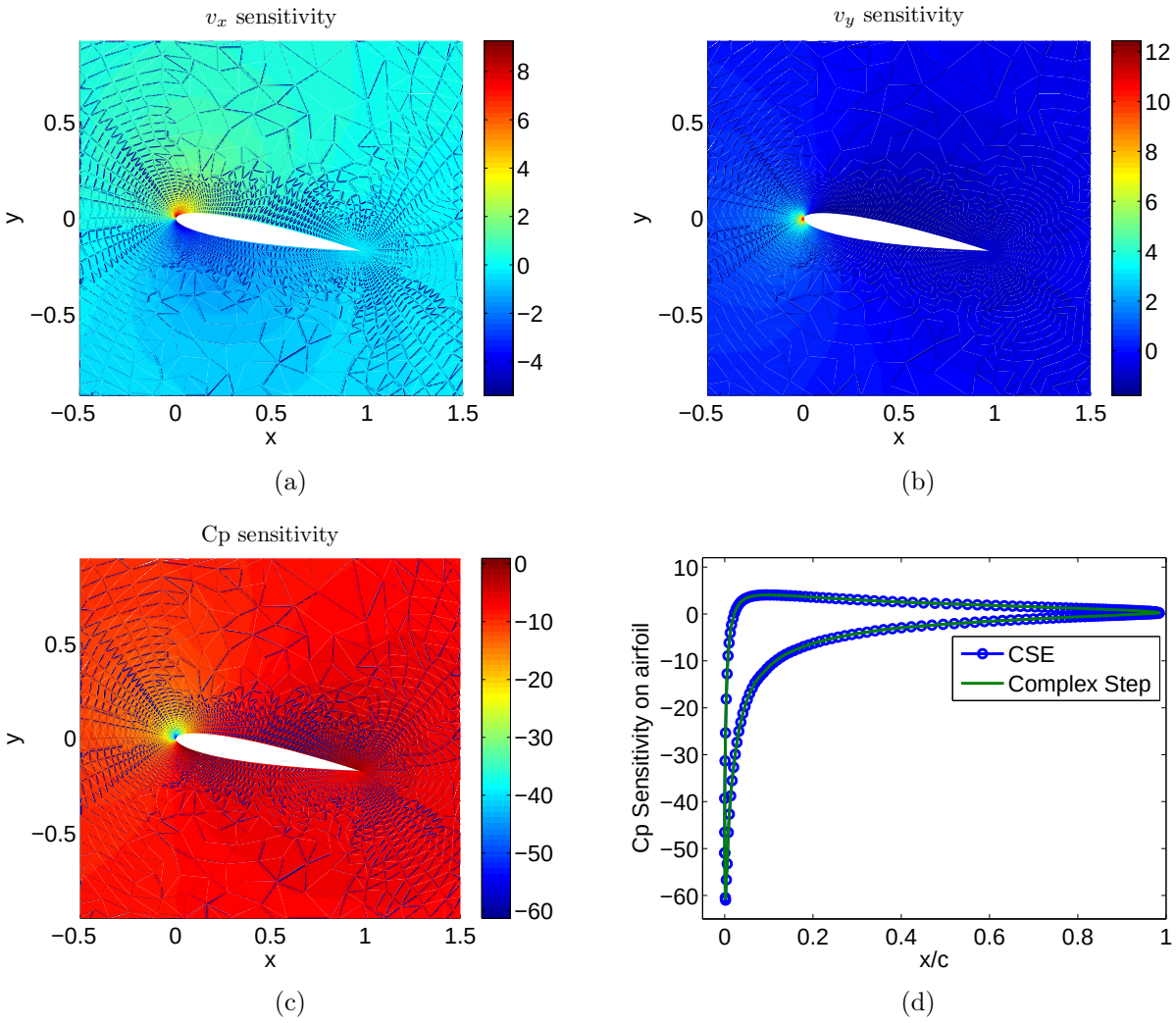

Figure 4.5: Sensitivity of flow velocity and pressure with respect to angle of attack.

For investigating the application of CSE for transient problems, the airfoil under unsteady gust load was investigated. The vertical gust is modeled using the usual discrete gust idealization of a one-minus-cosine pulse (Hoblit, 1988), so that

$$V_g(t) = \begin{cases} \frac{1}{2} V_{g,max} \left(1 - \cos \frac{t-\tau_0}{T_g}\right) & \tau_0 \leq t \leq T_g \\ 0 & \text{otherwise} \end{cases} \tag{4.101}$$

where $V_{g,max}$ is the maximum amplitude of the gust, τ_0 is the start of the gust, and T_g is the

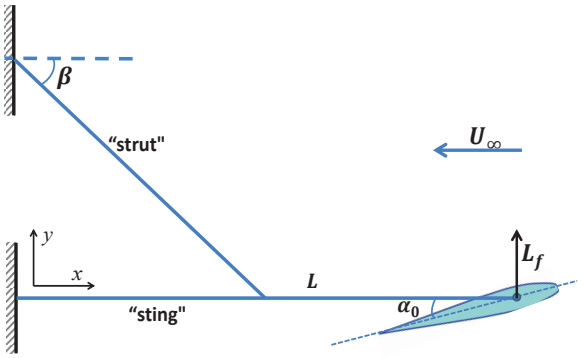

Figure 4.6: Joined beam with an airfoil model.

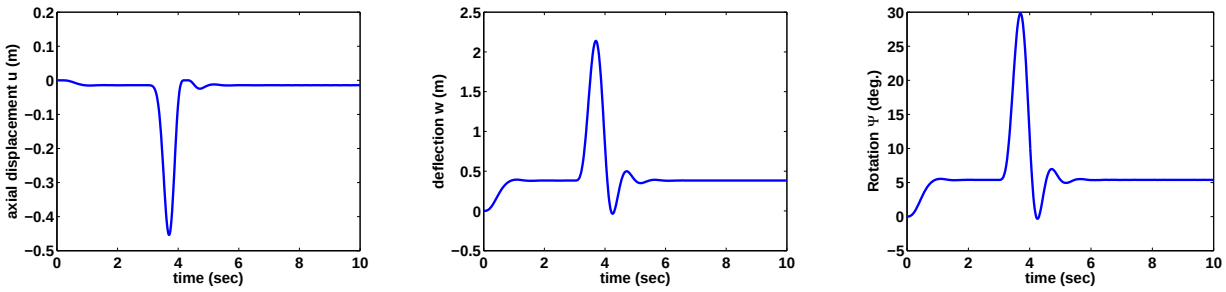

(a) (b) (c)

Figure 4.7: Joined beam gust response at sting tip

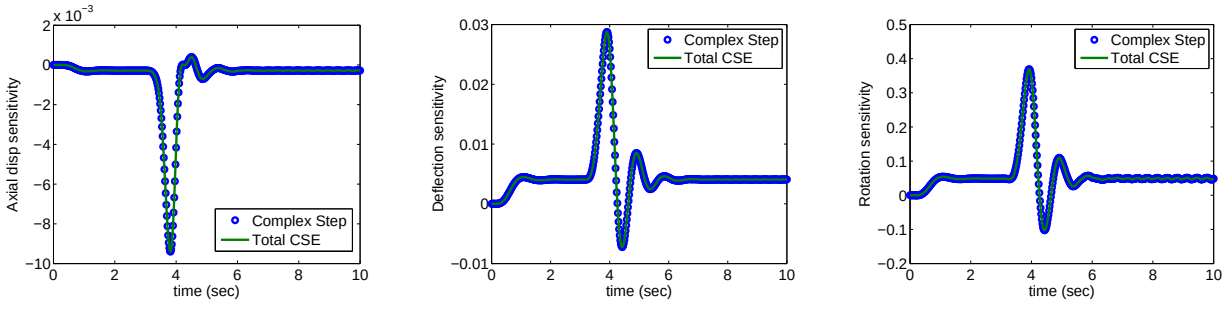

(a) (b) (c)

Figure 4.8: Joined beam gust response sensitivity with respect to beam length at sting tip

duration of the gust. Since the NACA 0012 is symmetric and the tip of the sting is mounted at the aerodynamic center of the airfoil, the aerodynamic moment is zero.

The dynamic typical section aerodynamic theory was used to obtain the aerodynamic load exerted on the tip of the sting. The life force was given as

$$L_f = qcC_{l_\alpha}\left(\alpha_0 + \Phi_{\text{tip}} - \frac{w_{\text{tip},t}}{U_\infty} + \alpha_{\text{gust}}\right) \tag{4.102}$$

where α_0 is the initial incidence angle, $w_{\text{tip},t}$ is the vertical deflection velocity of the beam tip, and α_{gust} is the change in angle of attack due to vertical gust.

The nonlinear Timoshenko beam theory accounts for moderately large rotations and nonlinear strains (Reddy, 2006). The displacement field can be given as

$$u_1 = u(x) - y\Phi, \quad u_2 = w(x), \quad u_3 = 0 \tag{4.103}$$

where Φ is the rotation of the cross section. Using the nonlinear strain-displacement relation (4.72) and retaining only the square of rotation of a transverse normal line in the beam as the only nonlinear strain term, we obtain

$$E_{11} = \left[\frac{\partial u}{\partial x} + \frac{1}{2}\left(\frac{\partial w}{\partial x}\right)^2\right] - y\frac{\partial \Phi}{\partial x}; \quad 2E_{12} = \frac{\partial w}{\partial x} - \Phi \tag{4.104}$$

where w is the vertical deflection, u is the axial displacement, Φ is the cross section rotation angle. Assuming linear elastic material behavior, the equation for the nonlinear Timoshenko beam with rotational inertia can be derived, which is a special case of (4.10)

$$\int_{x_l}^{x_u} \delta\boldsymbol{u}\cdot\boldsymbol{\rho}\boldsymbol{u}_{,tt} + \boldsymbol{D}(\delta\boldsymbol{u})\cdot\boldsymbol{A}(\boldsymbol{u})\, dx = \delta\boldsymbol{u}\cdot\boldsymbol{T}\,|_{x_l}^{x_u} \tag{4.105}$$

where

$$\delta \boldsymbol{u} = [\delta u \ \delta w \ \delta \Phi]^T \tag{4.106}$$

$$\boldsymbol{u}_{,tt} = [u \ w_{,tt} \ \Phi_{,tt}]^T \tag{4.107}$$

$$\boldsymbol{\rho} = \begin{pmatrix} \rho A & 0 & 0 \\ 0 & \rho A & 0 \\ 0 & 0 & \rho I \end{pmatrix} \tag{4.108}$$

and

$$\boldsymbol{D}(\delta \boldsymbol{u}) = [\delta u_{,x} \ \delta w_{,x} \ \delta \Phi_{,x} \ \delta \Phi]^T \tag{4.109}$$

$$\boldsymbol{A}(\boldsymbol{u}) = \begin{bmatrix} EA(u_{,x} + \frac{1}{2} w_{,x}^2) \\ EAw_{,x}(u_{,x} + \frac{1}{2} w_{,x}^2) + kGA(w_{,x} - \Phi) \\ EI\Phi_{,x} \\ -kGA(w_{,x} - \Phi) \end{bmatrix} \tag{4.110}$$

Following the procedure in Section. 4.3, the sensitivity equations can be derived and discretized by using the finite element method. The length of the sting is 6 m with membrane rigidity $EA = 1e8 \ N$, shear rigidity $kGA = 1e7 \ N$, bending rigidity $EI = 3e6 \ N \cdot m^2$, rotary inertia $\rho I = 50 \ kg \cdot m$ and mass per unit length $\rho A = 200 \ kg/m$. The strut was rigidly connected to the sting at the midspan of the sting with a 45 degree angle. The strut has membrane rigidity $EA = 1.4e7 \ N$, shear rigidity $kGA = 1e7 \ N$, bending rigidity $EI = 1.3e4 \ N \cdot m^2$, rotary inertia $\rho I = 18 \ kg \cdot m$ and mass per unit length $\rho A = 135 \ kg/m$. The inflow velocity $U_\infty = 70 \ m/s$ and air density $\rho_a = 1.2 kg/m^3$. The chord length of the airfoil is 3 m with a 3 degree initial angle of attack, α_0. The typical section has lift coefficient $C_{l\alpha} = 2\pi$. The one-minus-cosine gust (4.101) starts at $t = 3s$ and ends at $t = 4s$ with the

maximum amplitude $V_{g,max} = 15\ m/s$.

The transient gust response was investigated and the FSI responses at the sting tip are plotted in Fig. 4.7. Before the gust arrives at $t = 3s$, the joined beam structure reached steady state. After the gust arrives, the structure has a large deflection, and the nonlinear model captures the shortening effects as seen in subfigure 7(a). The transient gust response sensitivities with respect to the sting length were calculated by using the CSE method in total derivative form. The transient FSI response sensitivities at the sting tip are shown in Fig. 4.8. As can be seen from the plots, the gust response sensitivity closely matches the complex step results.

4.7 Conclusions

The shape sensitivity equations were derived in this paper for general transient nonlinear partial differential equations, such as the geometrically nonlinear elasticity and the potential flow. The discrete analytic method and continuum sensitivity equation in total derivative form, once discretized, were proven to be identical when they use the same: discretization, numerical integration and design velocity fields that are linear with respect to the design. These are the same assumptions for the equivalency proof for linear elasticity in Akbari et al (2010). In addition, the shape functions used for domain transformation also should be the same as those for design velocity calculation. Although the discrete analytic method is equivalent to the total form continuum method under these conditions, the advantage of the continuum method is that, if equivalence is not required, minimal information of the source codes for the original analysis problem is required.

4.8 Acknowledgements

The Air Force Office of Scientific Research sponsored this research under agreement number FA9550-09-1-0354. The authors gratefully acknowledge the support of AFOSR program manager Dr. Fariba Fahroo and the AFRL Senior Aerospace Engineers Dr. Raymond Kolonay, Dr. Phillip Beran, and Dr. Maxwell Blair.

Bibliography

Akbari J, Kim N, Ahmadi M (2010) Shape sensitivity analysis with design-dependent loadings–equivalence between continuum and discrete derivatives. Structural and Multidisciplinary Optimization 40(1-6):353–364

Arora JS (1993) An exposition of the material derivatives approach for structural shape sensitivity analysis. Computer Methods in Applied Mechanics and Engineering 105:41–62

Barthelemy BM, Haftka RT (1988) Accuracy analysis of the semianalytical method for shape sensitivity calculation. In: 29nd AIAA/ASME/ASCE/AHS/ASC Structures, Structural Dynamics, and Materials Conference, Washington, DC, AIAA

Bhaskaran R, Berkooz G (1997) Optimization of fluid-structure interaction using the sensitivity equation approach. In: 4th International Symposium on Fluid-Structure Interaction, Aeroelasticity, Flow-Induced Vibrations and Noise, ASME International Mechanical Engineering Congress and Exposition., Dallas, Texas, vol 1, pp 49–56

Borggaard J, Burns J (1994) A sensitivity equation approach to shape optimization in fluid flows. Tech. rep., Langley Research Center

Borggaard J, Burns J (1997) A pde sensitivity equation method for optimal aerodynamic design. Journal of Computational Physics 136:366–384

Choi KK, Kim NH (2005) Structural sensitivity analysis and optimization. Springer Science+Business media, New York

Choi KK, Twu SL (1988) On equivalence of continuum and discrete methods of shape sensitivity analysis. AIAA Journal 27(10):1418–1424

Christensen WP, Klarbring A (2009) An Introduction to Structural Optimization. Springer Science + Business media

Dems K, Haftka RT (1988) Two approaches to sensitivity analysis for shape variation of structures. Mech Struct& Mach 16(4):501

Dems K, Mroz Z (1985) Variational approach to first- and second-order sensitivity analysis of elastic structures. International Journal for Numerical Methods in Engineering 21:637–661

Etienne S, Pelletier D (2005) A general approach to sensitivity analysis of fluid-structure interactions. Journal of Fluids and Structures 21(2):169–186

Etienne S, Hay A, Garon A, Pelletier D (2006) Shape sensitivity analysis of fluid-structure interaction problems. In: 36th AIAA Fluid Dynamics Confernce, AIAA 2006-3217

Etienne S, Hay A, Garon aPD A (2007) Sensitivity analysis of unsteady fluid-structure interaction problems. In: 45th AIAA Aerospace Sciences Meeting, AIAA-2007-332

Haftka RT, Adelman HM (1989) Recent developments in structural sensitivity analysis. Structural Optimization 1:137–151

Haftka RT, Grandhi RV (1986) Structural shape optimization–a survey. Computer Methods in Applied Mechanics and Engineering 57:91–106

Haftka RT, Gurdal Z (1992) Elements of Structural Optimization, 3rd Ed. Kluwer Academic Publichsers, Dordrecht

Haug EJ, Arora JS (1978) Design sensitivity analysis of elastic mechanical systems. Computer Methods in Applied Mechanics and Engineering 15(1):35–62

Haug EJ, Rousselet B (1980) Design sensitivity analysis in structural mechanics. I. static response variations. Journal of Structural Mechanics 8(1):17–41

Haug EJ, Choi KK, Komkov V (1986) Design sensitivity analysis of structural systems, Mathematics in science and engineering., vol 177. Academic Press, Orlando

Hoblit FM (1988) Gust loads on aircraft : concepts and applications. AIAA education series, American Institute of Aeronautics and Astronautics., Washington, D.C.

Jameson A (1988) Aerodynamic design via control theory. Journal of Scientific Computing 3:233–260, URL http://dx.doi.org/10.1007/BF01061285, 10.1007/BF01061285

Johnson AA, Tezduyar TE (1994) Mesh update strategies in parallel finite element computations of flow problems with moving boundaries and interfaces. Computer Methods in Applied Mechanics and Engineering 119:73–94

van Keulen Fv, Haftka RT, Kim NH (2005) Review of options for structuraldesignsensitivity-analysis. part 1: Linearsystems. Computer Methods in Applied Mechanics and Engineering 194:3213–3243

Liu S, Canfield RA (2011) Continuum shape sensitivity for nonlinear transient aeroelastic gust response. In: 52nd AIAA/ASME/ASCE/AHS/ASC Structures, Structural Dynamics, and Materials Conference, Denver, Colorado, AIAA 2011-1971

Liu S, Canfield RA (2012) Continuum shape sensitivity method for fluid flow around an airfoil. In: 53st AIAA/ASME/ASCE/AHS/ASC Structures, Structural Dynamics, and Materials Conference, Honolulu, Hawaii, AIAA 2012-1426

Liu S, Wickert DP, Canfield RA (2010) Fluid-structure transient gust response sensitivity for a nonlinear joined wing model. In: 51st AIAA/ASME/ASCE/AHS/ASC Structures, Structural Dynamics, and Materials Conference, Orlando,Florda

Marchman JF (1999) Panel: A "smith-hess" type of 2-d panel code combining source panels and vortices for a single-element, lifting airfoil in incompressible flow. Virginia Tech, URL http://www.dept.aoe.vt.edu/ marchman/software/index.html

Olhoff N, Taylor JE (1983) On structural optimization. Journal of Applied Mechanics 50(4):1139–1151

Reddy JN (2006) An introduction to nonlinear finite element analysis. McGraw-Hill series in mechanical engineering, McGraw-Hill Higher Education, New York,NY

Squire W, Trapp G (1998) Using complex variables to estimate derivatives of real functions. SIAM Review 40(1):110–112

Stanley LGD, Stewart D (2002) Design sensitivity analysis : computational issues of sensitivity equation methods. Academic Press, Philadelphia

Tortorelli D, Michaleris P (1994) Design sensitivity analysis: Overview and review. Inverse Problems in Engineering 1(1):71–105

Turgeon E, Pelletier D, Borggaard J (1999) A continuous sensitivity equation approach to optimal design in mixed convection. AIAA 99-3625

Wickert DP, Canfield RA, Reddy JN (2009) Fluid-structure transient gust sensitivity using least-squares continuous sensitivity analysis. In: 50th AIAA/ASME/ASCE/AHS/ASC

Structures, Structural Dynamics, and Materials Conference, Palm Springs, California, AIAA-2008-1821

Yang RJ, Botkin ME (1986) The relationship between the variational approach and the implicit differentiation approach to shape design sensitivities. In: Bennett JA, Botkin ME (eds) The optimum shape: automated structural design, Plenum press, New York, pp 61–77

Chapter 5

Conclusions and Future Work

5.1 Conclusions

In this dissertation, the continuum sensitivity method has been investigated and applied to shape sensitivity analysis of nonlinear dynamic aeroelastic problems. The design derivatives are calculated by solving the CSEs, a system of linear partial differential equations. Although the CSE system is posed as a continuous system, it can be solved by using the same numerical method as that used by the analysis solver. The sensitivity system is always a linear system of equations, even when the original system is nonlinear. If the Newton-Raphson method is used for the nonlinear problems, the converged tangent stiffness matrix gives the coefficient matrix for solving the linear system of CSEs. The continuum sensitivity method is more efficient than the finite difference method, especially for nonlinear problems, because only one nonlinear analysis is required.

Continuum sensitivity systems are often posed in terms of local derivatives for fluids and total derivatives for solids. This work investigated both the local form and the total form

continuum sensitivity methods for fluid and structure applications. A comparison of the derivation, accuracy, and efficiency of these two methods was conducted. The local form CSE only requires the design velocity to be evaluated at the boundaries, while the total form CSE requires the design velocity to be evaluated throughout the whole domain. However, the local form CSE requires higher order derivative terms to be evaluated at the boundary. This is a common source of error that is not present in the total form CSE. For this reason, the total form CSE was shown to be more accurate than the local form CSE. However, the continuity requirement on design velocity for the total form CSE is higher, which makes the parametrization of the domain more difficult.

It has been shown in this dissertation that, once discretized, the sensitivity equations derived by the total form CSE and by the analytical discrete method for field problems are equivalent under the conditions that they have the same [1] finite element discretization, [2] numerical integration method, [3] shape deformation mapping that is linear with respect to the design parameter, and [4] shape functions for domain transformation and for design velocity field calculation. Although they are equivalent, the implementation of the total form CSE does not have to satisfy all those conditions. If equivalence is not required, the advantage of the continuum sensitivity method is that not as much information about the analysis source codes are required, which leads to an easier implementation of the sensitivity analysis by treating the analysis codes as a "black box." For the continuum sensitivity method, one needs to know only the governing partial differential equations, the numerical solutions and the spatial gradients of the solutions for the governing equations.

In this dissertation, the total form continuum sensitivity method was applied for the first time to nonlinear transient aeroelastic problems. For nonlinear problems, it is shown that the tangent stiffness matrix yields the desired sensitivity coefficient matrix for solving the sensitivity equations. The local form CSE was applied for the first time to built-up structures.

The difficulty in implementation has been pointed out and resolved (Liu and Canfield, 2013a). First comparison of the local form and the total form CSE method for static and transient aeroelastic problems has been made on their accuracy, efficiency and implementation (Liu and Canfield, 2013c). The equivalence of the discrete analytic method and the total form CSE method is proved for the first time for general nonlinear transient second-order partial differential equations that govern many field problems (Liu and Canfield, 2013b).

5.2 Future Work

In this research, the joined beam model in two dimensions which is representative of the joined wing sensorcraft, under gust load was assumed to be fixed at the roots. In reality, the rigid body motion is large when modeling the gust response of the whole aircraft. Investigating efficient and accurate methods for calculating the sensitivity of rigid body motion and elastic deformation of structures under gust loads with respect to changes of aircraft shape would be an interesting topic for the future work. In this situation, modeling of the large vehicle motion in fluid flow may require posing the equations in an arbitrary Lagrangian-Eulerian (ALE) reference frame. For shape design sensitivity, the issues of dealing with the design velocity field on the fluid mesh and the mesh velocity due to elastic deformation are worth to investigate.

This dissertation employed continuum shape sensitivity method for aeroelastic response using linear potential flow. Future work should consider including compressibility in the aerodynamic analysis using Euler's equations or other high-fidelity flow models.

Also of interest, is the application of different forms of CSE for the eigenvalue design sensitivity. For instance, the sensitivity of normal modes and modal shapes with respect to the structural shape parameters. In addition, the frequency response sensitivity of coupled

aeroelastic systems is also of interest. For example, the flutter modes and flutter speed sensitivities to aircraft shape changes are critical for the optimal design of an aircraft.

Implementation of the continuum sensitivity method in this research mainly focused on the direct approach. When the number of design variables is larger than the number of constraints, the adjoint approach is very efficient. Therefore, investigation of adjoint formulations and their benefits for different forms of the CSE method should be considered in the future work.

Bibliography

Liu, S., Canfield, R. A., 2013a. Boundary velocity method for continuum shape sensitivity of nonlinear fluid–structure interaction problems. Journal of Fluids and Structures. URL `http://dx.doi.org/10.1016/j.jfluidstructs.2013.05.003`

Liu, S., Canfield, R. A., 2013b. Equivalence of discrete analytic and continuum sensitivity methods for nonlinear differential equations. Accepted for publication in Structural and Multidisciplinary Optimization.

Liu, S., Canfield, R. A., 2013c. Two forms of continuum shape sensitivity method for fluid-structure interaction problems. Submitted to AIAA Journal.